

Dissertation zur Erlangung des Doktorgrades
der Fakultät für Chemie und Pharmazie
der Ludwig-Maximilians-Universität München

Elucidating the role of the *de novo* mutation R252P/R281P in DPP9

Hannah Fischer

aus

Landsberg am Lech, Deutschland

2024

Erklärung

Diese Dissertation wurde im Sinne von § 7 der Promotionsordnung vom 28. November 2011 von Herrn Prof. Dr. Veit Hornung betreut.

Eidesstattliche Versicherung

Diese Dissertation wurde eigenständig und ohne unerlaubte Hilfe erarbeitet.

München, den 10.10.2024

.....
Hannah Fischer

Dissertation eingereicht am: 10.06.2024

1. Gutachter: Prof. Dr. Veit Hornung

2. Gutachter: Prof. Dr. Klaus Förstemann

Mündliche Prüfung am: 13.09.2024

Auszüge dieser Arbeit wurden bereits in folgender Publikation veröffentlicht:

Wolf, C.*, **Fischer, H.***, Kühl, J., Koss, S., Jamra, R.A., Starke, S., Schultz, J., Ehl, S., Neumann, K., Schuetz, C., Huber, R., Hornung, V.#, and Lee-Kirsch, M.A.# (2023). Hemophagocytic lymphohistiocytosis–like hyperinflammation due to a de novo mutation in DPP9. JACI Volume 152, Issue 5, P1336-1344

* *Contributed equally*

Corresponding authors

Table of contents

1	Introduction	1
1.1	Immune System	1
1.1.1	Innate Immune System.....	2
1.1.2	Adaptive Immune System.....	4
1.2	Pattern recognition receptors.....	5
1.2.1	Toll-like receptors (TLRs).....	6
1.2.2	RIG-I-like receptors (RLRs).....	7
1.2.3	C-type lectin receptors (CLRs).....	8
1.2.4	Cytosolic DNA sensors	9
1.2.5	NOD-like receptors (NLRs).....	10
1.3	Inflammasomes	11
1.3.1	Inflammasome signalling	12
1.3.2	Inflammasome sensors.....	15
1.4	FIIND-containing inflammasome sensors	19
1.4.1	NLRP1	21
1.4.2	CARD8	22
1.4.3	NLRP1 and CARD8 activation.....	23
1.4.4	NLRP1 and CARD8 in diseases.....	33
1.5	Dipeptidyl peptidases 8 and 9 (DPP8/9).....	36
1.5.1	Physiological roles of DPP8/9	37
1.5.2	Pathophysiological roles of DPP9	39
2	Aims of this work.....	41
3	Material and Methods	42
3.1	Material	42
3.1.1	Antibodies.....	42
3.1.2	Cell lines.....	42

3.1.3	Chemicals	43
3.1.4	Commercial Kits	44
3.1.5	Media and Buffers	45
3.1.6	Equipment.....	46
3.1.7	Primer	47
3.1.8	Plasmids	48
3.1.9	Enzymes	49
3.1.10	Single-guide RNA (sgRNA).....	49
3.1.11	Software and Algorithms	50
3.2	Molecular Biology Methods	50
3.2.1	Generation of chemically competent <i>E. coli</i>	50
3.2.2	Polymerase Chain Reaction (PCR)	50
3.2.3	Agarose gel electrophoresis	51
3.2.4	Agarose gel extraction	51
3.2.5	Cloning.....	51
3.2.6	<i>E. coli</i> transformation.....	52
3.2.7	Plasmid isolation <i>E. coli</i>	52
3.3	Cell culture methods	53
3.3.1	Culturing of Cells	53
3.3.2	Seeding and Stimulation of Cells.....	53
3.4	Cell Biology Methods	54
3.4.1	Transfection of plasmids	54
3.4.2	ASC Speck Assay	54
3.4.3	Overexpression Assay	55
3.4.4	Inflammasome Activation Assay	55
3.4.5	Lentiviral transduction	55
3.5	Biochemical methods.....	56

3.5.1	Immunoblotting.....	56
3.5.2	Cytotoxicity assay	56
3.5.3	Enzyme-linked immunosorbent assay (ELISA)	57
3.5.4	Fluorescence microscopy.....	57
3.5.5	Live-cell microscopy.....	57
3.6	CRISPR/ Cas9 mediated knockout generation	58
3.6.1	Nucleofection of cells.....	58
3.6.2	Knockout identification by Sanger sequencing	58
3.7	Quantification and Statistical Analysis	58
4	Results	59
4.1	Identification of a <i>de novo</i> mutation in <i>DPP9</i>	59
4.2	R252 of DPP9 enhances protein stability.....	60
4.3	DPP9 R252P mutation induces structural alteration	62
4.4	DPP9 R252P/R281P mutation impairs DPP9 protein stability.....	63
4.5	DPP9 R252P/R281P mutation leads to activation of the NLRP1 and CARD8 inflammasome.....	65
4.6	DPP9 R252P/R281P mutant exerts a dominant-negative effect on NLRP1 inflammasome activation.....	71
4.7	DPP9 R252P/R281P mutant exerts a dominant-negative effect on CARD8 inflammasome activation	75
4.8	DPP9 knockout in keratinocytes leads to increased inflammation	77
4.9	DPP8 and DPP9 have redundant functions in N/TERT-1 keratinocytes	78
5	Discussion.....	81
5.1	Role of DPP9 in regulating inflammasome activation <i>in vivo</i>	81
5.1.1	DPP9 R252P mutation impairs protein stability	82
5.1.2	DPP9 R252P mutation results in inflammasome activation in a dominant-negative manner.....	83
5.1.3	Patient mutation induces CARD8 inflammasome activation	84
5.1.4	DPP9 R252P mutation may interfere with NLRP1 binding.....	86

5.1.5	DPP9 loss-of-function mutations are intolerated.....	87
5.1.6	Minimal amounts of DPP8/9 are sufficient for DPP8/9 inhibition....	88
5.2	Physiological role of DPP8/9 and NLRP1/CARD8 interaction	89
5.3	NLRP1 and CARD8 – Why both?	91
5.4	Dipeptidyl-peptidase (DPP) inhibitors	92
5.4.1	Selective DPP8/9 inhibitors.....	93
5.4.2	Prospects for therapeutic applications.....	94
5.5	Our work in the context of recent publications.....	94
5.6	Limitations of this study	95
6	Summary	97
7	Bibliography	98
8	List of abbreviations	129
9	Acknowledgements	132
10	Appendix	134
10.1	PolyPhen-2 report for the short isoform of DPP9	134
10.2	IC ₅₀ and KI' values of relevant DPP8 and DPP9 inhibitors	134
10.3	Batch processing scripts for ImageJ	135

1 Introduction

1.1 Immune System

The immune system is an essential defence mechanism that protects the body from exogenous and endogenous threats. Exogenous threats include microbes (bacteria, parasites, fungi, and viruses) and toxins, while endogenous threats can be aberrant cells in the body, such as cancer cells. The human body has evolved a complex defence mechanism consisting of an intricate network of organs, tissues, cells, and proteins that work in close synergy (Murphy et al., 2017).

The immune system is grouped into two arms: the innate immune system and the adaptive immune system. The innate immune system represents the body's first line of defence, providing an immediate response to intruding pathogens. This line of defence is non-specific and is found in all living multicellular species, including vertebrates, invertebrates, plants, and fungi. It is based on germline-encoded receptors, called pattern-recognition receptors (PRRs), that recognise a variety of conserved molecular patterns. Those molecules can be divided into two classes: pathogen-associated molecular patterns (PAMPs), which are characteristic of microbial pathogens, and damage-associated molecular patterns (DAMPs), which are host cell components released by damaged or dead cells. In general, the innate immune response can eliminate a large number of invading pathogens. However, in order to ensure the effective elimination of pathogens, the innate immune response in vertebrates activates the adaptive immune response (Abbas et al., 2018).

Unlike the innate immune system, the adaptive immune system recognises specific antigens and responds less rapidly to invading pathogens. The adaptive immune response includes humoral and cell-mediated immune responses carried out by white blood cells known as lymphocytes. B lymphocytes (B cells) are involved in humoral immunity by producing antibodies that bind to foreign antigens in the body and inactivate them. T lymphocytes (T cells) mediate cellular immune responses, ranging from detecting and destroying infected cells to secreting cytokines, which are chemical messengers that activate other immune cells. Importantly, the

adaptive immune response constantly adapts and develops an immunological memory, enabling the host to quickly eliminate previously encountered threats. This adaptability of acquired immunity results from somatic hypermutation, which produces antibodies with unique specificities through genetic mutations in antibody-coding genes and V(D)J recombination. This acquired immunity can provide lifelong protection against specific pathogens, depending on the severity and type of infection, but it cannot be inherited (Abbas et al., 2018).

The adaptive and innate immune responses are not mutually exclusive mechanisms; instead, they complement each other. Defects in either defence mechanism can lead to the host's susceptibility to infection and can trigger inappropriate responses. Dysregulation of the innate immune response can lead to autoinflammatory diseases, whereas aberrant changes in the adaptive immune response can mediate autoimmunity (Murphy et al., 2017).

1.1.1 Innate Immune System

The innate immune response is an immediate and rapid response to pathogens encountering the body. When microbes attempt to infect a host, they first encounter physical barriers, such as the skin, which serve as the first line of defence in the innate immune system. The outermost layer of the skin, the epidermis, protects the body from microbes and environmental factors such as ultraviolet (UV) radiation and chemicals (Lee et al., 2006). Additionally, the skin hinders pathogen colonisation by maintaining low water content, an acidic pH, and antimicrobial lipids deposited on its surface (Elias, 2007). Another physical barrier can be found on the surfaces of organs, which are lined with a mucus membrane consisting of immune cells and natural antibiotics to defend against pathogens. If a pathogen still manages to breach the physical barriers, it will then be exposed to both the humoral and cellular components of the innate immune system.

The humoral part of the innate immune response is mediated by a large variety of peptides and proteins, which include humoral lectins, such as collectins and ficolins, acute phase reactants, such as C-reactive protein (CRP), and antimicrobial peptides (Mantovani and Garlanda, 2023). These molecules interact with antigens

or microbial moieties and play a role in activating components of the complement system. The complement system consists of more than 30 proteins found in the plasma and membranes of cells. Activation of the complement system involves multiple steps of proteolysis and assembly, followed by cleavage of the third complement component (C3), whose cleaved parts C3b and C3a trigger different immune functions. On the one hand, binding of C3b to microbes or damaged cells leads to opsonisation and increased susceptibility to phagocytosis. On the other hand, C3b induces a cascade of polymerisation reactions leading to the assembly of a membrane attack complex (MAC). The assembly of MAC create pores in the membrane, which disrupt the cell membrane and cause the subsequent lysis of the cells, killing the pathogen. Additionally, small fragments of some complement components (e.g. C3a) act as chemoattractants that induce inflammation and recruit immune cells to the site of infection, subsequently leading to a cellular immune response (Bottazzi et al., 2010; Janeway et al., 2001).

The cellular part of the innate immune response consists of various effector immune cells, which respond rapidly to signals from invading pathogens or damaged cells. Upon sensing pathogens, those cells produce and secrete cytokines and chemokines. Cytokines were discovered in the 1960s and 1970s and are potent signalling molecules of a size between 5 and 25 kDa (Dinarello, 2007). They play a pivotal role in intercellular communication and are crucial for recruiting additional immune cells to the site of infection. Key inflammatory cytokines involved in the initiation of recruitment are the tumour necrosis factor (TNF), interleukin 1 β (IL-1 β) and interleukin 6 (IL-6). Neutrophils are the first cells to be attracted to the site of infection, followed by monocytes and lymphocytes, including T cells, natural killer cells, B cells, and mast cells. During inflammation, recruited monocytes can differentiate into macrophages and dendritic cells, which phagocytose pathogens and present antigens (Murphy and Weaver, 2017).

Cells of the innate immune system can ingest and eliminate pathogens or apoptotic cells, thereby playing an essential role in maintaining tissue homeostasis. This process is termed phagocytosis. The characterisation of cells responsible for phagocytosis, known as phagocytes, was first described by Ilya Metchnikoff (Schmalstieg and Goldman, 2008). Phagocytosis is initiated by recognising targets

via specific receptors expressed on the plasma membrane of phagocytes. This recognition triggers signalling cascades that result in the remodelling of cell membrane lipids and the actin cytoskeleton, allowing for the engulfment of particles and the formation of a phagosome. Engulfment of the particles leads to the formation of a phagosome. Phagosome maturation occurs within the cell and involves fusion and fission events between the phagosome and early and late endosomes. Ultimately, the phagolysosome – i.e. the mature phagosome – is created by fusion with lysosomes. The phagolysosome is progressively acidified, becomes highly oxidative, and is enriched with hydrolytic enzymes, eventually leading to its content degradation (Rosales and Uribe-Querol, 2017). In addition to its crucial role in the innate immune response, phagocytosis is also critical in initiating the adaptive immune response through two different mechanisms. Firstly, next to direct clearance of the pathogen, the recognition of phagocytic targets can result in the production and release of pro-inflammatory cytokines. These cytokines, such as TNF- α and IL-6, function as signalling molecules that attract lymphoid cells, including B cells and T cells, to the site of infection and coordinate the adaptive immune response. Secondly, during phagocytosis, professional phagocytes can process antigens of digested pathogens and present them on their cell surface to lymphocytes via their major histocompatibility complex (MHC) class II molecules (Flannagan et al., 2012).

1.1.2 Adaptive Immune System

The adaptive immune system, also known as the acquired immune system, becomes active following an initial exposure to an antigen, typically after a certain latency period. Unlike the innate immune system, the adaptive immune system is dependent on a smaller number of cells: B and T cells. Both are derived from hematopoietic stem cells in the bone marrow, with the B cells maturing within the bone marrow itself and the T cells migrating to the thymus to mature. Both cell types are activated by encountering antigens via their membrane-bound receptor and undergo clonal expansion after their activation. In contrast to B cell receptors, which can directly bind to antigens, T cell receptors can only recognise peptide fragments of antigens that are presented on the surface of other cells via MHC

molecules. As such, cytotoxic T cells, which express the CD8 receptor, recognise viral peptides presented via an MHC class I complex on infected cells and directly eliminate these cells. Helper T cells, which express the CD4 receptor, detect peptides presented via an MHC class II complex on professional antigen-presenting cells (APCs), such as dendritic cells, macrophages, and B cells. Upon activation, helper T cells secrete cytokines to orchestrate a targeted and effective immune response (Murphy et al., 2017).

1.2 Pattern recognition receptors

Innate immune responses are initiated by germline-encoded specialised receptors known as pattern recognition receptors (PRRs). These receptors are predominantly expressed on immune cells and recognise conserved molecular patterns, known as PAMPs and DAMPs, to initiate immune responses. This concept of sensing conserved molecular patterns resembles pattern-triggered immunity (PTI) observed in plants (Akira et al., 2006). However, in an evolutionary arms race, pathogens have evolved a variety of mechanisms, including virulence factors, also called pathogen effectors, to evade or counteract the host's immune response, such as the induction of PTI. These virulence factors are secreted by pathogens during infection (Lopes Fischer et al., 2020). While PTI involves direct recognition of conserved microbial patterns, the indirect detection of specific pathogen effectors initiates an immune response that is known as effector-triggered immunity (ETI) in the plant immune system (Bigeard et al., 2015).

In vertebrates, there are four major groups of PRRs, consisting of Toll-like receptors (TLRs), C-type lectin receptors (CLRs), Retinoic acid-inducible gene (RIG)-I-like receptors (RLRs) and NOD-like receptors (NLRs) (Amarante-Mendes et al., 2018). PRRs are found either membrane-bound or cytosolic in cells. Expressed on cell surfaces, they recognise extracellular pathogens, such as bacteria or fungi. Present in membranes of intracellular cell compartments, such as endosomes, they detect intracellular intruders like viruses. In the cytoplasm, they recognise different molecules arising from intracellular pathogens. Except for certain NLRs, PRR ligand recognition leads to the activation of transcription factors that ultimately

result in the upregulation of genes associated with cell autonomous or systemic defence pathways. A prominent subset of upregulated factors encompasses the so-called pro-inflammatory cytokines (Takeuchi and Akira, 2010).

1.2.1 Toll-like receptors (TLRs)

The initial member of the TLR family was identified in 1988 when the *Toll* gene, which is essential for establishing dorsoventral polarity during embryogenesis, was found in *Drosophila melanogaster* (Hashimoto et al., 1988). Subsequent research revealed the significance of Toll in the response of insects to a fungal infection (Lemaitre et al., 1996). TLRs are evolutionarily conserved across diverse organisms, ranging from worms to mammals. Currently, there are 10 described TLRs in humans (TLR1-10) and 12 in mice (TLR1-9, TLR11-13) located either on the cell membrane or on endolysosomal membranes. One of the first members of PRRs identified in humans was TLR4, initially named hToll owing to its similarity to the Toll protein in *Drosophila* (Medzhitov et al., 1997). TLRs can sense a variety of different PAMPs, including lipids (TLR1, TLR2, TLR6) and nucleic acids (TLR7, TLR8, TLR9). One example of nucleic acid sensing by TLRs is the recognition of oligoribonucleotides by TLR8, which are made recognisable by the lysosomal endoribonuclease RNase T2 (Greulich et al., 2019). Other ligands for TLRs are flagellin (TLR5), double-stranded RNA (dsRNA) (TLR3), and lipopolysaccharide (LPS) from gram-negative bacteria (TLR4) (Akira et al., 2006). These PAMPs are recognised by the extracellular leucine-rich repeat (LRR) domain of TLRs, which varies among the sensors. Additionally, TLRs possess a transmembrane domain and a cytoplasmic Toll/IL-1 receptor (TIR) domain. Sensing of a pathogen initiates the binding of the cytoplasmic TIR domain to signal transduction adaptors. Most TLRs utilise the adaptor myeloid differentiation primary response protein 88 (MyD88) adaptor, while TLR3 employs the TIR domain-containing adaptor-inducing IFN β (TRIF) adaptor. Recruiting these adaptors initiates a signalling cascade that activates several transcription factors, including the nuclear factor kappa light-chain enhancer of activated B cells (NF- κ B), the activator protein-1 (AP-1), and, in some cases, interferon regulatory factors (IRFs). Finally, TLR signalling leads to a pro-inflammatory response in cells (Nie et al., 2018). TLRs are

expressed in professional immune and most non-hematopoietic cells, including epithelial cells. However, TLRs have evolved primarily to recognise extracellular microbial components, allowing some pathogens to evade TLR detection. Consequently, additional pattern recognition receptors, especially cytosolic sensors, including RLRs and NLRs, operate concurrently and are widely expressed in most cell types (Cavlar et al., 2012).

1.2.2 RIG-I-like receptors (RLRs)

The RIG-I-like receptors (RLRs) are a family of cytoplasmic pattern recognition receptors that are crucial sensors for viral infection by recognising intracellular non-self RNA (Takeuchi and Akira, 2010). This family comprises of retinoic-acid inducible gene (RIG-I, encoded by *DDX58*), melanoma differentiation-associated gene 5 (MDA5, encoded by *IFIH1*), and laboratory of genetics and physiology 2 (LGP2). They consist of a central DEAD-box helicase/ATPase domain, characterised by the conserved Asp-Glu-Ala-Asp (DEAD) motif, and a C-terminal regulatory domain involved in viral RNA detection. RIG-I and MDA5 additionally contain two N-terminal caspase recruitment domains (CARDs), essential for initiating downstream signalling (Yoneyama and Fujita, 2008). Knockout studies in mice have shown that MDA5 is vital for the detection of picornavirus infections, such as encephalomyocarditis virus (EMCV), while RIG-I detects a wide range of viral infections, including influenza A, Japanese encephalitis and paramyxovirus infections (Gitlin et al., 2006; Kato et al., 2006). RIG-I recognises relatively short double-stranded RNA (dsRNA) (< 1 kb) and has been shown to detect viral RNA harbouring a 5'-triphosphate end, which can be found in negative ssRNA viruses and *in vitro*-transcribed RNA (Hornung et al., 2006; Pichlmair et al., 2006). Subsequent studies showed that RNA recognition by RIG-I requires base-pairing of the 5'-triphosphate RNA to a complementary RNA strand (Schlee et al., 2009; Schmidt et al., 2009) and that RIG-I also recognises 5'-diphosphate RNA (Goubau et al., 2014). In eukaryotes, the detection of 5'-triphosphate RNA is prevented by posttranscriptional RNA processing by either capping the 5'-triphosphate end or nucleoside modification of RNA (Hornung et al., 2006). MDA5 recognises dsRNA that is longer than 2 kb and the synthetic RNA ligand Poly(I:C) (Kato et al., 2008).

Endogenous dsRNA sensing by MDA-5 is prevented by adenosine deaminase acting on RNA 1 (ADAR1) through adenosine-to-inosine RNA editing (Liddicoat et al., 2015). LGP2 lacks the signalling CARD domain and was initially described as a negative regulator of MDA5-mediated and RIG-I-mediated virus recognition (Rothenfusser *et al.*, 2005; Saito et al., 2007; Yoneyama et al., 2005). However, subsequent studies in mice lacking LGP2 showed that LGP2 is required for antiviral responses mediated by RIG-I and MDA5, and it is assumed that LGP2 plays a supporting role in the assembly of MDA5 on dsRNA (Pippig et al., 2009; Satoh et al., 2010). Upon activation by RNA, RIG-I and MDA-5 recruit the signalling adaptor protein mitochondrial antiviral-signalling protein (MAVS). MAVS binds through homotypic CARD-CARD interactions and activates TANK-binding kinase 1 (TBK1) and I κ B kinase- ϵ (IKK ϵ). Subsequently, these kinases phosphorylate and, thus, recruit the two signalling mediators, the interferon regulatory factor 3 (IRF3) and 7 (IRF7). Phosphorylation of IRF3 and IRF7 and the activation of the NF- κ B signalling pathway leads to the expression of type-I interferons, initiating an antiviral response (Rehwinkel and Gack, 2020).

1.2.3 C-type lectin receptors (CLRs)

Another group of PRRs expressed in most cell types are the C-type lectin receptors (CLRs), which can be either soluble or membrane-bound. These receptors feature one or more extracellular carbohydrate-recognition domains (CRDs), enabling them to recognise carbohydrates present in microorganisms. This recognition leads to internalisation and degradation of the pathogen, followed by antigen presentation. Most of these CLRs function in a calcium-dependent manner to induce innate and adaptive immune responses. (Geijtenbeek and Gringhuis, 2009) Examples include dectin-1 and dectin-2, recognising fungal cell wall components such as β -glucan (Robinson et al., 2009; Taylor et al., 2007) and MINCLE (macrophage inducible Ca²⁺-dependent lectin receptor), which sense fungal infections such as *Candida albicans* and *Malassezia* infection (Yamasaki et al., 2009). Pathogen recognition by CLRs results in the production of cytokines, which in some cases has been associated with T-cell differentiation (Geijtenbeek and Gringhuis, 2009).

1.2.4 Cytosolic DNA sensors

Another important part of pattern recognition in cells is the cytosolic DNA recognition by different sensors. Initially, dsDNA sensing was attributed to Toll-like receptor 9 (TLR9), which recognises unmethylated CpG DNA (Hemmi et al., 2000). However, double-stranded B-form dsDNA was subsequently shown to trigger an antiviral response independently of Toll-like receptors (Ishii et al., 2006). Later, Z-DNA binding protein 1 (ZBP1), also known as the DNA-dependent activator of IFN regulatory factors (DAI), was implicated as the cytosolic DNA sensor triggering antiviral interferon- β (IFN- β) production (Takaoka et al., 2007). Subsequent studies have shown that DAI is redundant for innate immune responses (Ishii et al., 2008). However, DAI has been implicated in mediating virus-induced necrosis (Upton et al., 2012). Later, additional intracellular DNA sensors were discovered. These are PYHIN proteins characterised by an N-terminal pyrin domain and C-terminal DNA-binding HIN domain(s), named the PYHIN family of receptors (Hornung et al., 2009; Schattgen and Fitzgerald, 2011). They are only found in mammals and consist of five members in the human genome, including absent in melanoma 2 (AIM2) and interferon gamma-inducible protein 16 (IFI16) (Connolly and Bowie, 2014; Jin et al., 2012). AIM2 recognises cytosolic DNA and mediates caspase-1 inflammasome activation, leading to pyroptosis, mature interleukin IL-1 β and IL-18 secretion (Bürckstümmer et al., 2009; Fernandes-Alnemri et al., 2009; Hornung et al., 2009). IFI16 was shown to limit the transcription of diverse DNA viruses in the nucleus (Hotter et al., 2019). In addition, IFI16 was suggested to result in IFN- β induction by recruiting the adaptor stimulator of interferon genes (STING) after DNA stimulation (Unterholzner et al., 2010). In 2013, the key cytosolic DNA sensor that activates the STING signalling pathway was identified as the nucleotidyltransferase cyclic GMP-AMP synthase (cGAS) (Sun et al., 2013; Wu et al., 2013). Typically, cGAS is present in an inactive state in the cell, but upon binding to DNA, it undergoes a conformational change and becomes active. This activation results in the dimerisation of cGAS and the synthesis of the second messenger cyclic GMP-AMP (cGAMP) from ATP and GTP (Ablasser et al., 2013; Diner et al., 2013; Gao et al., 2013; Zhang et al., 2013). Upon binding of cGAMP, STING is activated and translocates to the Golgi, where it activates the serine/threonine kinase TBK1, which then phosphorylates itself, STING, and the

transcription factor IRF3. Lastly, phosphorylated IRF3 dimerises and translocates into the nucleus. This results in the production of type I interferons, such as IFN- β , and eventually triggers the expression of interferon-stimulated genes (ISGs) (Decout et al., 2021).

1.2.5 NOD-like receptors (NLRs)

The last and largest group of PRRs are the NOD-like receptors (NLRs), which play key roles in the innate immune response, including the modulation of signalling pathways, induction of various cell death processes, and mediation of adaptive immune responses (Chou et al., 2023). NOD-like receptors are highly conserved through evolution and were first identified in plants as nucleotide-binding sequence LRR (NBS-LRR) proteins belonging to the plant disease resistance (R) proteins (Baker et al., 1997). NBS-LRR proteins consist of a nucleotide-binding domain (NBD), an LRR domain, and variable N- and C-terminal domains. They are a crucial defence mechanism against various pathogens, such as bacteria, viruses, and fungi (McHale et al., 2006). In 2000, a large family of 22 human NBD-LRRs was identified based on the similarity of NBD and LRR domains to NBS-LRR proteins (Harton et al., 2002; Harton and Ting, 2000). Their founding member class II major histocompatibility complex (MHC) transactivator (CIITA) was identified in 1993 as a transactivator of MHC class II gene expression in hereditary MHC class II deficiency (Steimle et al., 1993). NLR family proteins are defined by a common nucleotide-binding and oligomerisation domain (NOD), also known as the NACHT domain (domain present in NAIP, CIITA, HET-E and TP-1) defined by Koonin and Aravind (Koonin and Aravind, 2000). The NACHT domain belongs to a subfamily of the AAA+ ATPases (ATPases associated with various cellular activities) called signal transduction ATPases with numerous domains (STAND) and consists of an NBD, two helical domains (HD1 and HD2) and a winged helix domain (WHD) (Hanson and Whiteheart, 2005). It contains Walker A and Walker B motifs, which are important for ATP binding and ATP hydrolysis. The precise mechanism of ATP's involvement in NLR activation remains unclear. However, ATP binding typically promotes the oligomerisation of NLRs, which is important for their activation (Danot et al., 2009). Additionally, NLRs possess C-terminal leucine-rich repeats (LRRs)

that recognise ligands. NLRs can be divided into different subfamilies based on their different N-terminal effector domains, including the acidic transactivation domain of CIITA (NLRA subfamily), the baculovirus inhibitor of apoptosis repeat (BIR) domain (NLRB subfamily), the caspase recruitment domain (CARD) domain (NLRC subfamily) and the pyrin (PYD) domain (NLRP subfamily). The human neuronal apoptosis inhibitory protein (NAIP), an example of the NLRB subfamily, was demonstrated to inhibit apoptosis (Listen et al., 1996). For the NLRC subfamily, NOD1 and NOD2 encoded by the *CARD4* and *CARD15* genes represent the earliest and best-characterised signalling NLRs. Both receptors recognise processed peptidoglycan fragments from bacteria, thereby inducing NF- κ B activation (Bertin et al., 1999; Inohara et al., 1999; Ogura et al., 2001). NOD2 senses peptidoglycan through the minimal fragment muramyl dipeptide (MDP) (Girardin et al., 2003), which requires *N*-acetylglucosamine kinase (NAGK) for its immunostimulatory activity, as revealed by a forward genetic screen (Stafford et al., 2022). The NLRP family consists of 14 known members in humans (NLRP1-NLRP14) that are involved in inflammation (Tschopp et al., 2003). Among the NLRs, certain sensors can assemble into high molecular weight complexes called inflammasomes, which generally result in the release of the pro-inflammatory cytokines IL-1 β and IL-18.

1.3 Inflammasomes

IL-1 β was one of the first cytokines to be discovered in the late 1970s as a factor secreted by activated macrophages that had a potent effect on other immune cells through its role in fever induction and regulation of immune responses (Broz and Dixit, 2016; Dinarello et al., 1977; Gery and Handschumacher, 1974; March et al., 1985). IL-1 β is initially synthesised as a biologically inactive precursor (pro-IL-1 β), remaining inside the cell until it is processed into an active molecule. This processing is carried out by the IL-1 β converting enzyme (ICE) (Black et al., 1989; Cerretti et al., 1992; Thornberry et al., 1992), which was later recognised as a member of the caspase family of proteases and renamed caspase-1 (Alnemri et al., 1996; Walker et al., 1994; Wilson et al., 1994). Subsequently, it was identified

that the activation of caspase-1 is facilitated by interaction with an adaptor molecule called apoptosis-associated speck-like protein containing a CARD (ASC) (Srinivasula et al., 2002). While it was shown that three proteins belonging to the initially named PYPAF (PYRIN-containing APAF-1-like protein) family are interaction partners of ASC and induce NF- κ B and caspase-1-dependent cytokine processing when co-expressed (Grenier et al., 2002; Manji et al., 2002; Wang et al., 2002), Tschopp and colleagues showed in a cell-free system that the formation of a high molecular weight complex induces the maturation of the pro-inflammatory cytokine pro-IL-1 β to IL-1 β . This molecular platform was subsequently coined by Martinon, Burns and Tschopp the term 'inflammasome' (Martinon et al., 2002).

1.3.1 Inflammasome signalling

Inflammasomes usually consist of a modular sensor protein, the adapter protein ASC (also known as PYCARD), and the effector cysteine protease caspase-1. The modular sensor proteins are present in the cells in an auto-inhibited state and are activated by diverse triggers, including PAMPs and DAMPs (Figure 1). Upon engagement, inflammasome sensors transform into an active open conformation, in which most inflammasome sensors recruit the adaptor protein ASC. ASC acts as a molecular glue between the sensor protein and pro-caspase-1 by forming large filaments through homotypic interactions. Its N-terminal PYD domain binds to the PYD domain of the sensor protein, and its C-terminal CARD domain interacts with the CARD domain of pro-caspase-1 (Lu et al., 2014) (Figure 1). These filaments establish a threshold-like signalling behaviour and serve as an activation platform for caspase-1 by proximity-induced autoproteolysis (Boucher et al., 2018; L. Zhang et al., 2015). Active caspase-1 then triggers the inflammatory response via proteolytic cleavage of the biologically inactive precursors of two of its most prominent substrates: the pro-inflammatory cytokines IL-1 β and IL-18 (Broz and Dixit, 2016) (Figure 1). In addition, activation of caspase-1 has been shown to induce a form of programmed cell death known as pyroptosis. Pyroptosis is characterised by the swelling of cells due to water influx, resulting in the rupture of cell membranes and the release of cytoplasmic contents, such as DAMPs (Bergsbaken et al., 2009; Jorgensen and Miao, 2015). However, how caspase-1

induces pyroptosis remained unclear until the mid-2000s, when gasdermin-D (GSDMD) was shown to be a substrate of inflammatory caspases, including caspase-1 (Shi et al., 2015). Cleavage of GSDMD results in an N-terminal fragment (GSDMD^{NT}) that inserts into the membrane, creating pores in the membrane, thereby mediating water influx and the release of IL-1 β and IL-18 (Mulvihill et al., 2018) (Figure 1). Lately, the cell surface protein ninjurin-1 (NINJ1) has been linked to inflammasome-driven pyroptosis by forming large pores into the plasma membrane (Degen et al., 2023; Kayagaki et al., 2021; Wang and Shao, 2021).

Pyroptosis is generally initiated by the activation of inflammatory caspases, including caspase-1, caspase-4 (caspase-11 in mice), and caspase-5. As described, caspase-1 is activated within the canonical inflammasome pathway. The related caspase-4 and caspase-5 are activated within the non-canonical pathway, which is triggered by the sensing of intracellular LPS from gram-negative bacteria independently of TLR4, following subsequent GSDMD cleavage (Kayagaki et al., 2015; Shi et al., 2014). While inflammatory caspases and GSDMD are key mediators of pyroptosis, pyroptosis can also be mediated by other gasdermins and apoptotic proteases under specific conditions. As such, studies revealed that the apoptotic initiator caspase-8 directly cleaves GSDMD to trigger pyroptosis during *Yersinia* infection (Demarco et al., 2020; Orning et al., 2018; Sarhan et al., 2018). Additionally, although other members of the gasdermin family are not cleaved by caspase-1 and caspase-11, some gasdermins possess other protease cleavage sites. In fact, the GSDMD homologue GSDME (also known as DFNA5) has been observed to be cleaved by the apoptotic caspase-3, proposing a switch from apoptosis to pyroptosis mediated by GSDME (Rogers et al., 2017; Wang et al., 2017).

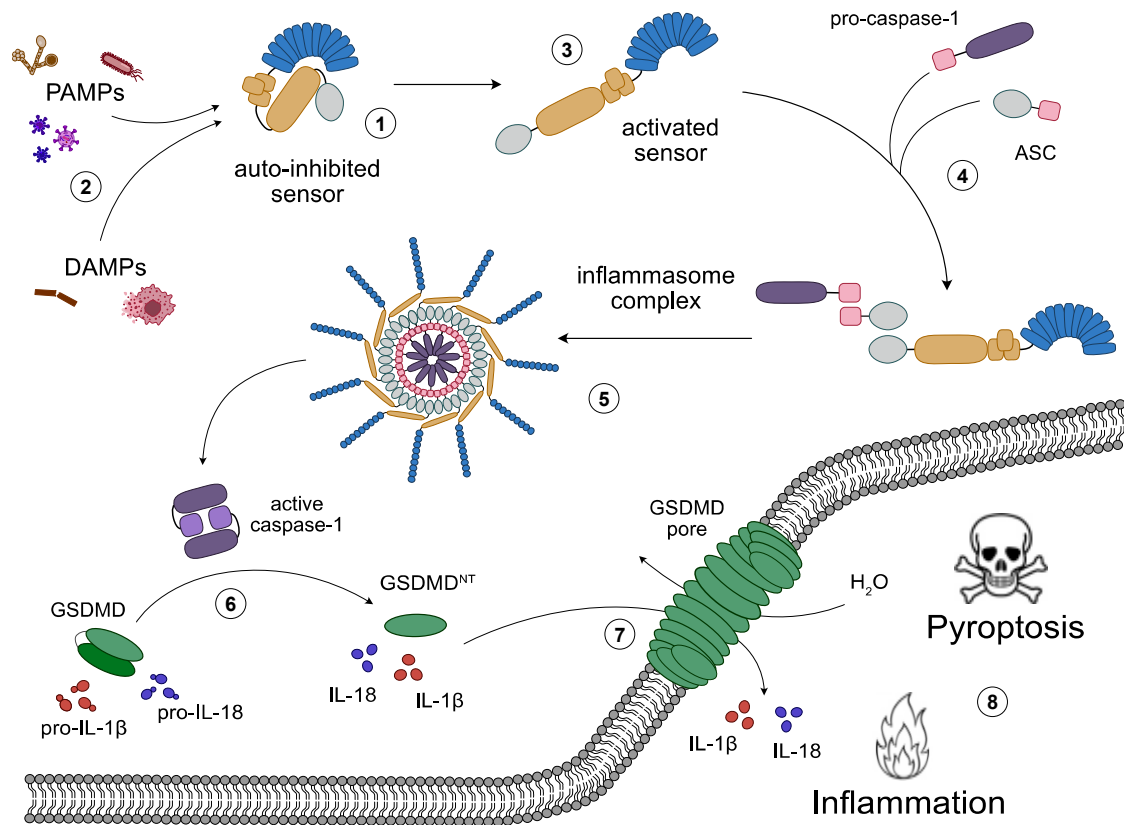


Figure 1: Inflammasome signalling pathway. (1) Inflammasome sensors are present in the cell in an autoinhibited state. (2) Upon recognition of pathogen- or damage-associated molecular patterns (PAMPs/DAMPs), inflammasome sensors get activated and transform into an open conformation (3). This activation leads to the recruitment of the effector caspase pro-caspase-1 and the adaptor molecule ASC (4), resulting in an inflammasome complex (5). Active caspase-1 cleaves the pro-inflammatory cytokines pro-IL-1β and pro-IL-18, as well as gasdermin-D (GSDMD) (6), leading to pore formation by the N-terminal part of GSDMD (GSDMD^{NT}) (7). Pore formation facilitates the release of mature IL-1β and IL-18 into the surrounding environment, accompanied by water influx into the cell, resulting in inflammation and pyroptosis (8).

Upon ligand binding and activation of the sensor protein, some inflammasome sensors assemble into a wheel-shaped structure (Figure 2). While wheel-shaped structures were recently presented for the NLRP3 inflammasome using cryo-electron microscopy (cryo-EM) (Hochheiser et al., 2022; Xiao et al., 2023), Hu et al. and Zhang et al. provided the first direct visualisation of this process by unravelling the structure of the NAIP–NLRC4 complex (Hu et al., 2015; L. Zhang et al., 2015). Once activated by a bacterial ligand, such as PrgJ or flagellin, which activate NAIP2 and NAIP5, respectively, a singular activated NAIP protein is sufficient to initiate NLRC4 oligomerisation via binding to an NLRC4 protein. After subsequent conformational changes, NLRC4 recruits in its open conformation additional NLRC4 proteins, which oligomerise, forming a wheel-like disc (Figure 2).

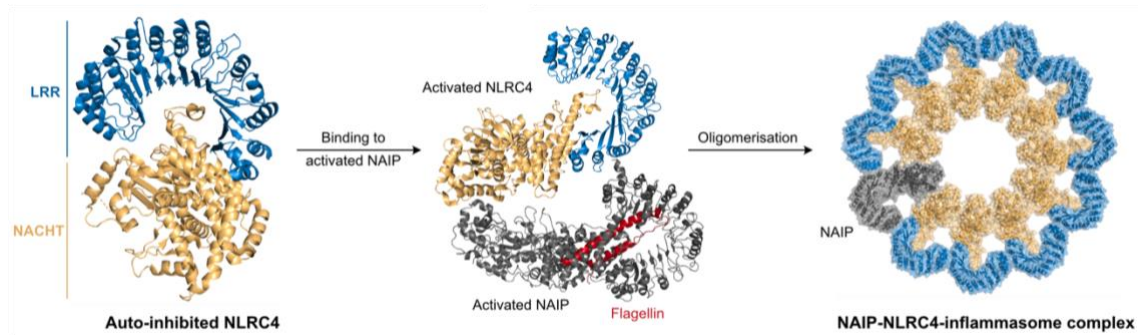


Figure 2: Inflammasome assembly of the NLRC4 inflammasome. Overview of NAIP-mediated NLRC4 oligomerisation into an NAIP-NLRC4-inflammasome complex. First, autoinhibited NLRC4 (PDB ID: 4KXF) binds to one activated NAIP (here NAIP5 with its ligand flagellin, PDB ID: 5YUD), leading to a conformational change of NLRC4 into an open conformation (PDB ID: 8FW2). In its open conformation, NLRC4 recruits additional NLRC4 proteins, forming an NAIP-NLRC4-inflammasome complex by oligomerisation (PDB ID: 3JBL).

1.3.2 Inflammasome sensors

To date, various sensor proteins that form inflammasomes upon activation have been identified. These proteins belong to the NLR family, with the exception of a few members, such as CARD8, AIM2, and PYRIN. While some inflammasome sensors directly sense PAMPs and DAMPs, resembling pattern-triggered immunity (PTI), others are activated indirectly by sensing changes in the cellular environment that occur after pathogen invasion, resembling effector-triggered immunity (ETI). Inflammasome sensors acting as classical PRRs include AIM2, NLRC4, NLRP1 and possibly NLRP6 and NLRP12. On the other hand, NLRP3 is typically activated not through direct PAMP recognition but indirectly in response to a wide range of stimuli that induce danger or stress signals in cells. Additional examples of inflammasome sensors indirectly sensing the presence of pathogens include Pyrin, NLRP1 and CARD8. An overview of selected inflammasome sensors and their distinct activators is shown in Figure 3, and each depicted inflammasome sensor is described in more detail in the following paragraphs.

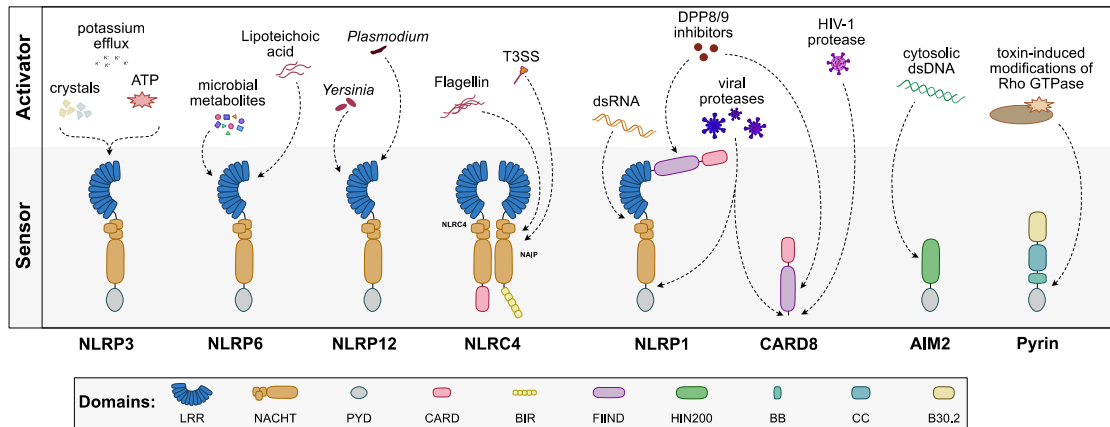


Figure 3: Schematic overview of human inflammasome sensors and their ligands. Domain representation of inflammasome sensors (middle panel) and their respective activators (top panel). While some sensors act as classical PRRs that detect PAMPs directly (NLRP4, AIM2, NLRP1, and possibly the less studied NLRP6 and NLRP12), inflammasome sensors can be activated indirectly via pathogenic effectors (NLRP3, Pypin, NLRP1, and CARD8).

NLRP3 inflammasome

NLRP3, known as NALP3 and cryopyrin, is the best-studied inflammasome sensor, consisting of a PYD, NACHT domain, and leucine-rich repeats. NLRP3 recognises various microbial and non-microbial activators ranging from pathogenic bacteria, such as *Staphylococcus aureus*, to viral and fungal pathogens, such as *Influenza A virus* and *Candida albicans*, respectively (Bauernfeind and Hornung, 2013). Various NLRP3 stimuli have been shown to result in K^+ efflux from cells and the dispersion of the trans-Golgi network (TGN), which in turn leads to the recruitment and activation of NLRP3 (Chen and Chen, 2018). As such, NLRP3 senses pore-forming toxins and bacterial ionophoric agents, such as nigericin, and endogenous DAMPs, including extracellular ATP (Mariathasan et al., 2006), uric acid crystals (Martinon et al., 2006), and environmental products, such as silica crystals (Hornung et al., 2008). The assembly of the fully functional NLRP3 inflammasome requires two steps: priming and activation. Priming is facilitated by TLRs, leading to NF- κ B activation and increased cellular expression of NLRP3, caspase-1 and pro-IL-1 β . In the activation step, NLRP3 senses a ligand and oligomerises, providing a scaffold for ASC filament formation through the interaction of the two PYD domains (Chou et al., 2023). Several groups identified the NIMA-related kinase 7 (NEK7) as an essential component of the NLRP3 inflammasome complex

(He et al., 2016; Schmid-Burgk et al., 2016; Shi et al., 2016). Although NEK7 had previously been reported to be indispensable for murine NLRP3 activation, it was later shown that NEK7 is redundant for human NLRP3 inflammasome formation by the inhibitor of nuclear factor kappa-B kinase subunit beta (IKK β)-mediated recruitment of NLRP3 to the *trans*-Golgi network (Schmacke et al., 2022).

NLRP6 inflammasome

NLRP6 comprises three domains, PYD, NACHT and LRR, and is mainly expressed in the intestine, lung, and liver. NLRP6 senses microbial metabolites, such as taurine (Levy et al., 2015), viral RNA (Wang et al., 2015), and bacterial lipoteichoic acid. Lipoteichoic acid derived from Gram-positive bacteria, such as *Listeria monocytogenes*, induces the formation of the NLRP6 inflammasome involving a rather unusual cascade that involves caspase-1 and the non-canonical inflammasome caspase-11 (Hara et al., 2018). Apart from its function in assembling inflammasomes, NLRP6 also plays an inflammasome-independent role in inhibiting inflammatory responses and signals, such as NF- κ B signalling, depending on physiological contexts (Zheng et al., 2021).

NLRP12 inflammasome

NLRP12 harbours an N-terminal PYD, a central NACHT and a C-terminal LRR domain and plays a diverse role in innate immunity. NLRP12 has been suggested to be an inflammasome sensor during *Yersinia* and *Plasmodium* infection by activating caspase-1 and pro-inflammatory cytokine release (Ataide et al., 2014; Vladimer et al., 2012). While the ligand for NLRP12 inflammasome activation remains unidentified, inflammasome activation after *Yersinia* infection was shown to be dependent on the virulence-associated type-III secretion system (T3SS) (Vladimer et al., 2012). Additionally, both infections showed a requirement for NLRP3 for the host defence. A recent study suggested that NLRP12 is involved in inflammation by forming a PANoptosome consisting of NLRP12, ASC, Caspase-8 and RIPK3. In this case, PANoptosis is triggered by heme, a DAMP released after red blood cell damage during infection, in combination with PAMPs (Sundaram et al., 2023). Besides its involvement in inflammasome formation, NLRP12 was shown to act as a negative regulator of inflammation (Tuladhar and Kanneganti, 2020).

NLRC4 inflammasome

NLRC4, in contrast to the described inflammasome sensors above, harbours an N-terminal CARD domain instead of the PYD domain. Detection of ligands involves direct upstream receptors called NLR family apoptosis inhibitory proteins (NAIPs) that recognise diverse pathogenic processes in mammals. Upon binding to ligands, NAIPs interact with NLRC4 and initiate NAIP/NLRC4 inflammasome complex assembly with one NAIP and several NLRC4 proteins. In contrast to mice expressing multiple NAIP paralogs, humans express only one functional NAIP (Tenthorey et al., 2014). Human NAIP senses virulence-associated bacterial proteins, such as flagellin and T3SS structural proteins. During *Salmonella* infection, full-length NAIP senses cytosolic flagellin, leading to NAIP/NLRC4 inflammasome assembly and subsequent cell death and IL-1 β secretion (Harton et al., 2002). The NAIP/NLRC4 inflammasome also recognises the needle subunit of the bacterial T3SS during *Chromobacterium violaceum* infection (Zhao and Shao, 2015).

AIM2 inflammasome

AIM2 is a member of the PYHIN protein family, structurally defined by an N-terminal PYD domain followed by one or two C-terminal hematopoietic interferon-inducible nuclear (HIN) domain(s). AIM2 is the only human member with true orthology among these species and harbours one HIN domain (Connolly and Bowie, 2014). This domain is important for binding to dsDNA in a sequence-independent manner (Jin et al., 2012). Unlike the other PYHIN proteins, AIM2 is predominantly expressed in the cytosol and recognises microbial DNA from intracellular pathogens. In addition, AIM2 can detect endogenous DNA in the cytosol following cell damage (Boss and Kirchhoff, 2020). In the absence of DNA, AIM2 exists in an autoinhibited state through the interaction of its HIN and PYD domains. Upon activation, multiple AIM2 molecules bind to dsDNA and expose their PYD domains, which in turn interact with ASC to form an inflammasome (Jin et al., 2012).

Pyrin inflammasome

Pyrin is a distinct inflammasome-forming receptor that only shares the PYD domain with other well-known inflammasome sensors described above. In addition to the

pyrin domain, it harbours a zinc finger domain (B-box), a coiled-coil domain, and a C-terminal B30.2 domain (Heilig and Broz, 2018). The pyrin inflammasome detects the inactivation of Rho guanosine triphosphatase (Rho GTPase) induced by bacterial toxins such as *Clostridium difficile* toxin B and *Clostridium botulinum* C3 toxin (Xu et al., 2014). This process shares similarities with the "guard" mechanism observed in plants.

1.4 FIIND-containing inflammasome sensors

Unique among inflammasome sensors, NLRP1 and CARD8 are the only FIIND-containing inflammasome sensors. Although NLRP1 was the first inflammasome identified in a landmark study by Martinon, Burns and Tschopp (Martinon et al., 2002), its function in host defence and the molecular activation mechanisms remained enigmatic for nearly two decades. This could be due to several factors, including its significant deviation in structure compared to other inflammasome sensors, its structural difference between humans and rodents, and its unusual expression in epithelial cells. Interestingly, the related inflammasome sensor CARD8 was first identified in 2018, which shares structural similarities and some common activation mechanisms (Johnson et al., 2018).

FIIND-containing inflammasome sensors contain an unusual C-terminal extension, consisting of a unique function-to-find (FIIND) domain and a CARD domain (Taabazuing et al., 2020). NLRP1 additionally contains the characteristic N-terminal NLRP domains, including PYD, NACHT, and leucine-rich repeats, which makes it the only NLR that contains both PYD and a CARD domain (Figure 4A). Unlike NLRP1, CARD8 lacks these structured N-terminal domains and only consists of a FIIND and CARD domain (Figure 4A). A distinct feature of the FIIND domain is that it undergoes post-translational processing called autoproteolysis under *steady-state* conditions, resulting in a break in the NLRP1/CARD8 polypeptide chain. The resulting fragments ZU5 (found in ZO-1 (zona occludens 1) and UNC5 (uncoordinated protein 5)) and UPA (conserved in UNC5, PIDD and Ankyrins) subdomains remain non-covalently associated with one another (Figure 4A) (Hollingsworth et al., 2021). Activation of NLRP1/CARD8 ultimately results in

the release of the C-terminal UPA-CARD fragment, enabling the formation of an inflammasome seed of CARD helical filaments and triggering a signalling cascade leading to inflammation and pyroptosis (Figure 4B). Compared to the NLRP1 inflammasome consisting of the adaptor ASC and caspase-1, the CARD8 inflammasome assembles independently of ASC (Robert Hollingsworth et al., 2021). A crystal structure of the auto-inhibited FIIND domain of rodent NLRP1 displayed the cleaved but still non-covalently associated ZU5 and UPA subdomains (Huang et al., 2021). It also showed that the first β -strand of the NLRP1 UPA subdomain inserts into the ZU5 fold, thereby establishing an auto-inhibited conformation (PDB ID: 7CRV) (Figure 4C). The FIIND domain shares structural similarity with UNC5b, a protein required during embryonic development, but interestingly does not undergo autoproteolysis (D’Oswaldo et al., 2011; Finger et al., 2012). However, autoproteolytic processing has been reported in other eukaryotic ZU5/UPA-containing proteins, such as the related p53-inducible protein with a death domain (PIDD), which acts as a molecular switch in programmed cell death (Wang et al., 2012, 2009).

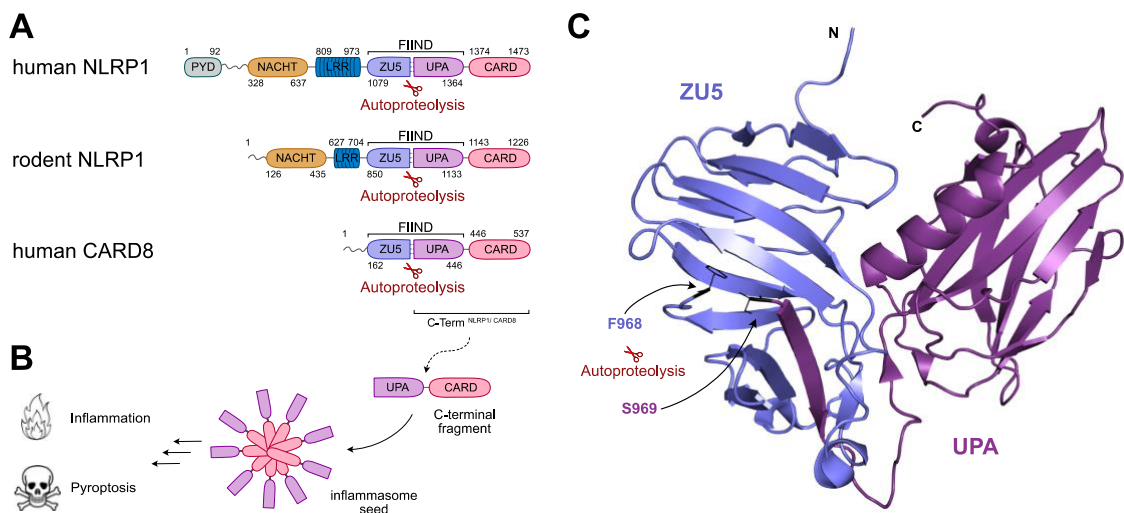


Figure 4: FIIND-containing inflammasome sensors. (A) Domain organisation of FIIND-containing inflammasome sensors with highlighted C-terminal domains. **(B)** Schematic of the inflammasome assembly of FIIND-containing inflammasome sensors. Released C-terminal UPA-CARD fragments form an inflammasome seed, resulting in inflammasome activation, which triggers inflammation and pyroptosis. **(C)** Crystal structure of the auto-inhibited FIIND domain of rodent NLRP1 in cartoon representation (PDB ID: 7CRV), displaying autocleavage of ZU5 (F968) and UPA (S969) labelled in black stick representation.

1.4.1 NLRP1

In 2007, the first study suggested that NLRP1 is activated by the bacterial cell wall component muramyl dipeptide (MDP) in the monocytic cell line THP-1 (Faustin et al., 2007), which loss-of-function data could not validate. Since it is known that MDP primes the NLRP3 inflammasome in THP-1 cells, these data could be attributed to NLRP3 rather than NLRP1 (Martinon et al., 2004). In the same year, more indicative studies showed UV-irradiation-induced IL-1 β secretion and NLRP1 expression in keratinocytes, the predominant cell type in the skin (Feldmeyer et al., 2007; Watanabe et al., 2007). In subsequent studies, NLRP1 was established as the key inflammasome sensor in human keratinocytes using CRISPR/Cas9, essential for sensing UV-B irradiation (Fenini et al., 2018; Zhong et al., 2016).

Differences between species

Throughout the years, most insights into NLRP1 biology have been derived from mouse models. However, the significant divergence between the biology of humans and mice is already visible when looking at the gene loci of NLRP1. While human NLRP1 is encoded by a single gene, up to seven *NLRP1* paralogues have been identified in mice by sequencing inbred mouse strains, with three to five of these paralogues being encoded depending on the individual mouse strain (Lilue et al., 2018). Additionally, the *NLRP1* alleles exhibit a high degree of polymorphism, most prominent in *NLRP1b* alleles (Sastalla et al., 2013). The majority of studies conducted on murine NLRP1 biology have focused on the NLRP1B protein, which is encoded by *NLRP1b*. *NLRP1a* has been shown to induce pyroptosis in haematopoietic progenitor cells and is also involved in inflammasome activation (Masters et al., 2012), whereas *NLRP1c* is missing the CARD domain and is considered a pseudogene (Sastalla et al., 2013). In line with this, NLRP1 shows the lowest conservation between humans and rodents of all known inflammasome-forming NLRs, with 50 % for mouse NLRP1B and 53 % for rat NLRP1A (Figure 5B). Comparing the canonical full-length protein sequences of human and rodent NLRP1 showed a higher relationship within rodents (Figure 5C).

Although mouse and human NLRP1 share structural similarities, including the NACHT, LRR, FIIND, and CARD domains, mice and rats lack the N-terminal PYD

domain (Figure 5A). In comparison to other NLR sensors using their PYD domain for ligand sensing, the PYD domain of human NLRP1 is proposed to function in an autoinhibitory manner (Chavarría-Smith et al., 2016; Zhong et al., 2016). Additionally, while human NLRP1 relies on the adaptor ASC for inflammasome activation, murine NLRP1B can either use ASC or directly activate caspase-1 (Broz et al., 2010; Vasconcelos et al., 2019). A further distinction between human and rodent NLRP1 homologues is their expression and functionality in different tissues. Human NLRP1 is predominantly expressed in epithelial barrier tissues, including keratinocytes (Zhong et al., 2016), bronchial epithelial cells (Robinson et al., 2020), and corneal epithelial cells (Griswold et al., 2022), whereas rodent NLRP1 is expressed in cells of the myeloid lineage. Notably, the linker region is rapidly evolving in both rodents and primates, indicating a strong evolutionary pressure on NLRP1 (Chavarría-Smith et al., 2016). In contrast to NLRP1, no CARD8 homologue exists in rodents (Bauernfried and Hornung, 2021).

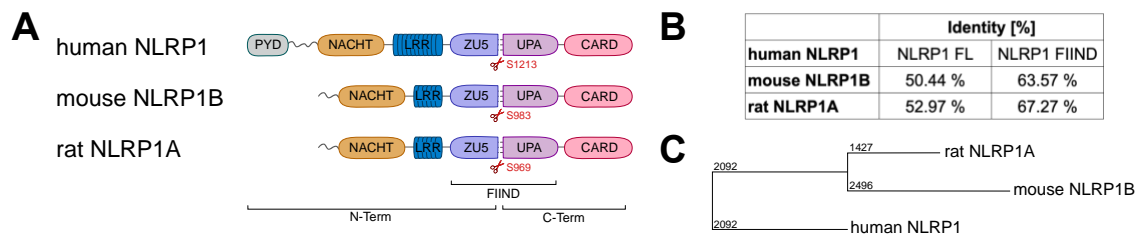


Figure 5: Comparison of human NLRP1 with rodent NLRP1. (A) Domain organisation of human NLRP1, mouse NLRP1B, and rat NLRP1A. Auto-proteolysis is specified in red. (B) Percentage identity of human NLRP1 compared to mouse NLRP1B and rat NLRP1A for the full-length protein sequence and the FIIND domain analysed using BLASTp. (C) Protein distance tree displaying the evolutionary relationship.

1.4.2 CARD8

Prior to its identification as the NLRP1-related inflammasome sensor activated by VbP, CARD8 was proposed to function in the inhibition of diverse proteins. As such, CARD8 was identified as a caspase-9 inhibiting factor upregulated in some cancer types and was, therefore, initially named the tumour-upregulated CARD-containing antagonist of caspase-9 (TUCAN) (Pathan et al., 2001). However, this could not be confirmed in other studies (Bouchier-Hayes et al., 2001; Razmara et al., 2002). CARD8 was later identified as an inflammasome-forming sensor, inducing

inflammasome activation in bone marrow-derived cells and human myeloid cancer cell lines (Ball et al., 2020; Johnson et al., 2020, 2018; Linder et al., 2020).

1.4.3 NLRP1 and CARD8 activation

Understanding the modes of activation for NLRP1 and the closely related CARD8 provides insights into their roles in innate immune regulation. While NLRP1 has been extensively studied, significantly fewer studies have been conducted on CARD8. To date, the most proximal mode of NLRP1 inflammasome activation across both mice and humans and human CARD8 inflammasome activation is the DPP8/9 inhibition (Okondo et al., 2018).

DPP8/9 inhibition: a common denominator for FIIND-containing inflammasome sensors

In 2018, Okondo et al. surprisingly showed that the pharmacological inhibitor Val-boroPro (VbP) activates the NLRP1B inflammasome (Okondo et al., 2018). VbP, also known as PT-100 or Talabostat, was initially found to have potent antitumour effects in mice (Adams et al., 2004) and was later demonstrated as a potent inhibitor of dipeptidyl peptidases (DPPs), such as DPP8/9 (Bachovchin et al., 2014). DPPs are a group of proteolytic enzymes that cleave off dipeptides from the N-terminus of proteins and peptides. While initially puzzling, the notion of NLRP1 inflammasome activation through DPP inhibition gained clarity with an independent study demonstrating a direct interaction between NLRP1 and DPP9, which was found to restrain inflammasome activation (Zhong et al., 2018). This interaction occurs via the FIIND domain of NLRP1, which is not only found in human and mouse NLRP1 but is also present in human CARD8. Indeed, when VbP was at first proposed to induce caspase-1-dependent pyroptosis in monocytes and macrophages by inhibiting DPP8/9 via an unknown mechanism, it was revealed to be independent of ASC (Okondo et al., 2017). This indicated a PRR directly interacting with caspase-1, which was later identified as the first ASC-independent inflammasome-forming sensor CARD8 (Ball et al., 2020; Johnson et al., 2020, 2018). Thus, DPP8/9 restrains NLRP1 and CARD8 inflammasome activation by binding to their FIIND domains under steady-state conditions.

As DPP8/9 inhibitors were found to activate the NLRP1 and CARD8 inflammasomes, recent structural studies of DPP9 complexes with NLRP1 or CARD8 shed more light on the activation mechanism (Hollingsworth et al., 2021; Huang et al., 2021; Sharif et al., 2021). DPP9 forms a ternary complex with either NLRP1 or CARD8, consisting of one DPP9 protein binding to one auto-processed by still non-covalently bound full-length NLRP1 (NLRP1^A) and one C-terminal fragment (NLRP1^B) (Hollingsworth et al., 2021; Huang et al., 2021) (Figure 6A). The complex assembly of DPP9 with NLRP1 or DPP9 with CARD8 is mediated by three interaction sites (Figure 6B), which are all located on the same side of DPP9 but differ in some of the involved residues between NLRP1 and CARD8 (Hollingsworth et al., 2021; Sharif et al., 2021).

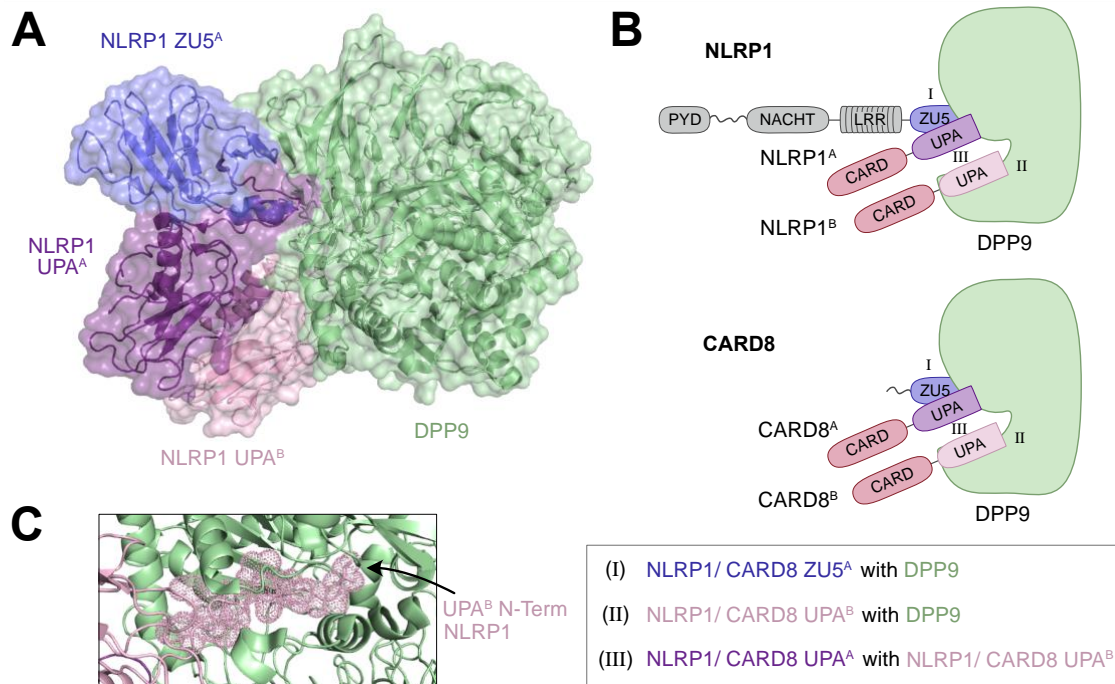


Figure 6: Interaction of DPP9 with FIIND-containing inflammasome sensors. (A) Cryo-EM map of the NLRP1-DPP9 complex (PDB ID: 6X6A) with transparent surface. **(B)** Model of the ternary NLRP1^A-NLRP1^B-DPP9 complex (top), the ternary CARD8^A-CARD8^B-DPP9 complex (middle) and the three interaction sites of NLRP1/ CARD8 with DPP9 (bottom). **(C)** Insertion of the N-terminal part of NLRP1 UPA^B into the DPP9 substrate tunnel (PDB ID: 6X6A).

The first interaction site, interface I (I), primarily involves the ZU5 of full-length NLRP1^A/ CARD8^A interacting with the WD40 β -propeller domain of DPP9. Even though UPA^A of the same FIIND shows only weak binding to DPP9, it is crucial for recruiting the C-terminal fragment of NLRP1^B/ CARD8^B, forming interface III (III). This interface is mediated by the interaction of both UPA (UPA^A and UPA^B)

subdomains. UPA^B also binds to the α/β -hydrolase domain of DPP9, forming interface II (II). Additionally, the N-terminal part of UPA^B is inserted as an extended polypeptide chain into the DPP9 substrate tunnel (Figure 6C). Mutations affecting either interface I or interface II led to the auto-activation of NLRP1 and subsequent inflammation and cell death, whereas mutations in interface III abolished the activity completely (Hollingsworth et al., 2021). In contrast to the NLRP1-DPP9 complex, where each monomer of the DPP9 dimer attaches to two NLRP1 copies (Hollingsworth et al., 2021), in the CARD8-DPP9 complex, one DPP9 monomer from the dimer binds to two CARD8 copies, in which the remaining DPP9 monomer does not interact with CARD (Sharif et al., 2021). This results in a 4:2 NLRP1:DPP9 stoichiometry for NLRP1 and a 2:2 CARD8:DPP9 stoichiometry for CARD8. Contrary to the ordered N-terminus of the UPA^B of NLRP1, the UPA^B of CARD8 is disordered and is not inserted into the DPP9 substrate tunnel (Sharif et al., 2021). Interestingly, the complex formation of NLRP1/CARD8 with DPP9 is independent of DPP9's enzymatic activity since the catalytically dead mutant of DPP9 is still able to bind NLRP1 and CARD8 (Andrew R. Griswold et al., 2019; Huang et al., 2021).

Inhibition of NLRP1 and CARD8 is critical for cells as it prevents auto-activation of the NLRP1/CARD8 inflammasome (Zhong et al., 2018). As described above, one freed C-terminal fragment of NLRP1/CARD8 is bound to DPP9 in addition to a full-length protein of NLRP1/ CARD8. VbP directly binds to the active site of DPP8 and 9, displacing the sequestered C-terminal fragment of NLRP1 and triggering inflammasome activation (Hollingsworth et al., 2021). In the context of CARD8, neither fragment of CARD8 is replaced by VbP, but the binding of the C-terminal part is inhibited (Sharif et al., 2021). Upon DPP8/9 inhibition by VbP, the C-terminal UPA-CARD fragments are released, leading to NLRP1/CARD8 inflammasome activation (Figure 7). Additionally, other structurally unrelated small molecule inhibitors that are selective for DPP8/9 inhibition trigger NLRP1/CARD8 inflammasome activation, such as 1G244 and the compound 8j (Okondo et al., 2018). Recently, the small molecule inhibitor CQ31 was shown to selectively cause CARD8 inflammasome activation by indirect inhibition of DPP8/9 (Rao et al., 2022). CQ31 inhibits specific M24B aminopeptidases, leading to the accumulation of Xaa-Pro-containing peptides that weakly bind to and inhibit DPP9 (Figure 7). This

results in the activation of the CARD8 inflammasome but not the NLRP1 inflammasome, likely due to NLRP1's interaction with the active site of DPP9. Notably, a recent study has shed some light on the downstream signalling of VbP-induced CARD8 inflammasome activation. It was shown that VbP-treated cells are susceptible to 20S proteasomal degradation of the whole N-terminus of CARD8, resulting in the release of a C-terminal fragment and subsequent inflammasome activation (Hsiao et al., 2022).

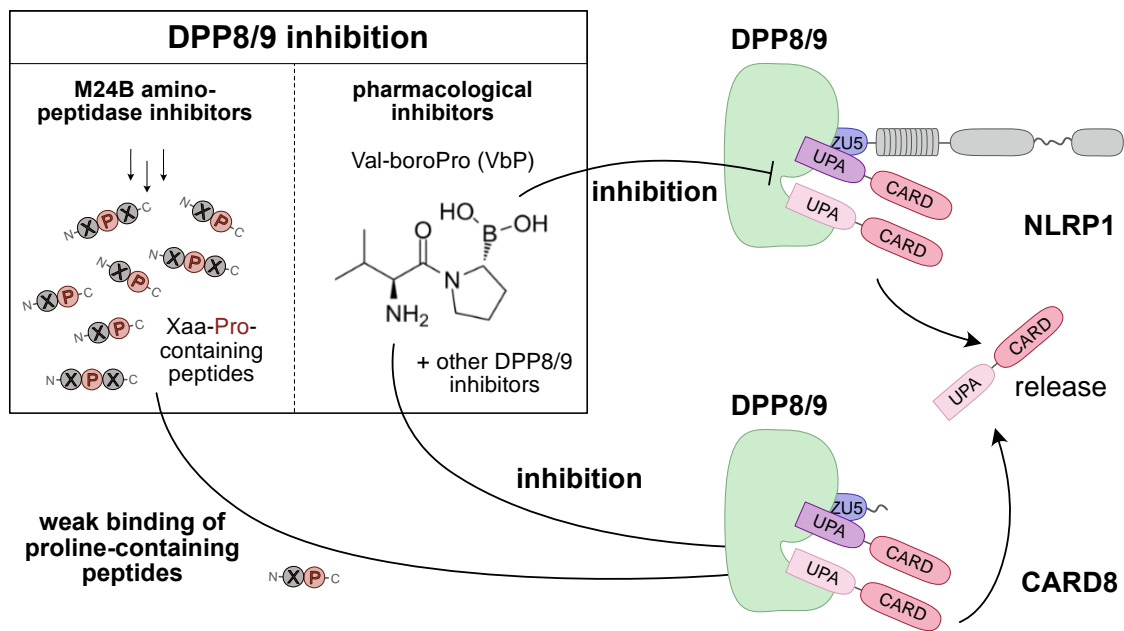


Figure 7: Human NLRP1 and CARD8 inflammasome activation by DPP8/9 inhibition. NLRP1 and CARD8 are activated by pharmacological inhibitors such as Val-boroPro (VbP), which inhibits the dipeptidyl dipeptidases DPP8 and 9 (DPP8/9). In addition, M24B aminopeptidase inhibitors lead to the accumulation of Xaa-Pro-containing peptides that weakly bind to DPP8/9 and inhibit CARD8.

Notably, no physiological condition that would inhibit these DPPs has yet been identified (Barry et al., 2023). However, it is conceivable that both NLRP1 and CARD8 could sense DPP8/9 inhibition as a result of the pathogenic activity of invaders, thereby acting as sensors for cellular perturbation.

Of note, in addition to VbP-mediated NLRP1/CARD8 inflammasome activation, several studies showed that *Toxoplasma gondii* activates human and rodent NLRP1 (Cirelli et al., 2014; Ewald et al., 2014; Gorfou et al., 2014), which has been best studied for rat NLRP1. Notably, the sensitivity to *T. gondii* is highly variable between different rat strains and has been shown to be similar to DPP9 sensitivity

(Cirelli et al., 2014; Gai et al., 2019). However, the exact mechanism by which NLRP1 is activated by *T. gondii* in rodents is still unknown and requires further studies.

NLRP1 activation by protease activity

During research on host-pathogen interactions, the virulence factor lethal toxin (LT), which contains a functional protease lethal factor (LF) and protective antigen (PA), was identified as the cause of severe pathologies in the host following *Bacillus anthracis* infection. In 1993, mice injected with sterile LT exhibited a severe inflammatory response, leading to systemic shock and death (Hanna et al., 1993). This inflammatory response was attributed to macrophages producing high amounts of IL-1 after *B. anthracis* infection (Hanna et al., 1993). Later, mouse NLRP1B was identified as the susceptibility factor for macrophage cell death after LT administration (Boyden and Dietrich, 2006; Moayeri et al., 2010). Interestingly, only the NLRP1B variant of certain mouse strains responds to LT (Hellmich et al., 2012; Newman et al., 2010). In 2012, it was shown that site-specific cleavage at the N-terminus of NLRP1B between lysine K44 and leucine L45 by the lethal factor (LF) protease induces inflammasome activation (Hellmich et al., 2012; Levinsohn et al., 2012) (Figure 8A). However, the exact molecular mechanism by which the lethal factor protease activates the NLRP1B inflammasome remained unclear.

Central model for NLRP1B activation by “functional degradation”

A study using a modified NLRP1B allele with an additional tobacco etch virus (TEV) cleavage site showed that cleavage alone is sufficient for inflammasome activation (Chavarría-Smith and Vance, 2013). Years later, two studies proposed a central model for NLRP1B activation, which they termed “functional degradation” or “N-end rule” pathway based on the degradation of NLRP1B (Chui et al., 2019; Sandstrom et al., 2019; Xu et al., 2019). The proteolytical cleavage at the N-terminus of NLRP1B creates a novel N-terminus (Figure 8). This neo-N-terminus undergoes ubiquitination mediated by the ubiquitin ligase UBR2, which triggers the progressive degradation of the ubiquitinated N-terminus. Due to the autoproteolytic cleavage site of NLRP1B, only the N-terminal fragment is degraded, and the non-

covalently linked C-terminal fragment is released, leading to downstream inflammasome activation (Figure 8B). This model is further supported by a study showing that the E3 ligase IpaH7.8 of *Shigella flexneri* directly ubiquitylates NLRP1B, targeting it for proteasomal degradation (Sandstrom et al., 2019). The detection of the presence of specific pathogen effectors in cells, such as toxins or proteases, indicates a form of "trip-wire" immunity or mammalian effector-triggered immunity (ETI) for NLRP1, which is similar to plants (Dangl and Jones, 2001).

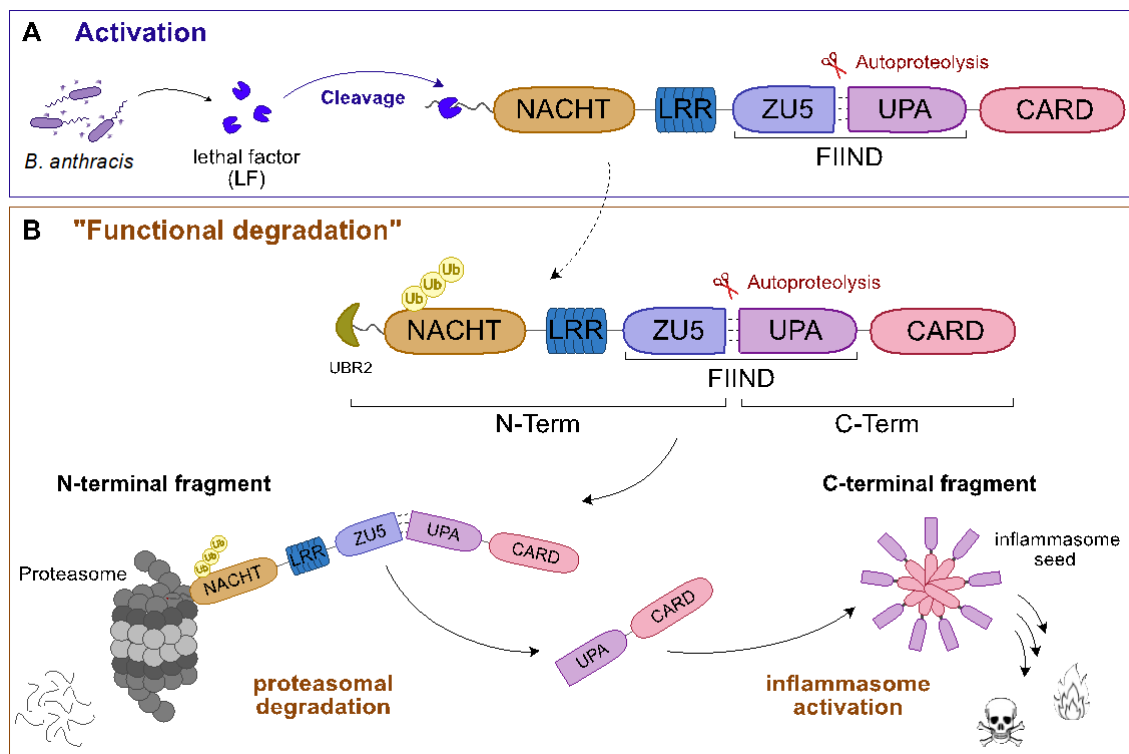


Figure 8: NLRP1B inflammasome activation by "functional degradation". (A) Mouse NLRP1 is activated by proteasomal cleavage of the N-terminus by *B. anthracis* lethal factor (LF). (B) The neo-N-terminus undergoes ubiquitination mediated by the ubiquitin ligase UBR2, which targets NLRP1B for proteasomal degradation. Due to the auto-proteolytic cleavage site of NLRP1B, the non-covalently attached C-terminal part is released. This leads to inflammasome activation by inflammasome seed formation and subsequent pyroptosis.

Protease activity activates both NLRP1 and CARD8

In 2020, it was shown that viral 3C proteases directly cleave NLRP1 between glutamine Q130 and glycine G131 sites located in the disordered region of NLRP1 during enterovirus infection (Robinson et al., 2020) (Figure 9). This triggers a

pathway called "functional degradation", as previously described for mouse NLRP1B inflammasome activation. Later, diverse viral proteases of the *Picornaviridae* family, which includes enterovirus, were shown to activate the NLRP1 inflammasome (Tsu et al., 2021). Additionally, closely related 3CL proteases of coronavirus were linked to NLRP1 activation in lung epithelial cells by cleavage of NLRP1 between glutamine Q333 and glycine G334 sites (Planès et al., 2022) (Figure 9). This study further suggests that the 3CL protease suppresses inflammasome activation by inactivation of GSDMD (Planès et al., 2022). Noteworthy, human CARD8 can also be activated by protease activity. As such, a study showed CARD8 inflammasome activation induced by human immunodeficiency virus (HIV-1) protease activity in the presence of non-nucleoside reverse transcriptase inhibitors (NNRTIs) (Figure 9) (Wang et al., 2021). NNRTIs are antiretroviral drugs used to treat HIV-1 infection by blocking the HIV-1 reverse transcriptase. These drugs promote the dimerisation of the GAG-Pol polyprotein, which leads to premature activation of HIV-1 protease. This, in turn, triggers CARD8-mediated caspase-1 activation (Wang et al., 2021). Recently, VbP was shown to be able to overcome the need for NNRTIs in CARD8 inflammasome activation during HIV-1 infection and is able to increase the clearance of residual HIV-1 in CD4⁺ T cells (Clark et al., 2023). Additionally, CARD8 was indicated to recognise protease activity in acute HIV-1 infection. They show direct site-specific cleavage of CARD8 between the two phenylalanines at positions 59 and 60 (F59, F60) (Figure 9). They also suggested that CARD8-specific recognition of HIV-1 infection leads to inflammasome activation (Kulsuptrakul et al., 2023). A very recent study suggests that CARD8 dictates the HIV-1 and simian immunodeficiency virus (SIV-1) disease progression and pathogenesis (Wang et al., 2024). Furthermore, other viral proteases were shown to activate the CARD8 inflammasome, such as the coronavirus 3C-like protease (3CL), which can cleave CARD8 after glutamine at positions 37 and 61 (Q37 and Q61) (Figure 9) (Tsu et al., 2023). Interestingly, they show that a human polymorphism, an S39P substitution in CARD8, reduces the recognition of coronavirus 3CL protease. However, this polymorphism confers a specificity switch for sensing enteroviral 3C proteases (Tsu et al., 2023). Lastly, protease cleavage of CARD8 after glycine at position G38 (G38) through the Coxsackie virus B3 (2A and 3C proteases) was shown to induce CARD8 inflammasome formation in endothelial cells (Figure 9) (Nadkarni et al., 2022).

The activation of NLRP1 and CARD8 by viral proteases suggests that both NLRP1 and CARD8 function as a molecular “trap”, initiating an immune response upon sensing danger signals (Barry et al., 2023).

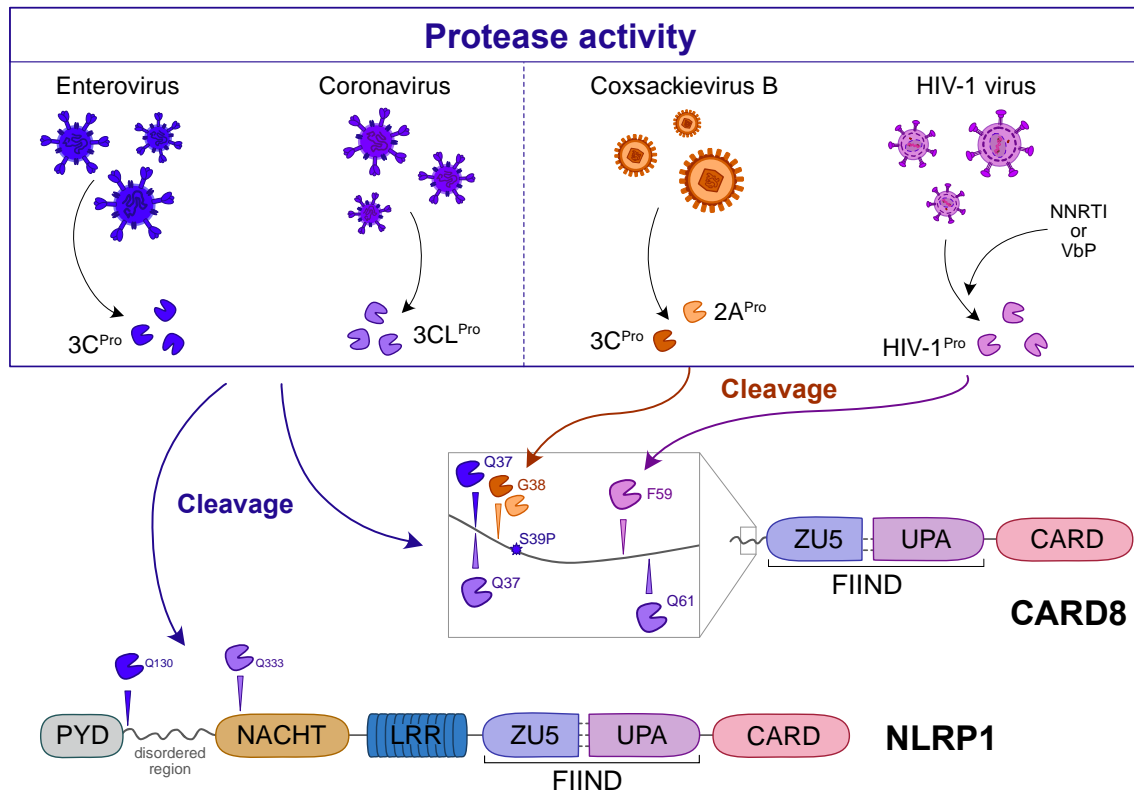


Figure 9: Human NLRP1 and CARD8 inflammasome activation by protease cleavage. Human NLRP1 and CARD8 are activated by different viral proteases, such as enteroviral protease (3C^{Pro}) and coronaviral protease (3CL^{Pro}). In addition, CARD8 is activated by the coxsackievirus B proteases (2A^{Pro} and 3C^{Pro}) and HIV-1 protease (HIV-1^{Pro}). All proteases cleave within the unstructured N-terminal part of CARD8 and the disordered region or the NACHT domain of NLRP1. The HIV-1 virus was shown to require non-nucleoside reverse transcriptase inhibitors (NNRTIs) or VbP as an additional trigger to activate HIV-1 protease.

NLRP1 activation by ribotoxic stress

Early on, UV-B irradiation was identified as an activator of human NLRP1, although the exact activation mechanism remained unclear (Feldmeyer et al., 2007; Fenini et al., 2018) (Figure 10A). In 2022, UV-B irradiation was linked to the ribosomal stress response through the induction of RNA damage (Jenster et al., 2022; Robinson et al., 2022). RNA damage results in ribosome stalling and/or ribosome collisions, which are sensed by specific stress-activated kinases, such as p38,

JNK, and ZAK α (Vind et al., 2020; Wu et al., 2020). Subsequently, ZAK α and, to a lesser extent, p38 hyper-phosphorylate serine residues in the disordered region of NLRP1, located between the PYD and NACHT domain (Robinson et al., 2022). The same study further demonstrated NLRP1 inflammasome activation by known ribotoxic stress inducers, such as the antibiotic products anisomycin, hygromycin, and doxyvinenol (Figure 10A). In addition, several bacterial toxins targeting human ribosome elongation factors, namely eukaryotic elongation factors 1 and 2 (EEF1/2), have been reported to activate the NLRP1 inflammasome by inducing ribotoxic stress sensed by ZAK α (Figure 10A). These include the bacterial exotoxins Diphtheria toxin (DT) from *Corynebacterium diphtheriae*, Exotoxin A (ExoA) from *Pseudomonas aeruginosa*, and Cholix toxin from *Vibrio cholera* targeting EEF2 (Pinilla et al., 2023; Robinson et al., 2023), as well as Sid1 from *Legionella pneumophila* targeting EEF1 (Robinson et al., 2023). As mouse NLRP1 lacks the disordered region undergoing phosphorylation that is present in human NLRP1, mouse NLRP1 is not activated by ribotoxic stress (Robinson et al., 2022).

NLRP1 activation by nucleic acid sensing

NLRP1 was proposed as a nucleic acid sensor of dsRNA and synthetic analogues mimicking dsRNA and dsDNA. Bauernfried et al. showed that long dsRNA binds directly to human NLRP1 predominantly through its leucine-rich repeat domain (Figure 10B) (Bauernfried et al., 2021). This interaction activates the ATPase NACHT domain of NLRP1, yet its relevance for the activation process remains to be determined. However, based on the previously identified activation mechanisms, one can infer that it induces a conformational change and triggers the release of the biologically active C-terminal fragment by N-terminal degradation. Bauernfried et al. used the Semliki Forrest Virus (SFV), which is a positive-sense single-stranded RNA alphavirus, as a viral infection model, producing dsRNA during viral replication. Notably, dsRNA does not activate mouse NLRP1 and the closely related human CARD8 (Bauernfried et al., 2021). Additionally, this study demonstrated dsRNA binding to NLRP1 following transfection of the synthetic dsRNA analogue Poly(I:C) (Figure 10B). In 2022, other alphaviruses have been shown to activate NLRP1 through the activation of the p38

pathway (Figure 10B). They suggest that viral activation of NLRP1 is dependent on the mitogen-activated protein kinase p38 and partially dependent on ZAK α (Jenster et al., 2022). As such, additional studies are required to elucidate the precise mechanism of dsRNA-mediated NLRP1 activation. In addition to dsRNA sensing, the synthetic dsDNA analogue Poly(dA:dT) was proposed to activate NLRP1 activation independent of NLRP1 ATPase activity (Zhou et al., 2023). In this study, Poly(dA:dT) sensing was shown to be independent of the cytosolic dsDNA sensor AIM2 and the cGAS-STING pathway. Since Poly(dA:dT) was found to not bind directly to NLRP1 and no dsRNA intermediates could be found in the cells, the authors speculated that it triggers another response, such as global cellular stress, which is subsequently sensed by NLRP1 (Zhou et al., 2023).

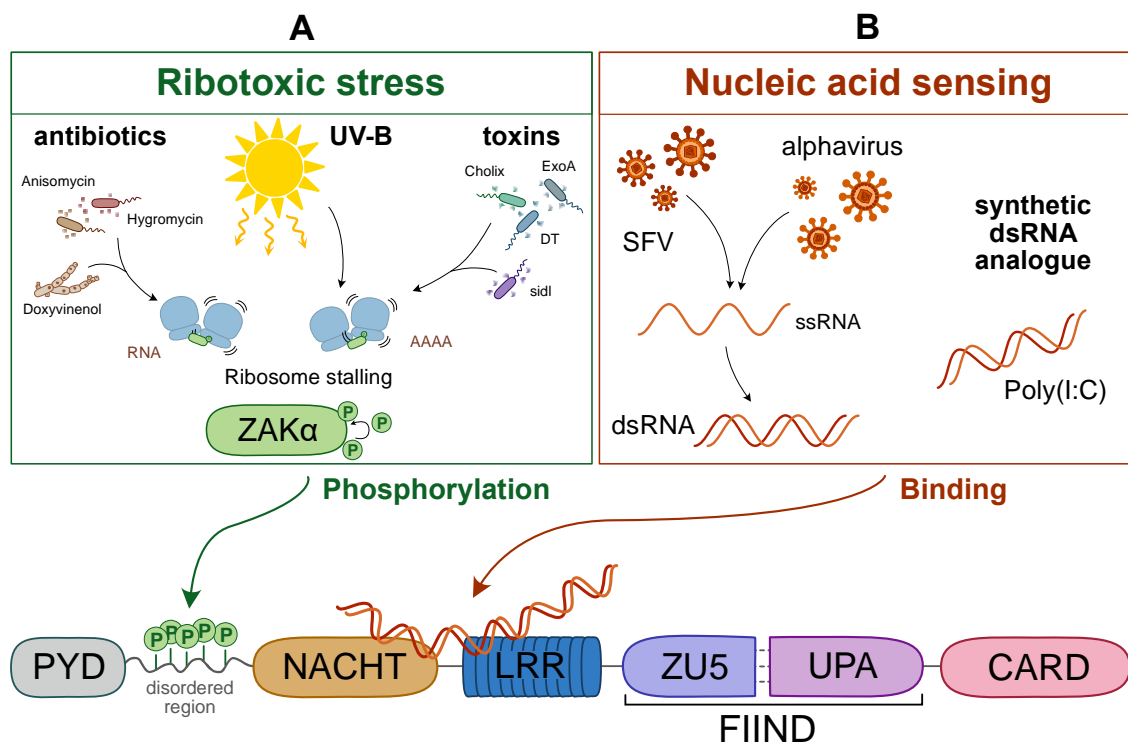


Figure 10: Human NLRP1 inflammasome activation by ribotoxic stress and nucleic acid sensing. (A) Various triggers mediate the activation of human NLRP1 through the induction of ribotoxic stress. These include antibiotics produced by bacteria and fungi, as well as several bacterial toxins, which induce ribosome stalling in cells. UV-B irradiation induces RNA damage, leading to ribosome stalling, which in turn activates ZAK α . ZAK α hyper-phosphorylates serine residues in the disordered region of NLRP1 between the PYD and NACHT domains. **(B)** Nucleic acids, such as dsRNA generated by Semliki-Forrest-Virus (SFV), and synthetic ligands, such as Poly(I:C) mimicking dsRNA, activate the NLRP1 inflammasome by binding to NLRP1.

Regulation of NLRP1 by reductive stress

A recent structural study on NLRP1 showed that oxidised thioredoxin-1 (TRX-1) directly binds to the NACHT domain of NLRP1 (Zhang et al., 2023). Cellular assays demonstrated that oxidised TRX-1 serves as a suppressor of NLRP1 in an ATP-dependent process, acting as a regulatory checkpoint for NLRP1 inflammasome activation. Abrogation of the TRX-1-NLRP1 interaction has been suggested to result from cellular perturbations, such as reductive stress, by accelerating proteasomal degradation of the N-terminal fragment of NLRP1 (Ball et al., 2022; Wang et al., 2023; Zhang et al., 2023). In addition, complementary studies indicated that protein folding stress also leads to accelerated N-terminal NLRP1 degradation, resulting in NLRP1 inflammasome activation (Orth-He et al., 2023). Importantly, even though accelerated N-terminal degradation takes place, this mostly does not cause inflammasome activation on its own since the freed C-terminal fragments are sequestered by DPP8/9.

Understanding the molecular basis of NLRP1/CARD8 inflammasome activation provides insights into its role in innate immune regulation, which is important for understanding the underlying mechanisms of NLRP1/CARD8-induced pathology.

1.4.4 NLRP1 and CARD8 in diseases

NLRP inflammasomes, such as NLRP1 and CARD8, are frequently implicated in the pathogenesis of chronic inflammation and the associated chronic diseases. As such, polymorphisms in *NLRP1* are genetically linked to susceptibility to various autoimmune disorders, such as generalised vitiligo (Jin et al., 2007b, 2007a), Addison's disease and type 1 diabetes (Magitta et al., 2009; Żurawek et al., 2010), rheumatoid arthritis (Sui et al., 2012), and systemic sclerosis (Dieudé et al., 2011). Various gain-of-function mutations in human NLRP1 described in patients have been associated with several autoinflammatory diseases, skin inflammation and skin cancer, as shown in Figure 11. Zhong et al. identified three germline missense mutations of NLRP1 (A54T, A66V and M77T) located in its PYD, which resulted in multiple self-healing palmoplantar carcinoma (MSPC) phenotypes in these

patients. They also found an in-frame deletion (F787-R843 deletion) in NLRP1, resulting in the loss of part of the linker between the NACHT and LRR domains with loss of the first LRR domain, causing familial keratosis lichenoides chronica (FKLC). All mutations described in this study led to increased inflammasome activation with elevated IL-1 β secretion in the patients (Zhong et al., 2016). In the same domain of NLRP1, another patient with an NLRP1 variant (A59P) has been described, showing dyskeratosis of the cornea and mucous membranes and elevated levels of IL-1 β and IL-18 (Herlin et al., 2020). Autoinflammation with arthritis and dyskeratosis (AIADK) with increased caspase-1 and IL-18 levels was found in three patients and linked to two different mutations in NLRP1, one in the NACHT-LRR interface (R726W) and one in the FIIND domain (P1214R) (Grandemange et al., 2017). Additionally, a homozygous NLRP1 variant also in the NACHT-LRR interface (T755N) was associated with juvenile-onset recurrent respiratory papillomatosis (JRRP) in two brothers (Drutman et al., 2019). Another study described siblings with an NLRP1 variant in the LRR domain (L813P) that caused different degrees of severity in the siblings, ranging from multiple keratoacanthomas for the milder phenotype to a severe phenotype of FKLC with manifestations of psoriasis and atopic dermatosis (Li et al., 2023). A study investigating the impact of rare genetic variations in multiple sclerosis cases provided the first link between NLRP1 and neurodegenerative disease, as a missense mutation in the NACHT domain of NLRP1 (G578S) caused multiple sclerosis and malignant melanoma in two siblings (Maver et al., 2017). Another mutation in the FIIND domain of NLRP1 (M1184V) has been associated with an increased risk for autoimmune diseases like asthma (Moecking et al., 2021). In later studies, the M1184V variant of NLRP1 was shown to stabilise the FIIND domain, leading to increased autoproteolysis and enhanced binding of DPP9 to NLRP1 (Moecking et al., 2022). An NLRP1 missense variant in the linker region of NLRP1 between the PYD and NACHT domain (L155H) was proposed to increase the risk of developing preeclampsia (Pontillo et al., 2015).

In addition to gain-of-function mutations causing severe phenotypes in patients, some loss-of-function mutations in DPP9, a key inhibitor of NLRP1, have been found to cause autoimmune diseases by unleashing NLRP1 inflammasome activation (Figure 11) (Harapas et al., 2022; Wolf et al., 2023). Harapas et al.

describe three unrelated families with immune-related defects such as pancytopenia, increased susceptibility to infection and poor growth, and skin manifestations. These conditions are associated with biallelic rare variants in the *DPP9* gene that result in knockout or hypomorphic alleles, resulting in an inability to inhibit NLRP1. Only one mutation of their patients is located in the α/β -hydrolase domain (one patient with a homozygous mutation resulting in a premature stop codon Q851*), whereas three of the mutations are located in the β -propeller domain of DPP9 (two related patients with homozygous stop-gained mutation R111*, and one patient with an early stop-gained mutation S214* in addition to a missense mutation G167S) (Figure 11). Their findings outline a previously unrecognised Mendelian disorder resulting from germline *DPP9* deficiency. Experiments with patient cells and two animal models, mouse and zebrafish, showed that the pathology is predominantly driven by abnormal activation of the NLRP1 inflammasome (Harapas et al., 2022).

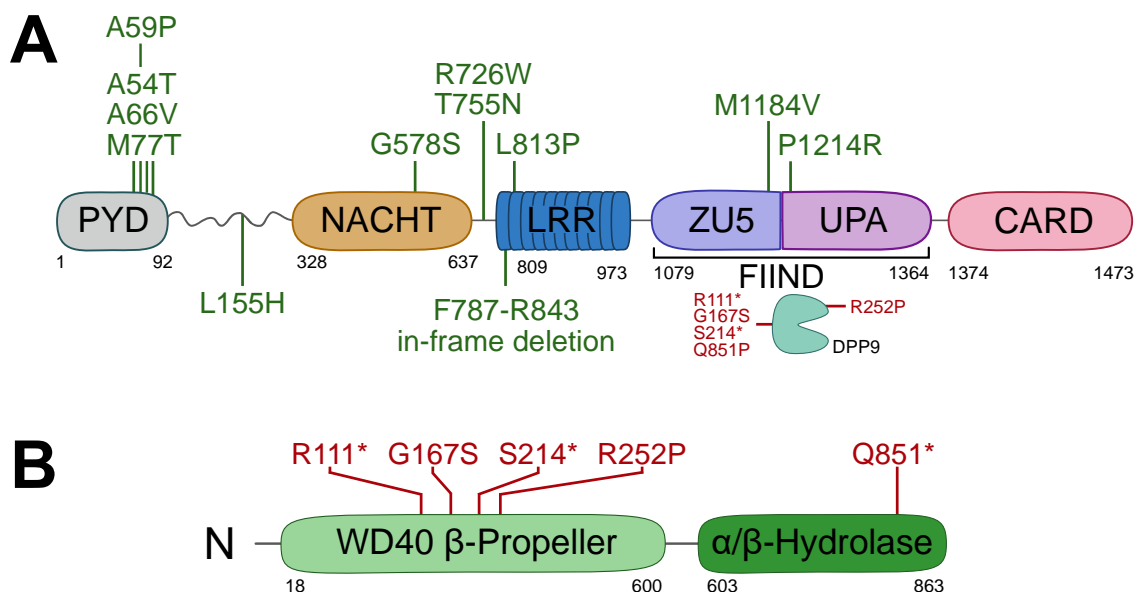


Figure 11: Mutations triggering NLRP1 inflammasome activation. (A) Domain representation of human NLRP1. Gain-of-function mutations (marked in green) of NLRP1 highlight its role in disease. Loss-of-function mutations in DPP9 (marked in red) trigger constitutive NLRP1 activity. (B) Domain representation of human DPP9. Loss-of-function mutations (marked in red) of DPP9 lead to constitutive NLRP1 and CARD8 inflammasome activation.

In contrast to NLRP1, there are fewer studies on CARD8. CARD8 has been linked to increased inflammation in a variety of diseases in several studies. In 2014, it was shown that cryopyrin-associated periodic syndromes (CAPS)-associated

NLRP3 mutants are unable to bind to CARD8, thereby blocking CARD8-dependent inhibition of NLRP3 (Ito et al., 2014). Another study reported a CARD8 frameshift variant that is unable to bind to NLRP3 and causes a form of CAPS in patients (Cheung et al., 2017). Mao et al. described a valine-to-isoleucine substitution at position 44 (V44I) in three related patients, causing CD-like intestinal inflammation (Mao et al., 2018). They found that this CARD8 variant leads to increased IL-1 β production in addition to elevated NLRP3 inflammasome activation. Although CARD8 has been proposed to suppress NLRP3 activity, more studies are needed to unravel the CARD8-mediated regulation of NLRP3. Additionally, the CARD8 rs2043211 polymorphism causing a premature stop codon was associated with Crohn's disease (CD) (McGovern et al., 2006b; Schoultz et al., 2009) but could not be validated in a meta-analysis of several reports (Z.-T. Zhang et al., 2015). Moreover, CARD8 was associated with inflammatory bowel disease (McGovern et al., 2006a).

Collectively, these diverse autoimmune and inflammatory disorders caused by NLRP1 and CARD8 emphasise the significance of tight control of inflammasome sensors.

1.5 Dipeptidyl peptidases 8 and 9 (DPP8/9)

DPP8 and 9 are dipeptidyl peptidases (DPPs) belonging to the enzymatically active members of the S9b family, which includes the fibroblast activation protein (FAP) and the extensively studied proteins DPP4, and DPP8/9 themselves (Ross et al., 2018). Members of the S9b family are known to function as dimers, with the rare ability to remove N-terminal Xaa-Pro dipeptides (Geiss-Friedlander et al., 2009; Lee et al., 2006). Each monomer contains a WD40 β -propeller domain and an α/β -hydrolase domain. The C-terminal α/β hydrolase domain harbours the catalytic triad for DPP9, comprising Ser730, His840 and Asp808 (Ross et al., 2018). This triad is structurally located between both domains. The S9b family members DPP4 and FAP are extracellular proteases circulating in body fluids and expressed on the plasma membrane of cells. DPP4 is the best-characterized member and is involved in glucose homeostasis by controlling the activity of incretin hormones, essential

regulators of blood glucose levels and insulin secretion (Green et al., 2006). Thus, DPP4 has emerged as an appealing drug target for which small molecule ligands have been identified that successfully treat type II diabetes mellitus (Lambeir et al., 2008).

In 2000, research on DPP4 homologues led to the discovery of a novel post-proline dipeptidyl aminopeptidase called DPP8, sharing 27 % amino acid identity and 51 % similarity with DPP4 (Abbott et al., 2000). Furthermore, this study identified a gene that is closely related to *DPP8*, which has been named *DPP9*. In 2002, DPP9 was then first cloned and recombinantly expressed (Abbott et al., 2000; Olsen and Wagtmann, 2002). Unlike DPP4, DPP8 and DPP9 are intracellular proteins present in the cytosol and nucleus of cells (Abbott et al., 2000; Ajami et al., 2004; Justa-Schuch et al., 2014). DPP8 and DPP9 exhibit a high degree of similarity, with 60% overall amino acid identity and greater than 90% identity in their active sites (Bjelke et al., 2006). Due to their structural and functional similarities to DPP4, DPP8 and DPP9 were first primarily used as a counter-screen for DPP4 selective inhibitors. Both are ubiquitously expressed in vertebrate tissues, with DPP9 being more abundant in cells and highly expressed in lymphocytes and epithelial cells (Chowdhury et al., 2013). Nevertheless, although DPP8 and DPP9 share cellular localisation and enzymatic specificity, indicating partial redundancy, there is growing evidence that they may also serve distinct physiological roles.

1.5.1 Physiological roles of DPP8/9

Throughout the years, the identification of DPP8/9 substrates has accumulated evidence that DPP8/9 may be involved in several physiological processes. As dipeptidyl peptidases generate dipeptides, which are of small size, the identification of endogenous substrates using classical proteomic approaches is challenging. However, N-terminal labelling of the cleaved peptide allowed protease substrate profiling and enabled the identification of the first natural substrate of DPP9, the RU1₃₄₋₄₂ antigenic peptide (VPYGSFKHV) (Geiss-Friedlander et al., 2009). Elevated presentation of this antigen by silencing of DPP9 indicated that DPP9 may be involved in peptide turnover and antigen presentation (Geiss-Friedlander et al., 2009). Subsequent screening for endogenous substrates of DPP8/9 using

similar methods with N-terminal labelling led to the identification of additional endogenous substrates (Geiss-Friedlander et al., 2009; Kleifeld et al., 2010; Wilson et al., 2013). The known substrates of DPP9 include the tyrosine kinase Syk (Justa-Schuch et al., 2016), the adenylate kinase 2 (AK2) (Finger et al., 2020), and the breast cancer type 2 susceptibility protein (BRCA2) (Bolgi et al., 2022). The cleavage of these substrates by DPP9 activity suggests that DPP9 is involved in B-cell signalling, mitochondrial homeostasis, and DNA repair. While B-cell signalling via Syk and DNA repair via BRCA2 showed specificity for DPP9 activity, the involvement in mitochondrial homeostasis via AK2 was indicated for both DPP8 and DPP9. Independently of its enzymatic activity, DPP9 has been shown to bind to protein ligands using the β -propeller domain, such as SUMO-1 (Pilla et al., 2012) and filamin A (Justa-Schuch et al., 2016). Nevertheless, further research is required to unravel the involvement of DPP8/9 and its enzymatic activity in different physiological processes.

Previous research has demonstrated that the inhibition of DPP9 results in the suppression of T-cell proliferation as well as neonatal lethality in mice. This effect was postulated to be a crucial immunomodulatory function of DPP9 (Gall et al., 2013; Kim et al., 2017; Lankas et al., 2005; Reinhold et al., 2009). However, subsequent findings demonstrated that DPP9 inhibition results in inflammasome activation and subsequent pyroptotic cell death, which indicates that the immunomodulatory role of DPP9 can be attributed to its key role in regulating inflammasome activation.

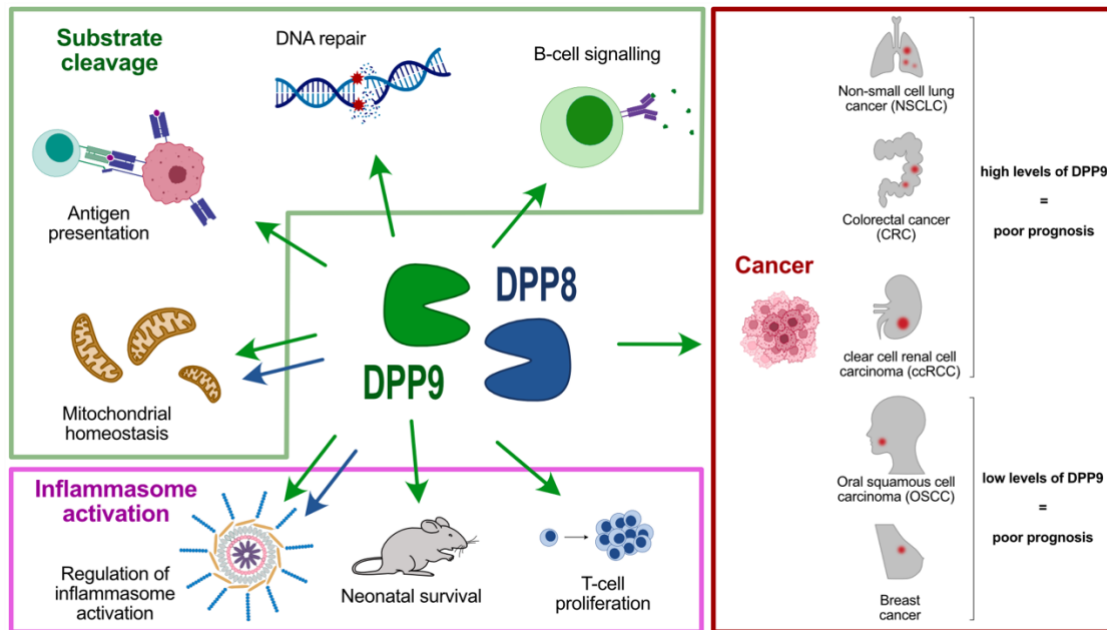


Figure 12: The roles of DPP8/9 in health and disease. DPP8 and DPP9 are linked to essential aspects of cellular biology by their enzymatic activity, which involves the cleaving of substrates. DPP8/9 play a pivotal role in the regulation of inflammasome activation. Dysregulation of DPP9 is associated with pathophysiological conditions, such as different types of cancer. Potential roles of DPP8/9 are indicated with green (DPP9) and blue (DPP8) arrows.

1.5.2 Pathophysiological roles of DPP9

DPP9 is of increasing interest in immunology and cancer biology, given that its dysregulation is associated with pathophysiological conditions (Ross et al., 2018).

Several cancer-related studies have demonstrated that dysregulation of DPP9 is involved in the proliferation, migration, invasion, and apoptosis of tumour cells. A correlation between high levels of DPP9 and poor prognosis for patients has been indicated for several types of cancer, such as non-small cell lung cancer (NSCLC) (Tang et al., 2017), colorectal cancer (CRC) (Saso et al., 2020), and clear cell renal cell carcinoma (ccRCC) (Chang et al., 2023). Conversely, studies in other types of cancer, such as oral squamous cell carcinoma (OSCC) (Q. Wu et al., 2020) and breast cancer (Bolgi et al., 2022), highlight a correlation between low levels of DPP9 and poor prognosis in these patients. Overall, these findings suggest that DPP9 plays diverse roles in different types of cancer, but the precise role of DPP9 is not fully understood yet.

More recently, elevated DPP9 levels were associated with the severity of disease progression in COVID-19 patients (Pairo-Castineira et al., 2021; Sharif-zak et al., 2022). While the precise involvement of DPP9 in the pathogenesis of COVID-19 remains unclear, DPP9 may be a promising indicator for assessing the risk in COVID-19 patients.

Finally, DPP9 is also associated with immune-associated defects and diseases via its pivotal role as a negative regulator of the NLRP1 and CARD8 inflammasome (Harapas et al., 2022; Wolf et al., 2023).

2 Aims of this work

Inflammasomes are intracellular multimeric signalling complexes helping the host's immune system to distinguish between self and non-self. Activation of inflammasome sensors leads to inflammasome assembly, resulting in cell death and pro-inflammatory cytokine release (Broz and Dixit, 2016). Thus, inflammasome activation must be tightly controlled to avoid excessive inflammation. Mutations in genes encoding inflammasome sensors are associated with various hereditary autoinflammatory syndromes (Lamkanfi and Dixit, 2012). Recently, the Min Ae Lee Kirsch group found a patient exhibiting severe infancy-onset hyperinflammation with strongly elevated serum levels of the pro-inflammatory cytokines IL-18 and IL-1 β , indicating inflammasome activation (Wolf et al., 2023). Genetic analysis of this patient unveiled a *de novo* mutation from arginine to proline at position 252 (R252P) in dipeptidyl peptidase 9 (DPP9), a direct interaction partner of NLRP1 and CARD8. Recently, DPP9 has been described to cause autoinflammation in patients partly due to inflammasome activation by biallelic loss-of-function mutations (Harapas et al., 2022).

This study aimed to investigate the molecular basis of this patient's phenotype. To this end, the potential role of the R252P mutation on DPP9's stability was assessed by modelling R252P in a previously determined structure of DPP9. To investigate the impact of the DPP9 mutant on the stability of the protein, overexpression of either wild-type or mutant DPP9 in HEK293T cells was conducted. Using functional assays in HEK293T cells, the impact of this mutation on NLRP1 and CARD8 inflammasome activation was then determined. We additionally exploited different human cell lines, including immortalised N/TERT-1 keratinocytes and the monocytic cell line THP-1, to study the impact of this DPP9 mutant on inflammasome signalling. Moreover, we also addressed the role of DPP8 and DPP9 for inflammasome activation using a loss-of-function approach in N/TERT-1 keratinocytes.

3 Material and Methods

3.1 Material

Consumables (both sterile and non-sterile) were purchased from Corning, Eppendorf, Greiner, Sarstedt, Thermo Fisher Scientific or TPP.

3.1.1 Antibodies

The following antibodies were used in this study.

Table 1: Antibodies.

Antibody	Source	Catalogue number
Primary antibodies		
Mouse anti-human NLRP1	Biologend	#679802
Mouse anti-human DPP9	R&D Systems	#MAB5419-SP
Human anti-human IL-1 β	AG Hornung	N/A
Anti- β -actin antibody (C4): sc-47778 HRP-coupled	Santa Cruz Biotechnology	#sc-47778 HRP
Mouse anti-HA (6E2) HRP-coupled	Cell Signalling Technology	#2999S
Secondary antibodies		
Anti-human IgG, HRP-coupled	Sigma-Aldrich	#A0293-1ML
Anti-rabbit IgG, HRP-coupled	Cell Signalling Technology	#7074S
Anti-mouse IgG, HRP-coupled	Cell Signalling Technology	#7076S

3.1.2 Cell lines

The following cell lines were used in this study.

Table 2: Cell lines.

Cell line	Source	Specification
HEK293T	ATCC [®] CRL-3216	Created by transformation of human embryonic kidney cells

HEK293T-RFP	AG Hornung	Created by lentiviral transduction of RFP to HEK293T and selected for low specking cells
THP-1	ATCC® TIB-202	Monocytic leukaemia cell line
N/TERT-1	J. Rheinwald	Obtained by immortalisation of human primary keratinocytes by transduction with a TERT transgene and spontaneous loss of p16INK4a expression
N/TERT-1 NLRP1 KO	AG Hornung	Pool KO created by CRISPR/CAS9 gene editing (Bauernfried et al., 2021)
N/TERT-1 DPP9 KO	This study	Pool KO created by CRISPR/CAS9 gene editing
N/TERT-1 DPP8 KO	This study	Pool KO created by CRISPR/CAS9 gene editing
N/TERT-1 DPP8/9 dKO	This study	Pool KO created by CRISPR/CAS9 gene editing

3.1.3 Chemicals

The following chemicals were used in this study.

Table 3: Chemicals.

Chemical	Source	Catalogue number
Dulbecco's phosphate-buffered saline (DPBS)	Thermo Fisher Scientific	#14190169
DMEM Medium (high glucose)	Thermo Fisher Scientific	#41965062
RPMI 1640 Medium	Thermo Fisher Scientific	#21875-034
DMEM Medium (high glucose, no glutamine, no calcium)	Thermo Fisher Scientific	#21068028
Ham's F12 Medium	Thermo Fisher Scientific	#11765054
Penicillin-Streptomycin (10,000 U/ml)	Thermo Fisher Scientific	#15140163
Foetal Calf Serum (FCS)	Thermo Fisher Scientific	#10270106
Hepes solution, 1 M, pH 7.0-7.6, sterile-filtered, BioReagent	Sigma-Aldrich	#H0887-100ML
Sodium pyruvate	Thermo Fisher Scientific	#11360088
Non-essential amino acids	Thermo Fisher Scientific	#11140050
GlutaMAX	Thermo Fisher Scientific	#35050061
EpiLife™ defined growth supplement	Thermo Fisher Scientific	#S0125
bovine pituitary extract (BPE)	Thermo Fisher Scientific	#13028014
Calcium chloride	Sigma-Aldrich	#C7902
epidermal growth factor (EGF)	Max-Planck-Institute of Biochemistry, Munich	N/A

EDTA	Thermo Fisher Scientific	#15575020
0.05 % Trypsin-EDTA	Thermo Fisher Scientific	#25300054
Recombinant Cas9 protein from <i>S. pyogenes</i>	Max-Planck-Institute of Biochemistry, Munich	N/A
Nuclease-free Duplex Buffer	IDT	#11-05-01-12
tracrRNA	IDT	#1072533
phorbol 12-myristate 13-acetate (PMA)	Enzo Life Sciences	#BML-PE160
Pam3CSK4	InvivoGen	tIrl-pms
Val-boroPro	APExBIO	#B3941
Anisomycin	Biomol	#Cay11308-10
Poly(I:C) HMW	Invivogen	#tIrl-pic
Propidium iodide (PI)	MP Biomedicals	#0219545810
PEI Max	Polysciences	#24765-1
Blasticidin	Thermo Fisher Scientific	#A1113903
Gibson Master Mix	Max-Planck-Institute of Biochemistry, Munich	N/A
FastDigest Green Buffer (10x)	Thermo Fisher Scientific	#B72
Phusion™ High-Fidelity Buffer (10x)	Thermo Fisher Scientific	#F518-L
Phusion™ High-Fidelity DNA Polymerase	Thermo Fisher Scientific	#F-530XL
Agarose	Biozyme	#840004
Serva DNA stain	Serva	#39803
6x DNA loading dye	Thermo Fisher Scientific	#B72
Thermo Scientific GeneRuler 1 kb DNA Ladder	Thermo Fisher Scientific	#SM0313
Thermo Scientific GeneRuler 100 bp DNA Ladder	Thermo Fisher Scientific	#SM0244
Thermo Scientific PageRuler Prestained 10-180 kDa Protein Ladder	Thermo Fisher Scientific	#26616
Immobilon Forte Western HRP substrate	Sigma-Aldrich	#WBLUF0500

3.1.4 Commercial Kits

The following commercial kits were used in this study.

Table 4: Commercial Kits.

Commercial Kit	Source	Catalogue number
Human IL-1 β ELISA Set II	BD Biosciences	#557953
CyQUANT™ LDH Cytotoxicity Assay	Invitrogen	#C20301
Qiagen Maxiprep Kit	Invitrogen	#K210017
QIAquick Gel Extraction Kit	Qiagen	#28706
P3 Primary Cell Nucleofection Kit	Lonza	#V4XP-3032

3.1.5 Media and Buffers

Media and buffers were prepared using the following ingredients.

Table 5: Media and Buffers.

Media/ Buffer	Ingrediencies
LB Medium	5 g Yeast extract 10 g Tryptone 10 g NaCl Fill up to 1 L with H ₂ O Autoclave before usage
LB Agar	5 g Yeast extract 10 g Tryptone 10 g NaCl 5 g Agar Fill up to 1 L with H ₂ O Autoclave before usage
Mini-Prep Puffer P1	50 mM Tris pH 8.0 10 mM EDTA 100 µg/mL RNase A
Mini-Prep Puffer P2	200 mM NaOH 1 % SDS
Mini-Prep Puffer N3	4.2 M Guanidinium hydrochloride 0.9 M Potassium acetate pH 4.8
Mini-Prep Puffer PE	10 mM Tris pH 7.5 80 % Ethanol
TAE Puffer	40 mM Tris pH 8.0 20 mM acetic acid 1 mM EDTA
Direct lysis buffer	0.2 mg/mL Proteinase K 1 mM EDTA 1 mM CaCl ₂ 3 mM MgCl ₂ 1 % Triton X-100 10 mM Tris pH 7.5
10x PBS	1.37 M NaCl 27 mM KCl 100 mM Na ₂ HPO ₄ 18 mM KH ₂ PO ₄ pH 7.4
PBS-T	1x PBS 0.5 % Tween-20
6x Lämmli sample buffer	450 mM Tris-HCl pH 6.8

	600 mM DTT 60 % Glycerine 12 % SDS 0.03 % Bromophenol
10x Tris-Glycine running buffer (Westernblot)	290 g Tris 1440 g Glycine Fill up to 10 L with H ₂ O
Transfer buffer (Westernblot)	200 mL 10x Tris-Glycine Puffer 400 mL Ethanol (EtOH) 1400 mL H ₂ O

3.1.6 Equipment

The following laboratory equipment was used in this study.

Table 6: Laboratory Equipment and Machines.

Laboratory Equipment	Source	Catalogue number
96-well Ibidi glass-bottom black plate	Ibidi	#89626
Novex™ WedgeWell™ 12% Tris-Glycine Mini Gels, 15-well	Thermo Fisher Scientific	#XP00125BOX
EconoSpin Silica Membrane Mini Spin Column	Epoch Life Science	#1910-250
Nitrocellulose membrane, 0.45 µm	GE Life Sciences	#10600002
Machines		
SYNENTEC CellaVista Imager	SYNENTHEC, Elmshorn, Germany	N/A
Olympus 203/0.50 Objective	Olympus, Hamburg, Germany	N/A
Leica DMI8 inverted microscope	Leica	N/A
HC PL FLUOTAR L 20×/0.40 DRY objective lens	Leica	N/A
HC PL FLUOTAR 10×/0.32 DRY objective lens	Leica	N/A
ORCA-Flash4.0 LT+ Digital CMOS camera	Hamamatsu	N/A
4 D Nucleofector	Lonza	N/A

3.1.7 Primer

The following primers were designed using SNAPGENE and dissolved in water. All Gibson cloning primers contain an overhang, which is highlighted in bold. For site-directed mutagenesis, the nucleotides are lowercase letters.

Table 7: Primer.

Name	Sequence (5' to 3')
DPP9 fwd_pFUGW	GGTCGACTCTAGTTCGAGCAGCTAGCATG CGGAAGGTAA GAAACTGCGCC Forward primer for Gibson Assembly Cloning of HF-p2/3
DPP9 rev_pFUGW	GCAACCCCAACCCCGGATCCTCAGAGGTATTCCTGTAGAAA GTG Reverse primer for Gibson Assembly Cloning of HF-p2/3/6/7
pFUGW_HA-eGFP- blast_PCR1_fwd	ATACGACGTACCAGATTACGCTGGCGGGCAGCGT GAGC AAGGGCGAGGAGC Forward primer for Gibson Assembly Cloning for the PCR1 of adding an HA-Tag of HF-p1
pFUGW_HA-eGFP- blast_PCR2_fwd	GTCGACTCTAGTTCGAGCAGCTAGCATGTACCCATACGACG TACCAGATTACGCTGG Forward primer for Gibson Assembly Cloning for the PCR2 of adding an HA-Tag of HF-p1
pFUGW_HA-eGFP- blast_rev	AAGGCGCAACCCCAACCCCGGATCCTTACTTGTACAGCTC GTCCAT Reverse primer for Gibson Assembly Cloning of HF-p1/10/11
shortDPP9_fwd	GCAGGTCGACTCTAGTTCGAGCAGCTAGCATGGCCACCAC CGGGACCCCAACG Forward primer for Gibson Assembly Cloning of HF-p4/5
short_DPP9rev	GCAACCCCAACCCCGGATCCTCAGAGGTATTCCTGTAGAAA GTGCA Reverse primer for Gibson Assembly Cloning of HF-p4/5/8/9
forHA_shortDPP9	TACCCATACGACGTACCAGATTACGCTGGCGGGCAGCG CCACCACCGGGACCCCAACG Forward primer for Gibson Assembly Cloning for the PCR1 of adding an HA-Tag of HF-p8/9
forHAinpFUGW_short DPP9 fwd	CAGGTCGACTCTAGTTCGAGCAGCTAGCATGTACCCATACG ACGTACCAGATT Forward primer for Gibson Assembly Cloning for the PCR2 of adding an HA-Tag of HF-p8/9
HA_DPP9 fwd_pFUGW	CAGGTCGACTCTAGTTCGAGCAGCTAGCATGTACCCATACG ACGT Forward primer for Gibson Assembly Cloning of HF-p6/7
DM036_GFP_fwd_mi ddle	AGGAATACCTCGGCGGGCGGCGGCAGCGTGAGCAA Forward primer for Gibson Assembly Cloning of fragment 2 of HF-p8/9/10/11

DM036_DPP9_rev_middle1	GCTGCCGCCGCCGCCGAGGTATTCCTGTAGAAAGTGCAGC Reverse primer for Gibson Assembly Cloning of fragment 1 of HF-p8/9/10/11
R281P_fwd	AGAGTTCGACCCCTTCACTGG Forward primer for site-directed mutagenesis using Gibson Assembly Cloning of fragment 2 of HF-p3/5/7/9
R281P_rev	CCAGTGAAGgGGTCGAACTC Reverse primer for site-directed mutagenesis using Gibson Assembly Cloning of fragment 1 of HF-p3/5/7/9
DPP9_R281P_SeqPrimer	CCTCCTACGACTTCCACAGC Sequencing primer for DPP9 mutant
DPP9 Forward Sequencing Primer	CCCGGATGGACCCCAAAT Sequencing primer for DPP9
pFUGW_rev_seq	TGAAGAATGTGCGAGACCCAGG Sequencing primer for pFUGW BamHI outside
hUBC_fwd_seq	TGAAGCTCCGGTTTTGAAC Sequencing primer for pFUGW NheI outside
DPP8 KO_fwd	GCTAAAAGCATTTTTTCTTGCCCTCCC Forward primer for DPP8 KO PCR
DPP8 KO_rev	ACAACAAAATCGAATTCTTCAAATTATAGGCTTTTCTTTAATGA Reverse primer for DPP8 KO PCR

3.1.8 Plasmids

The following plasmids were generated using Gibson Assembly Cloning.

Table 8: Plasmids.

Name	Identifier	Source
pFUGW_HA-eGFP_blast	HF-p1	This study
pFUGW_IDPP9_blast	HF-p2	This study
pFUGW_IDPP9-R281P_blast	HF-p3	This study
pFUGW_sDPP9_blast	HF-p4	This study
pFUGW_sDPP9-R252P_blast	HF-p5	This study
pFUGW_HA-IDPP9_blast	HF-p6	This study
pFUGW_HA-IDPP9-R281P_blast	HF-p7	This study
pFUGW_HA-sDPP9_blast	HF-p8	This study
pFUGW_HA-sDPP9-R252P_blast	HF-p9	This study
pFUGW_IDPP9-eGFP_blast	HF-p10	This study
pFUGW_sDPP9-eGFP_blast	HF-p11	This study
pFUGW_hsCARD8	N/A	AG Hornung
pFUGW_hsNLRP1	N/A	AG Hornung

pcDNA3.1_pro-IL1 β	N/A	AG Hornung
pcDNA3.1_ASC-mCherry	N/A	AG Hornung
pcDNA3.1_GSDMD	N/A	AG Hornung
pcDNA3.1_Caspase-1	N/A	AG Hornung
pMDLg/pRRE	N/A	AG Hornung
pRSV-rev	N/A	AG Hornung
pCMV-VSV-G	N/A	AG Hornung

3.1.9 Enzymes

The following enzymes were used in restriction assays in FastDigest Green Buffer (10x).

Table 9: Enzymes.

Enzyme	Source	Product number
NheI	Thermo Fisher Scientific	FD0974
BamHI	Thermo Fisher Scientific	FD0054

3.1.10 Single-guide RNA (sgRNA)

The sgRNAs were designed using the SYNTHEGO sgRNA design web tool, purchased from IDT, and dissolved in IDT Nuclease-free Duplex Buffer.

Table 10: Single-guide RNAs.

Target gene	Name	Target site including the PAM site (5' to 3')
<i>DPP8</i>	DPP8_gRNA1 (SBA)	GCAATGGAAACAGAACAGCT GGG
	DPP8_gRNA2 (SBA)	TAATAGATTCTGTCTGAAT GAGG
<i>DPP9</i>	DPP9_gRNA_left	CTGGGGACAGCCAGGGGCT caagg
	DPP9_gRNA_right	TCCAGGAGGAAAAGCACGCC CGGG

3.1.11 Software and Algorithms

Table 11: Software.

Software	Source
Affinity Designer v1.9.0	Affinity
Graphpad Prism 9	Graphpad
Snappgene v4.3.11	Snappgene
Pymol v2.5.5	Pymol (Schrödinger and DeLano, 2020)
ChimeraX v1.6.1	UCSF ChimeraX (Pettersen et al., 2021)
JPred 4	Web tool (Drozdetskiy et al., 2015)
MPI Bioinformatics Toolkit	Web tool (Zimmermann et al., 2018)
MolView v2.4	Web tool (Copyright © Herman Bergwerf)

3.2 Molecular Biology Methods

3.2.1 Generation of chemically competent *E. coli*

The production of chemically competent *E. coli* (DH5 α or Top10) was performed as described by Rachel Green and Elizabeth J. Rogers (Green and Rogers, 2013).

3.2.2 Polymerase Chain Reaction (PCR)

PCRs were performed according to the manufacturer's instructions to generate inserts for cloning.

Table 12: Standard PCR reaction.

Component	50 μ L reaction
Template DNA	10 ng
5 x Phusion TM HF Buffer	10 μ L
10 mM dNTPs	1 μ L
Forward Primer (10 μ M)	2.5 μ L
Reverse Primer (10 μ M)	2.5 μ L
H ₂ O	Fill up to 49.5 μ L
Phusion TM High-Fidelity DNA Polymerase (2 U/ μ L)	0.5 μ L

Table 13: Standard PCR program.

Cycle step	Temperature	Time	Cycle
Initial Denaturation	98 °C	30 sec	1
Denaturation	98 °C	10 sec	30 x
Annealing	60 °C	20 sec	
Extension	72 °C	20 sec/ kb	
Final extension	72 °C	7 min	1

3.2.3 Agarose gel electrophoresis

For agarose gel electrophoresis, a 1.5 % agarose weight/volume (w/v) solution was prepared and melted in 1 x TAE, supplemented with 0.001 % volume/volume (v/v) of DNA stain. Samples were mixed with 4 x loading dye before loading. The gel was run at 120 V for 30-60 min.

3.2.4 Agarose gel extraction

For the purification of PCR products and digested vectors, the desired fragments were cut out of the gel using a scalpel. They were then purified using the QIAquick Gel Extraction Kit and eluted in water.

3.2.5 Cloning

For cloning, firstly, the vector was cut with restriction enzymes. 10 µg of plasmid DNA were digested for 3 hours at 37 °C. Afterwards, the restriction enzymes were heat-inactivated at 80 °C for 5 min.

Table 14: Standard reaction for a digest.

Component	50 µL reaction
Plasmid DNA (vector)	10 µg
10 x FastDigest Green Buffer	10 µL
Enzyme 1	1 µL
Enzyme 2	1 vL
H ₂ O	Fill up to 50 µL

After gel electrophoresis and gel extraction, Gibson assembly cloning was performed by incubating cut vector (50 ng) and PCR products (in a ratio of 1:3) in Gibson assembly mix for 1 hour at 50 °C. Afterwards, 4 µL of the Gibson reaction was used for *E. coli* transformation. For Gibson assembly with more than one fragment, the 1:3 ratio was calculated for the complete insert length and then split for each fragment.

Table 15: Standard Gibson Assembly reaction.

Component	10 µL reaction
2 x Gibson Master Mix	5 µL
Plasmid DNA backbone (vector)	50 ng
DNA insert (PCR)	150 ng total
H ₂ O	Fill up to 10 µL

3.2.6 *E. coli* transformation

For transformation, chemically competent *E. coli* (DH5α or Top10) were thawed on ice. Then, 4 µl Gibson reaction mix was added and incubated on ice for 30 min. A heat shock at 42 °C for 30 - 45 seconds was performed. After 2 min incubation time on ice, 500 µl LB medium was added, and the bacteria were shaken for 30 - 60 min at 37 °C and 300 rpm. The bacteria were then plated on selection plates with 100 µg/ml ampicillin.

3.2.7 Plasmid isolation *E. coli*

For plasmid isolation from *E. coli*, buffers P1, P2, N3 (buffer components listed in Chapter 3.1.5) and Mini Spin columns were used for a mini prep according to the protocol of the QIAprep Spin Miniprep Kit. For Maxi preps, the Qiagen kit was used according to the manufacturer's instructions.

3.3 Cell culture methods

3.3.1 Culturing of Cells

Human embryonic kidney (HEK293T) cells were cultured in DMEM⁺⁺⁺. Dulbecco's Modified Eagle Medium (DMEM) (high glucose) was supplemented with 10 % foetal calf serum (FCS), 1 mM sodium pyruvate and 1 % penicillin-streptomycin.

THP-1 cells were cultured in RPMI⁺⁺⁺. Roswell Park Memorial Institute (RPMI) 1640 was supplemented with 10 % FCS, 1 mM sodium pyruvate and 1 % penicillin-streptomycin.

N/TERT-1 cells were cultured in N/TERT medium. A 1:2 mixture of Ham's F12) and DMEM (high glucose, no glutamine, no calcium) was supplemented with 1 % non-essential amino acids, 10 mM HEPES, 2 mM GlutaMAX, 0.1 mM CaCl₂, 0.5 % EpiLife defined growth supplement, 25 µg/ml bovine pituitary extract (BPE), 20 ng/ml epidermal growth factor (EGF), and 1 % penicillin-streptomycin.

All cell lines were incubated at 37 °C with 5 % CO₂ and frozen in FCS with 10 % DMSO.

3.3.2 Seeding and Stimulation of Cells

Hek293T cells were washed with 1 x DPBS once and then incubated for 5 min at 37 °C with 0.05 % Trypsin-EDTA. Detached cells were harvested in DMEM⁺⁺⁺, counted with a Bio-Rad cell counter, and seeded as indicated in the different assays in the cell biology methods Chapter 3.4). THP-1 cells were counted in suspension and differentiated into macrophages overnight in 10 cm dishes at 1×10^6 cells per mL with 100 ng/mL of phorbol-12-myristate-13-acetate (PMA). The following day, cells were washed twice with DPBS, detached with DPBS + 2 mM EDTA, and seeded at 8×10^4 cells per well (96-well tissue culture plate in 100 µL of RPMI⁺⁺⁺). THP-1 cells were primed the next day with 2 µg/mL pam3CSK4 for 4 hours and stimulated with VbP for 24 hours.

N/TERT-1 cells were washed with 1 x DPBS once and then incubated for 10 min at 37 °C with 0.05 % Trypsin-EDTA. Detached cells were harvested in DMEM⁺⁺⁺, spun down, resuspended in an appropriate amount of N/TERT-1 media, and counted. Cells were seeded at 5×10^4 cells per well (96-well tissue culture plate in 100 μ L of N/TERT-1 media) for stimulation assays or seeded at 2×10^4 cells per well (96-well tissue culture plate in 100 μ L of N/TERT-1 media) for live-cell microscopy. The following day, N/TERT-1 cells were stimulated with VbP, Anisomycin, and Poly(I:C) for 24 hours.

3.4 Cell Biology Methods

3.4.1 Transfection of plasmids

For transfection of plasmids, HEK293T cells were seeded at $1.5 - 2 \times 10^4$ cells per well in a 96-well tissue culture plate in 100 μ L of DMEM⁺⁺⁺ and 1×10^6 cells per well in a 6-well tissue culture plate in 2 mL of DMEM⁺⁺⁺. The cells were transfected with different plasmids listed in Chapter 3.1.7 using GeneJuice (0.5 μ L/ per 200 ng of DNA) the following day and incubated for 24 h.

3.4.2 ASC Speck Assay

HEK293T cells that stably express ASC coupled to a red fluorescent protein (RFP) were seeded at 1.5×10^4 cells per well in a 96-well Ibidi glass-bottom black plate in 100 μ L of DMEM⁺⁺⁺. The cells were transfected on the next day with plasmids coding for human NLRP1 alone or together with the short or long isoform of wild-type DPP9 (sDPP9 wt/ IDPP9 wt) or mutant DPP9 (sDPP9_R252P, IDPP9_R281P) at indicated concentrations using 0.75 μ L of GeneJuice per well according to the manufacturer's protocol. The cells were imaged 24 hours later using the SYNENTEC CellaVista Cell Imager using an Olympus 203/0.50 Objective. For the quantification of the ASC specks, the total area was examined from brightfield images for the normalisation between wells, and the number of ASC specks was

counted from fluorescent images using an optimised processing function of 'Count Fluo Dots'.

3.4.3 Overexpression Assay

HEK293T cells were transfected with plasmids coding for the short or long isoform of wild-type DPP9 (sDPP9 wt/ IDPP9 wt) or mutant DPP9 (sDPP9_R252P, IDPP9_R281P) according to the manufacturer's protocol. To keep the DNA concentration for each well constant, a plasmid encoding for HA-eGFP was co-transfected. The following day, the wells were washed once with 1 x DPBS, then lysed in 50 μ L 1 x Lämmli and transferred in fresh PCR tubes for immunoblotting.

3.4.4 Inflammasome Activation Assay

HEK293T cells were transfected on the next day with plasmids coding for inflammasome components with the following concentrations: 2 ng ASC, 5 ng GSDMD, 20 ng caspase-1, and 25 ng pro-IL-1 β . Additionally, plasmids coding for human NLRP1/ human CARD8 alone or together with the short or long isoform of wild-type DPP9 (sDPP9 wt/ IDPP9 wt) or mutant DPP9 (sDPP9_R252P, IDPP9_R281P) at indicated concentrations were co-transfected using 0.75 μ L of GeneJuice per well according to the manufacturer's protocol. DNA concentrations were kept constant by co-transfecting HA-eGFP. 24 hours later, the supernatant was replaced with fresh medium containing 4 μ M VbP and incubated for 4 hours. 30 min before the 4-hour stimulation ended, designated wells for the maximal lysis were treated with 10 x Lysis Buffer (Cytotoxicity Kit), and afterwards, the supernatant was harvested into a fresh supernatant plate.

3.4.5 Lentiviral transduction

HEK293T cells were seeded at 1.2×10^6 cells per well in a 6-well plate (tissue culture plate) in 2 mL of DMEM⁺⁺⁺. The cells were transfected on the next day with 0.75 μ g transfer plasmid of HA-tagged constructs in the pFUGW_Blasticidin backbone together with the lentiviral packaging plasmids pMDLg/pRRE (1.125 μ g),

pRSV-rev (0.375 µg), and pCMV-VSV-G (0.75 µg) using PEI Max according to the manufacturer's protocol. The lentiviral supernatant was harvested after 48 hours and filtered through a 0.45 µm pore filter. THP-1 cells were transduced at a density of 1×10^6 cells per mL in a 6-well plate (tissue culture plate) in a 1:2 mixture of viral supernatant and fresh RPMI⁺⁺⁺ media. N/TERT-1 cells were seeded at 1×10^6 cells per T-25 flask (tissue culture flask) and transduced the following day in a 1:2 mixture of viral supernatant and fresh N/TERT-1 media. 48 hours later, the cells were selected using respective media with 5 µg/ mL of blasticidin. THP-1 cells were kept at a density of 0.5×10^6 cells per mL for the following three days, and N/TERT-1 cells were seeded at 1.5×10^6 cells per T-25 flask (tissue culture flask) for the first split in selection media.

3.5 Biochemical methods

3.5.1 Immunoblotting

For immunoblotting, the lysed cells in 1 x Lämmli Buffer were boiled for 5 min at 95 °C and then loaded next to the PageRuler™ Prestained Protein Ladder onto a denaturing TRIS-Glycine SDS-PAGE running at 80 V for 10 min, followed by 1 h at 120 V, and finally blotted onto 0.45 µm nitrocellulose membranes. After blocking in 3 % milk, the membranes were incubated at 4 °C overnight in the primary antibody, which was diluted 1:1000 in 3 % milk with 0.002 % sodium azide. The next day, the membranes were washed three times with PBS-T and incubated at room temperature (RT) for one hour in the respective secondary antibody, which was diluted 1:10000 in 3 % milk. Afterwards, the membranes were washed three times with PBS-T and detected using the Immobilon Forte Western HRP substrate for detection. All the antibodies used are listed in the table in Chapter 3.1.1.

3.5.2 Cytotoxicity assay

For the measurement of cytotoxicity, the lactate dehydrogenase (LDH) release of cells was measured according to the manufacturer's protocol. For the results, the

only medium control was subtracted for the background, and then the values were normalised to a lysis control done in the same experiment.

3.5.3 Enzyme-linked immunosorbent assay (ELISA)

The human IL-1 β ELISA was performed according to the manufacturer's protocol.

3.5.4 Fluorescence microscopy

For the detection of the fluorescently labelled DPP9 isoforms, HEK293T cells were seeded at 4×10^5 cells per well in a 12-well plate (tissue culture plate) in 1 mL of DMEM⁺⁺⁺. The following day, 200 ng of plasmids encoding for GFP-tagged short and long isoforms of DPP9 were transfected using GeneJuice. After 24 h, MitoBrilliant646 (1:1000) and Hoechst (1:1000) were added and incubated for 30 min. Afterwards, cells were imaged using a Leica DMI8 inverted microscope equipped with an HC PL FLUOTAR L 20 \times /0.40 DRY objective lens and ORCA-Flash4.0 LT+ Digital CMOS camera (Hamamatsu). Merged images were generated using Fiji/ImageJ.

3.5.5 Live-cell microscopy

For the live-cell microscopy, N/TERT-1 keratinocytes were seeded at 2×10^4 cells per well in a 96-well glass-bottom black plate (Ibidi) in 100 μ L of DMEM⁺⁺⁺. After 24 h, propidium iodide (PI, 1:1000) was added, and the cells were imaged 24 h every 30 min using the Leica DMI8 inverted microscope equipped with an HC PL FLUOTAR 10 \times /0.32 DRY objective lens and ORCA-Flash4.0 LT+ Digital CMOS camera (Hamamatsu). For the quantification of PI-positive cells and the total number of cells, batch processing of Fiji/ImageJ was used on the images. The codes used are printed in the appendix.

3.6 CRISPR/ Cas9 mediated knockout generation

3.6.1 Nucleofection of cells

For the knockouts generation, CRISPR/ Cas9 ribonucleoproteins (RNPs) were assembled by hybridising two different sgRNA (each one 100 pmol) and tracrRNA (200 pmol) for 5 min at 95 °C and following incubation at room temperature (RT) for 30 min. Afterwards, the sgRNA:tracrRNA duplex was mixed with 80 pmol of recombinant Cas9 protein and incubated for 15 min at RT. N/TERT-1 cells were trypsinised, harvested in DMEM⁺⁺⁺, and washed with DPBS. For nucleofection, 1.5×10^6 cells were resuspended in 20 μ L of P3 Primary Cell Nucleofector Solution with Supplement 1 (supplement to P3 solution ratio: 1 to 5.5). Afterwards, the prepared RNPs were mixed with the cell suspension and electroporated with the DS-138 program in the X Unit of a 4 D Nucleofector. The nucleofected cells were transferred into a T-25 cell culture flask with pre-warmed media. The pool knockout was verified by immunoblotting or Sanger sequencing.

3.6.2 Knockout identification by Sanger sequencing

For Sanger sequencing, 1×10^6 cells were lysed in 1 x Direct Lysis Buffer. Afterwards, sanger sequencing was performed according to the provider's protocol at Eurofins Genomics using the forward primer of the PCR for sequencing.

3.7 Quantification and Statistical Analysis

Statistical significance was examined using a two-way ANOVA with Dunnett's correction for multiple testing, a one-way ANOVA with Sidak's correction for multiple testing, or a paired t-test using GraphPad Prism 9: **** $p \leq 0.0001$; *** $p \leq 0.001$, ** $p \leq 0.01$, * $p \leq 0.05$, ns = not significant. For multiple comparisons in one graph, the major tick indicates the reference bar. Data are presented as mean \pm SEM as indicated.

4 Results

4.1 Identification of a *de novo* mutation in *DPP9*

A patient exhibiting severe pancytopenia and infancy-onset hyperinflammation was referred to the Min Ae Lee-Kirsch group (Wolf et al., 2023). To find the underlying cause of the severe symptoms, whole exome sequencing was performed on the DNA of the patient and his parents. Sequencing unveiled a heterozygous *de novo* mutation in *DPP9* in the patient, a single base change from G to C at position 755, altering the amino acid residue from arginine (Arg, R) to proline (Pro, P) (Figure 13A). This mutation in *DPP9* is a non-synonymous single-nucleotide polymorphism (nsSNP), a subtype of SNVs, which is not present in the parents (Figure 13, A and B). To investigate the conservation of this arginine residue (R252), a multiple species alignment was done. This showed a high degree of conservation of R252 in a highly conserved protein region between the different species (Figure 13C).

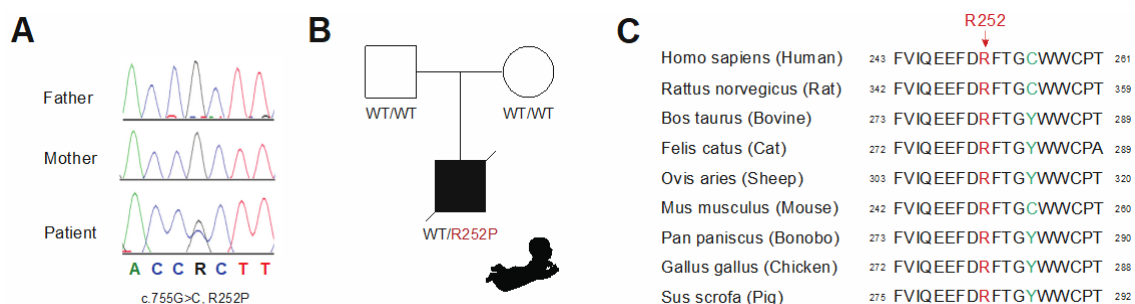


Figure 13: The *de novo* R252P patient mutation is localised in a conserved region of *DPP9*. (A) Electropherograms of the family display a heterozygous mutation (c.755G>C, R252P) in the patient that is absent in the parents (Wolf et al., 2023). (B) Pedigree showing *DPP9* genotype of individuals of the patient's family. (C) Multiple species alignment shows the high conservation of R252 (marked in red) in the *DPP9* protein sequence. The adjacent sequence to R252 is highly conserved except for the amino acids marked in green.

To assess the probability of the mutation having functional effects or damaging the protein, a prediction tool for the possible impact of non-synonymous SNPs on the protein was utilised. Polymorphism Phenotyping v2 (PolyPhen-2) prediction employs sequence, phylogenetic, and structural information to judge the impact of an amino acid change (Adzhubei et al., 2010). PolyPhen-2 categorised the R252P

mutation as “probably damaging”, indicating an effect on the protein function (Figure 31, Appendix).

4.2 R252 of DPP9 enhances protein stability

Arginine is a positively charged amino acid essential in forming secondary structures (Gupta and Uversky, 2024). To assess the structural significance of R252, a crystal structure of DPP9 (PDB ID: 6EOQ) was utilised. DPP9 forms functional homodimers (Ross et al., 2018), with R252 (shown in bright orange) located within the WD40 β -propeller domain and the core of the DPP9 protein (Figure 14, A and B). R252 is structurally neighbouring the catalytically active S730 residue of the DPP9 active site (shown in red), located in the α/β -hydrolase domain (Figure 14C).

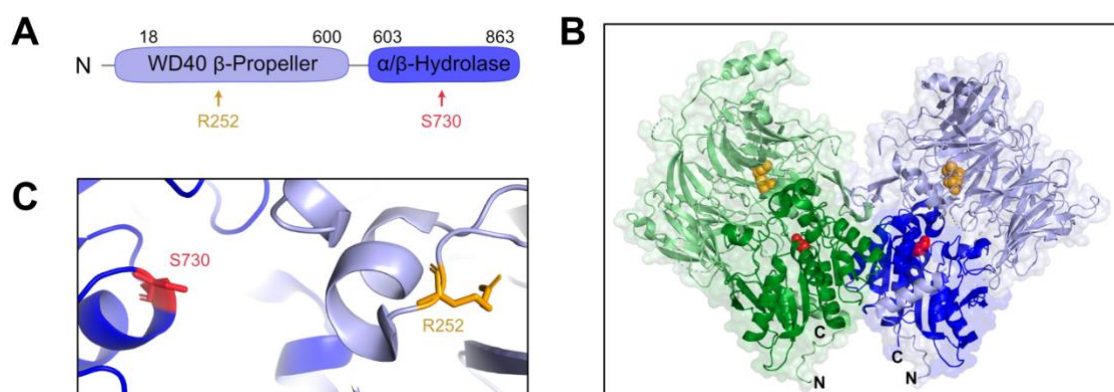


Figure 14: R252 is located in the core of the DPP9 protein. (A) Domain organisation of DPP9, depicting the location of R252 (bright orange) and the catalytically active S730 (red). (B) DPP9 homodimer (PDB ID: 6EOQ) is in cartoon representation with a transparent surface with R252 (bright orange) and S730 (red) in spheres representation. (C) Close-up view on R252 (bright orange) and S730 (red) labelled in stick representation.

A closer look at the local environment of R252 in an electrostatic potential map of DPP9 revealed that R252 is embedded in a hydrophobic pocket formed by the protein segment spanning residues A242 to W258 adjacent to the R252 residue (Figure 15, A and B). Nestled in this pocket, R252 is surrounded by a hydrophobic environment created by predominantly hydrophobic amino acid residues marked in white, including A242, I246, F250, F253 and W257 (Figure 15B), with the exception of the glutamic acid residue at position 278 (E278). Arginine generally

builds electrostatic interactions and forms salt bridges and hydrogen bonds with negatively charged residues. The side chain of R252 establishes polar contacts with structurally close amino acid residues, depicted in a close-up view (Figure 15D). These interactions include a salt bridge with the side chain of E278. In addition, R252 forms hydrogen bonds with three amino acid backbones, specifically the carbonyl oxygen of W254 and the amino acids I352 and A353 (Figure 15D). Thus, R252 plays an essential role in constructing structural features by forming polar contacts and occupying a surface pocket in the core of the protein. This indicates a pivotal role in stabilising the secondary structure and three-dimensional architecture of DPP9.

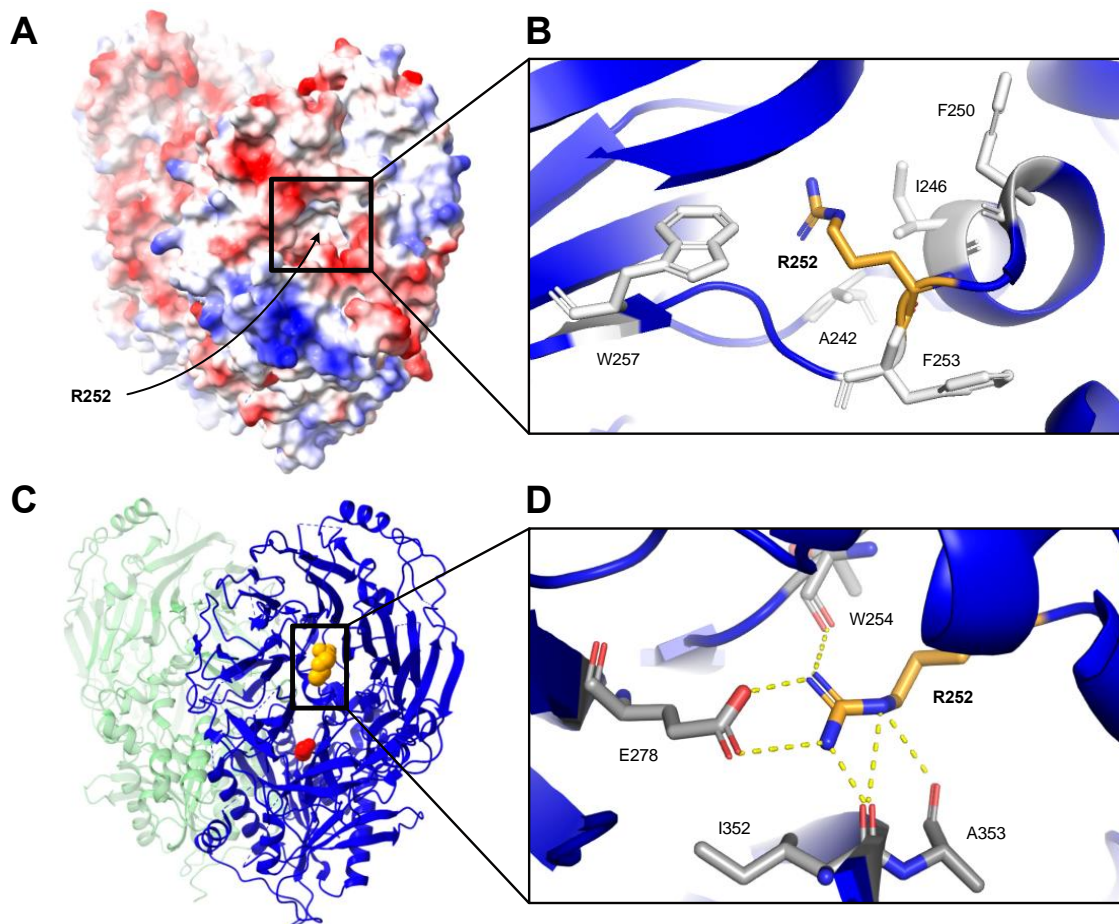


Figure 15: R252 is important for the stability of DPP9 protein. (A) Electrostatic potential map of DPP9 (PDB ID: 6EOQ) with hydrophobic pocket around R252. (B) Hydrophobic amino acids lining R252 (bright orange) are depicted in white stick representation. (C) Cartoon presentation of a DPP9 homodimer (PDB ID: 6EOQ) with R252 (bright orange) and S730 (red). (D) Close-up view of R252 (bright orange) in one monomer of the DPP9 dimer. Interaction partners are labelled in grey stick representation with polar interactions marked in yellow.

4.3 DPP9 R252P mutation induces structural alteration

The patient exhibits a heterozygous substitution of arginine to proline. In contrast to the positively charged arginine side chain, the side chain of proline has no charge and forms a distinctive cyclic structure (Figure 16A). Proline constitutes 6.3 % of all protein composition and is required for tight turns in loops between secondary structural elements, introducing rigidity into protein chains (Chow et al., 2018). Even though proline is crucial for the protein structure by its *cis*- and *trans*-isomerisation in the backbone and maintains protein stability, it disrupts secondary structure elements, such as α -helices and β -sheets (Morgan and Rubenstein, 2013). To investigate whether the R252P mutation affects the structure of DPP9, different protein secondary structure prediction (PSSP) tools were used to predict the adjacent secondary structure elements (Zimmermann et al., 2018). Three different algorithms, including PSIPRED (Jones, 1999), SPIDER3 (Heffernan et al., 2017), and PSSPRED4 (Yan et al., 2013), predict an α -helix formation N-terminally adjacent to or spanning R252 (highlighted in red) (Figure 16B). However, this predicted α -helix formation is lost in the R252P mutant, suggesting structural differences (Figure 16B). The protein secondary structure prediction server JPred 4 (Drozdetskiy et al., 2015) predicted an α -helix spanning ten amino acid residues for wild-type DPP9, ranging from F244 to R252 to F253 (Figure 16C). Furthermore, we analysed the WD40 β -propeller of DPP9, which harbours the R252P mutation, using RaptorX, a protein structure property prediction tool: The analysis revealed a decreased probability of α -helix formation for the mutant compared to the wild-type sequence (Figure 16D). For illustrative purposes, arginine was replaced with proline in the DPP9 crystal structure (PDB ID: 6EOQ) (Figure 16E). R252 of wild-type DPP9 is located next to an α -helix that starts at T243 and ends at the adjacent D251. In wild-type DPP9, the side chain of R252 forms polar contacts with four amino acids, as shown by the yellow lines (as described in the previous chapter). Additionally, arginine interacts with the nitrogen hydrogen in the backbone with the carbonyl oxygen of I246 located in the adjacent α -helix. In contrast to R252, P252 is unable to form polar contacts and hydrogen bonds with backbone DNA; instead, it introduces van-der-Waals clashes, indicating steric interactions (Figure 16E). Thus, this mutation may significantly impact the structure of DPP9.

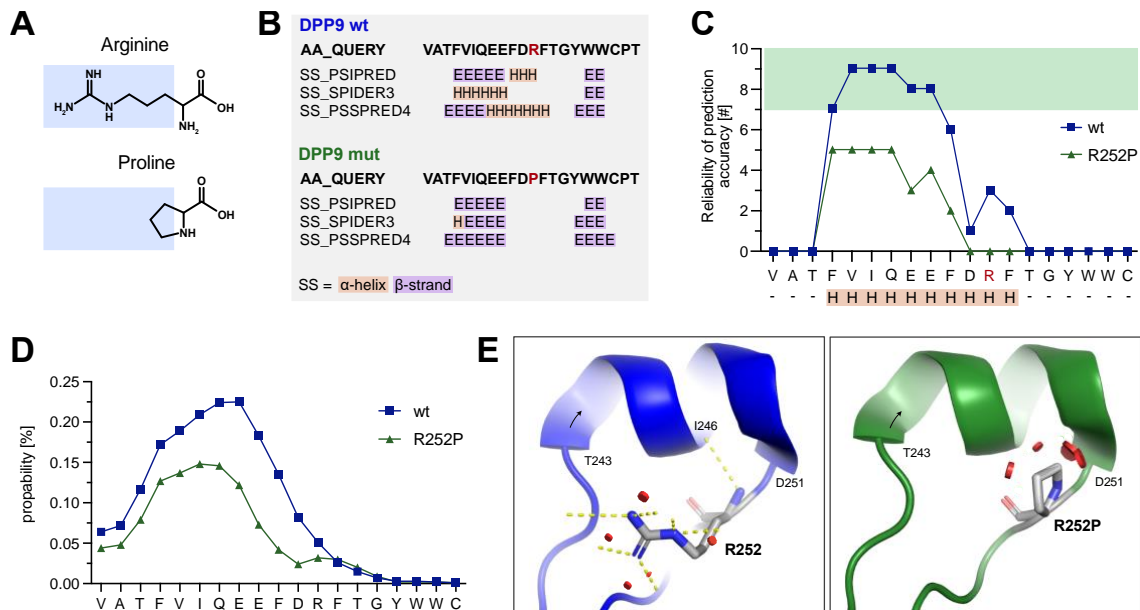


Figure 16: R252P mutation may affect the secondary structure of DPP9. (A) Amino acid structure of arginine and proline. The side chains are highlighted in light blue. (B) Secondary structure prediction of the displayed sequence (QUERY) using three different prediction methods (PSIPRED, SPIDER3, PSSPRED4). AA = amino acid, SS = secondary structure. (C) Secondary structure prediction using JPred4 for the displayed sequence of DPP9. The graph depicts the reliability of prediction accuracy for the predicted formation of an α -helix for DPP9 wt and R252P mutant (bottom; H = α -helix) with a reliable prediction highlighted in a green square. (D) Secondary structure prediction using RaptorX for the WD40 β -propeller of DPP9. The probability of forming an α -helix for the sequence adjacent to R252 is shown. (E) Close-up view of an illustration of R252 and R252P in atom-specific coloured stick representation adjacent to an α -helix in the DPP9 crystal structure (PDB ID: 6EQQ). The α -helix is spanning the protein fragment from T243 to D251. Polar contacts are depicted with yellow lines. Major van-der-Waals clashes are shown in red.

4.4 DPP9 R252P/R281P mutation impairs DPP9 protein stability

Cells express two isoforms of DPP9: a short isoform (863 aa) and a long isoform (892 aa) that carries an additional N-terminal nuclear localisation signal (NLS) (Figure 17A). To examine the cellular localisation of both isoforms, HEK293T cells were transfected with GFP-tagged versions of the short or long isoform of DPP9 (constructs scheme in Figure 17B) and analysed using fluorescence microscopy. As expected, the short isoform of DPP9 is localised to the cytosol, whereas the long isoform of DPP9 is present in the nucleus (Figure 17C). This observation is consistent with the literature (Ajami et al., 2004; Justa-Schuch et al., 2014).

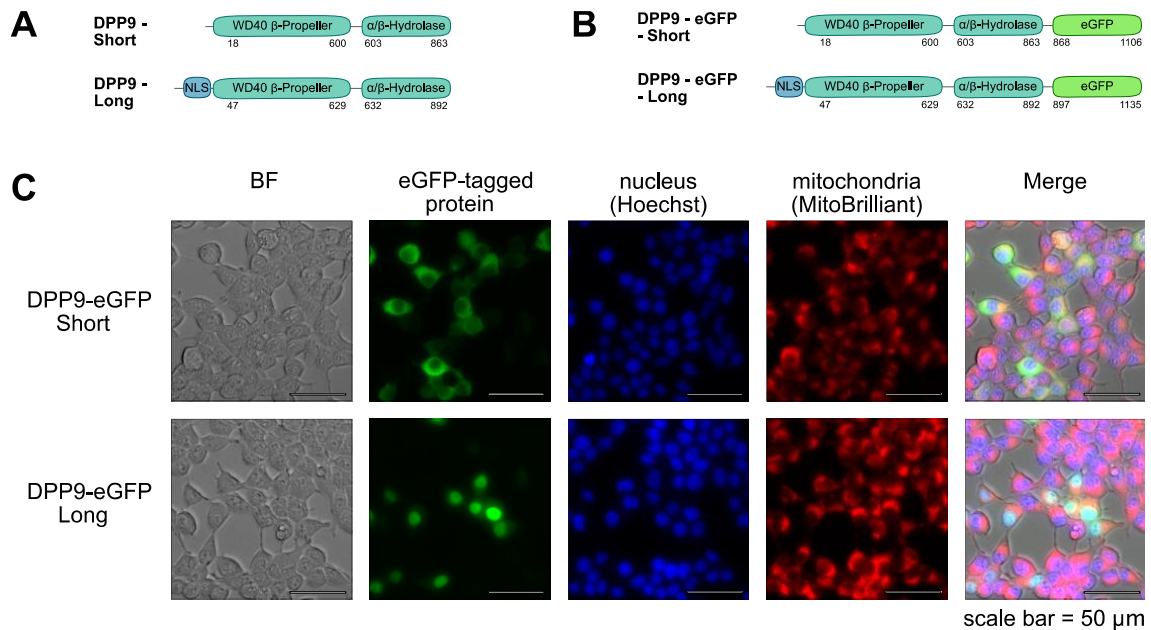


Figure 17: Cellular localisation of the short and long isoforms of DPP9. (A) Domain organisation of the short and long isoform of DPP9, carrying an additional N-terminal nuclear localisation signal (NLS). (B) Domain organisation of the C-terminal eGFP-tagged short and long isoform of DPP9. (C) HEK293T cells were transiently transfected with plasmids encoding for an eGFP-tagged short or long isoform of DPP9 (DPP9-eGFP). After 24h, the localisation of the two DPP9 isoforms is shown by microscopy with additional immunofluorescence staining for the nucleus (Hoechst) and mitochondria (MitoBrilliant646).

The structural model indicates that the patient mutation may cause instability of DPP9 by disrupting the adjacent α -helix. To examine the effect of the mutation on the stability of DPP9, HEK293T cells were transiently transfected with plasmids encoding wild-type and mutant DPP9 (sDPP9 R252P and IDPP9 R281P the short and long isoform, respectively). Cells were transfected with decreasing amounts of plasmid DNA. Immunoblotting showed significantly diminished protein levels of mutant DPP9 in comparison to the respective sample transfected with a plasmid encoding wild-type DPP9 (Figure 18, A and B). Quantification of the immunoblotting for the short isoform of DPP9 revealed a decreased expression of sDPP9 R252P with 52 %, 26 %, and 31 % of sDPP9 wild-type expression (200 ng, 100 ng and 50 ng of sDPP9, respectively) (Figure 18C). Compared to the short isoform, the long isoform of DPP9 showed an even greater reduction in expression of IDPP9 R281P with 28 % and 15 % of IDPP9 wild-type expression (200 ng and 100 ng of IDPP9, respectively) (Figure 18D).

Additionally, patient-derived induced pluripotent stem cells (iPSCs) of the patient also showed decreased DPP9 levels (Data not shown) (Wolf et al., 2023). Collectively, these data show that the R252P/R281P mutation impairs the stability of the DPP9 protein, resulting in reduced expression levels of mutant DPP9.

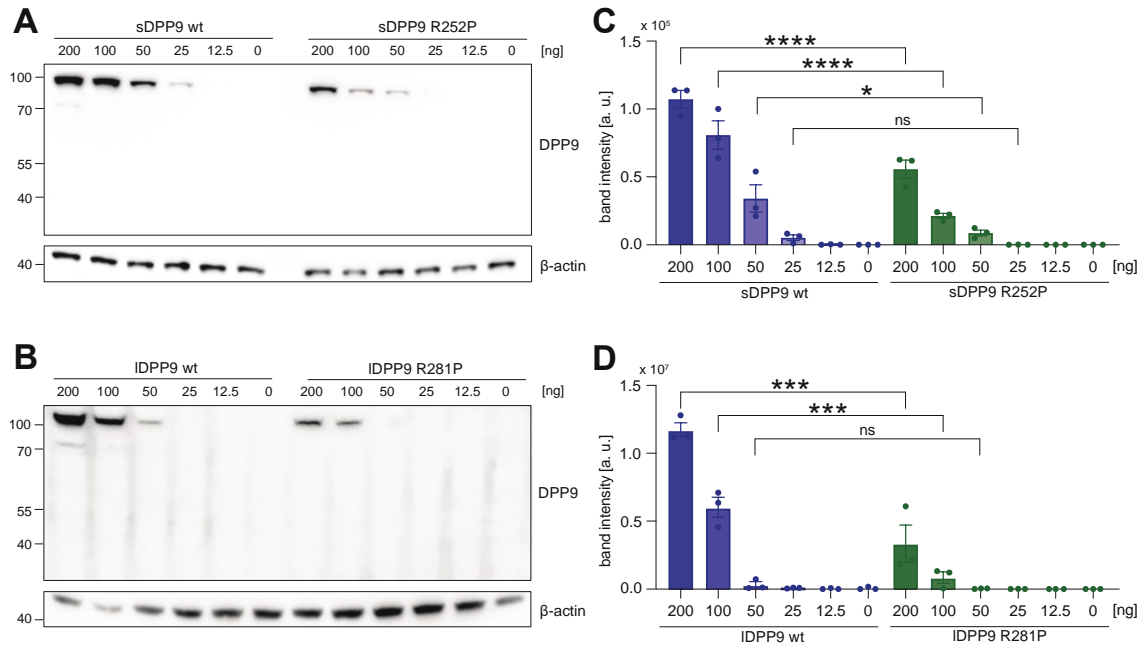


Figure 18: The DPP9 R252P/R281P mutation impairs protein stability. (A, B) HEK293T cells were transiently transfected with plasmids encoding wild-type DPP9 (wt) or mutant DPP9 (R252P/R281P) at the specified concentrations. The expression levels were examined 24 hours later via immunoblotting. One representative immunoblot of three independent experiments is shown. (C, D) Quantification of the band intensities of three independent experiments was done and summarised as mean \pm SEM. A 2-way ANOVA with the Sidak multiple comparisons test was used to perform the statistics. **** $p < 0.0001$; *** $p < 0.001$; * $p < 0.05$; ns = not significant. s = short isoform, l = long isoform.

4.5 DPP9 R252P/R281P mutation leads to activation of the NLRP1 and CARD8 inflammasome

DPP9 functions as an inhibitor of NLRP1 and plays a critical role in regulating NLRP1 inflammasome activation (Taabazuing et al., 2020). NLRP1 inflammasome activation leads to oligomerisation of the adaptor protein ASC, which in turn forms filaments, also known as ASC specks, and thereby provides a platform for caspase-1 activation. To examine whether the R252P/R281P mutation in DPP9 affects the inhibition of the NLRP1 inflammasome activation by DPP9, inflammasome activation assays were performed. To this end, we used HEK293T

cells stably expressing ASC fused to a red fluorescent protein (RFP) tag (ASC-RFP), allowing ASC speck formation to be visualised and quantified by fluorescence microscopy. Transient transfection of the inflammasome sensor NLRP1 alone at increasing concentrations resulted in increased ASC speck formation in cells, indicating inflammasome activation. As a control, the DPP9 wild-type and mutant for both isoforms were transiently transfected without an inflammasome sensor, showing no ASC speck formation (Figure 19, A and D). To investigate the inhibitory role of DPP9 in regulating NLRP1 inflammasome activation, co-expression of NLRP1 and sDPP9 or IDPP9 was performed in the same setting. Expression of the short and long isoforms of wild-type DPP9 resulted in a concentration-dependent reduction of ASC speck formation. At the highest concentration of DPP9, a 1:10 ratio of NLRP1:DPP9, ASC specks were halved for both isoforms (Figure 19, B and E), visualised by microscopy (Figure 19, C and F). In comparison, the co-expression of increasing concentrations of IDPP9 R281P and NLRP1 showed no decrease in ASC specks (Figure 19E). For the short isoform of DPP9, sDPP9 R252P, the level of ASC specks was not affected at lower concentrations of mutant DPP9. However, high concentrations of sDPP9 R252P (1:7 and 1:10 ratio of NLRP1:DPP9) showed a decrease in ASC specks (Figure 19B).

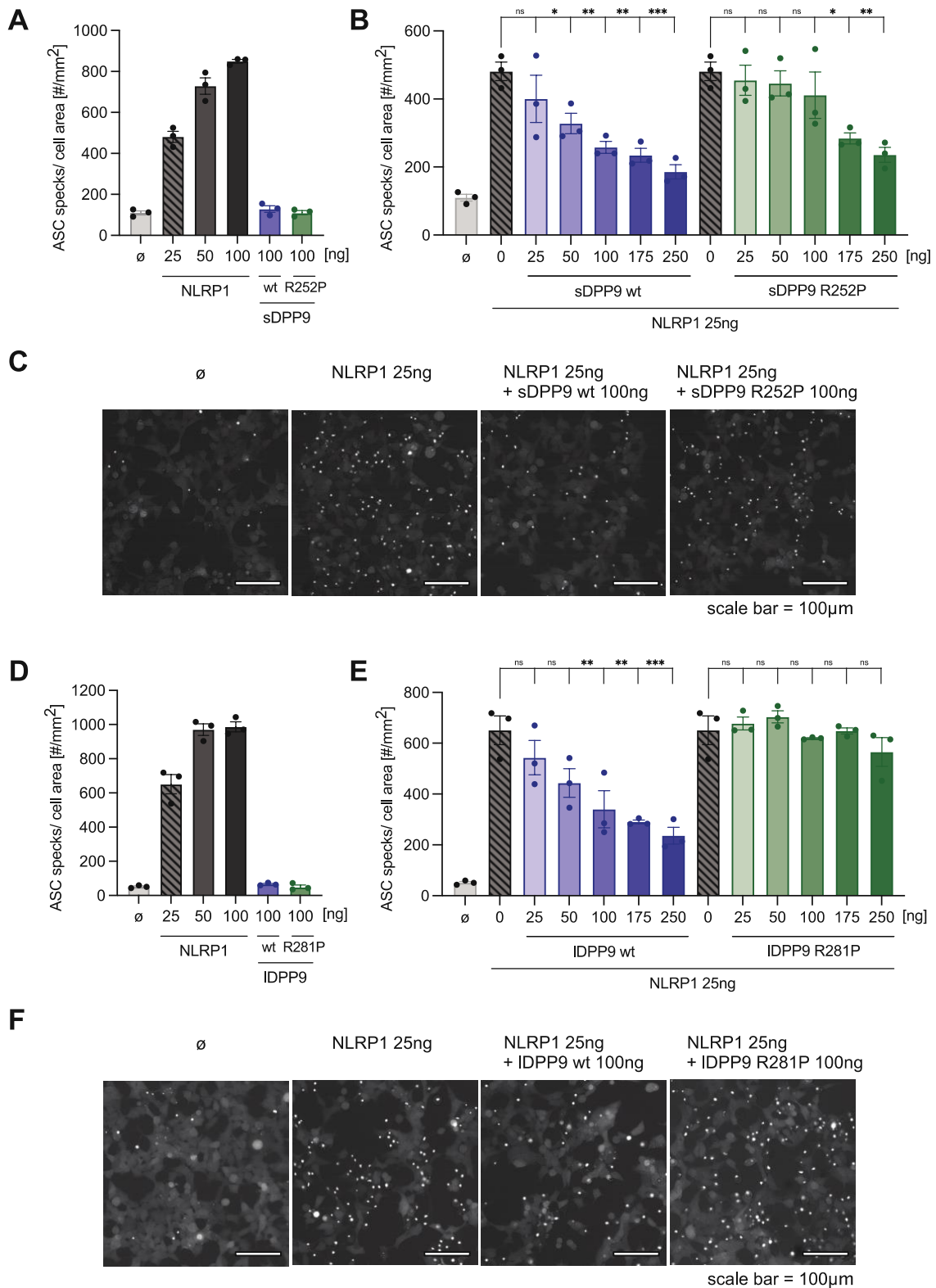


Figure 19: DPP9 R252P/ R281P mutant fails to inhibit NLRP1 inflammasome assembly. (A-F) HEK293T cells expressing ASC linked to a red fluorescent protein (RFP) were transiently transfected with plasmids encoding NLRP1, wild-type DPP9 (wt) or mutant DPP9 (R252P/R281P) at the respective concentrations. **(A, B, D, E)** ASC specks were determined 24 hours later using fluorescence microscopy. The number of ASC specks per cell area was quantified in three independent experiments and summarised as mean \pm SEM. A 1-way ANOVA with Dunnett's multiple comparisons test was used to perform the statistics. *** $p < 0.001$; ** $p < 0.01$.

0.01; * $p < 0.05$; ns = not significant. (C, F) Representative fields of view of B and E of one of three independent experiments are shown. s = short isoform, l = long isoform.

Compared to the NLRP1 inflammasome, which assembles with the adaptor ASC, the CARD8 inflammasome is ASC-independent (Figure 20A) (Taabazuing et al., 2020). To confirm ASC-independent CARD8 inflammasome activation, transient transfection of either NLRP1 or CARD8 with increasing concentrations was performed in HEK293T cells expressing ASC-RFP. Compared to NLRP1, which showed a dose-dependent ASC speck formation, CARD8 did not lead to ASC speck formation, demonstrating ASC-independent inflammasome activation (Figure 20B).

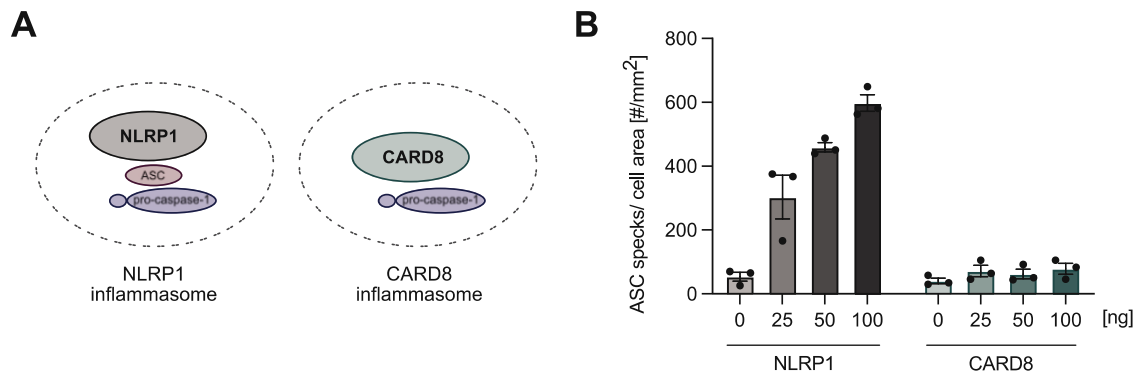


Figure 20: CARD8 inflammasome assembly is independent of the adaptor ASC. (A) Schematic illustration of NLRP1 and CARD8 inflammasome assembly. (B) HEK293T cells expressing ASC-RFP were transiently transfected with plasmids encoding NLRP1 or CARD8 at the respective concentrations. ASC specks were examined 24 hours later using fluorescence microscopy. Quantification of the ASC specks per cell area of three independent experiments was done and summarised as mean \pm SEM.

To assess NLRP1 and CARD8 downstream inflammasome activation, LDH release as a measure of pyroptotic cell death and the pro-inflammatory cytokine IL-1 β were determined in an additional inflammasome assay. To this end, the inflammasome sensor NLRP1 or CARD8 and inflammasome components ASC, caspase-1, pro-IL-1 β , and GSDMD were transiently transfected into HEK293T cells. Upon inflammasome activation, caspase-1 is activated and induces the maturation of IL-1 β by cleaving pro-IL-1 β and additionally cleaves GSDMD, creating pores in the membrane that allow the release of LDH and IL-1 β (Broz and Dixit, 2016). Indeed, increasing concentrations of NLRP1 or CARD8 both resulted in increased

secretion of IL-1 β and elevated levels of LDH release, confirming inflammasome activation (Figure 21, A and C; Figure 22, A and C). Co-expression of wild-type DPP9 and NLRP1 or CARD8 resulted in diminished IL-1 β secretion and LDH release, demonstrating a strong inhibition of NLRP1 and CARD8 by DPP9 (Figure 21, B and D; Figure 22, B and D). Conversely, co-expression of mutant DPP9 R252P/ R281P and NLRP1 or CARD8 resulted in persistent and markedly elevated IL-1 β secretion along with an increase in LDH release (Figure 21, B and D; Figure 22, B and D). This indicates that the R252P/R281P mutant DPP9 lacks the ability to suppress NLRP1 and CARD8 inflammasome activation.

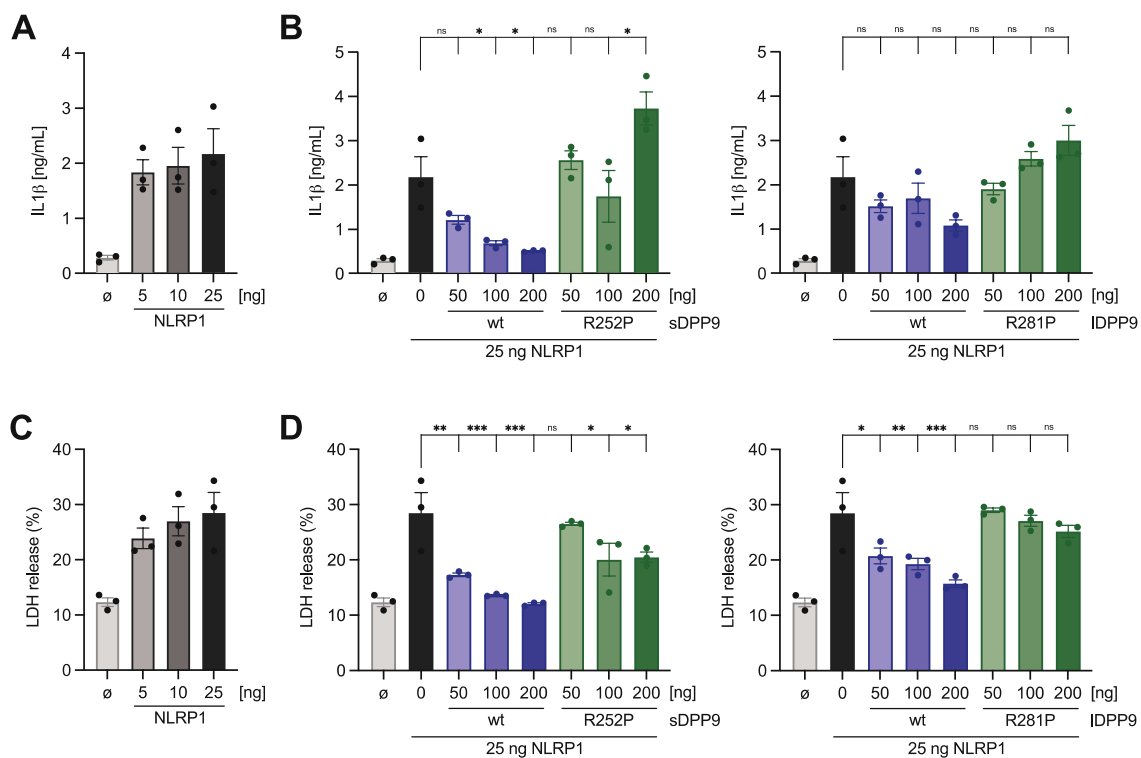


Figure 21: DPP9 R252P/R281P mutant fails to inhibit NLRP1 inflammasome activation. (A-D) HEK293T cells were transiently transfected with plasmids encoding for NLRP1 and inflammasome components and/ or wild-type DPP9 (wt) or mutant DPP9 (R252P/R281P) at the specified concentrations for 24 hours. IL-1 β release was determined using ELISA, and LDH release was measured using a cytotoxicity assay after 4 hours of treatment with 4 μ M Val-boroPro. Data from three independent experiments are summarised as mean \pm SEM. A 1-way ANOVA with Dunnett's multiple comparisons test was used to perform the statistics. ***p < 0.001; **p < 0.01; *p < 0.05; ns = not significant. s = short isoform, l = long isoform.

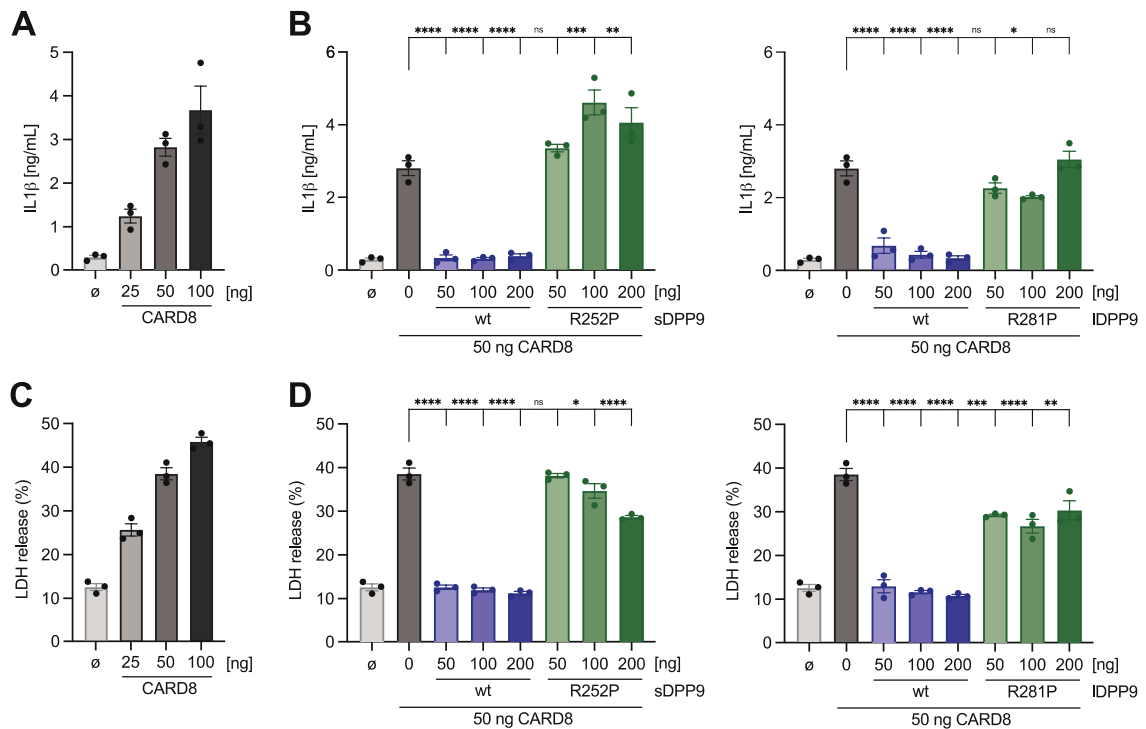


Figure 22: DPP9 R252P/ R281P mutant fails to inhibit CARD8 inflammasome activation. (A-D) HEK293T cells were transiently transfected with plasmids encoding for CARD8 and inflammasome components and/ or wild-type DPP9 (wt) or mutant DPP9 (R252P/R281P) at the specified concentrations for 24 hours. IL-1 β release was determined using ELISA, and LDH release was measured using a cytotoxicity assay after 4 hours of treatment with 4 μ M Val-boroPro. Data from three independent experiments are summarised as mean \pm SEM. A 1-way ANOVA with Dunnett's multiple comparisons test was used to perform the statistics. ****p < 0.0001; ***p < 0.001; **p < 0.01; *p < 0.05; ns = not significant. s = short isoform, l = long isoform.

To summarise, wild-type DPP9 inhibits NLRP1-mediated ASC speck formation and suppresses NLRP1 inflammasome activation, resulting in subsequent IL-1 β secretion and LDH release. In contrast, mutant DPP9 (sDPP9 R252P, IDPP9 R281P) is unable to suppress ASC speck formation and signalling downstream of NLRP1 inflammasome activation, indicating impaired inhibition of NLRP1 inflammasome activation. As for NLRP1, the activation of the CARD8 inflammasome can be inhibited by wild-type DPP9, resulting in decreased LDH and IL-1 β release. However, mutant DPP9 (sDPP9 R252P, IDPP9 R281P) is unable to inhibit CARD8 inflammasome activation.

4.6 DPP9 R252P/R281P mutant exerts a dominant-negative effect on NLRP1 inflammasome activation

NLRP1 is expressed in various cell types, such as monocytes and macrophages. Additionally, NLRP1 has also been shown to be highly expressed in keratinocytes, which are abundant in the skin (Zhong et al., 2016). A cellular model to study endogenous NLRP1 inflammasome activation is the N/TERT-1 cell line, an immortalised but primary cell-like keratinocyte cell line (Zhong et al., 2018). Zhong *et al.* showed that N/TERT-1 cells express NLRP1 and DPP8/9 and that the NLRP1 inflammasome can be activated by DPP8/9 inhibition using the small molecule inhibitor Val-boroPro (VbP) (Zhong et al., 2018). Although VbP activates NLRP1 and CARD8, human keratinocytes were shown to be dependent only on NLRP1 inflammasome activation (Griswold et al., 2022). Additionally, N/TERT-1 keratinocytes were shown to express pro-IL-1 β constitutively, eliminating the need for priming in these cells (Bauernfried et al., 2021). To investigate the effect of mutant DPP9 in a physiological model, transgenic N/TERT-1 keratinocytes were generated via lentiviral transduction using hemagglutinin (HA) -tagged constructs: either wild-type DPP9, mutant DPP9 (sDPP9 R252P, IDPP9 R281P), or green fluorescent protein (GFP). The expression of these transgenes was evaluated by immunoblotting for the HA-tag, which showed expression of all heterologous constructs (Figure 23A). Compared to wild-type DPP9, the expression of mutant DPP9 was significantly lower for the short and the long isoform, with 45 % and 10 % of wild-type DPP9 levels, respectively (Figure 23B). Immunoblotting for DPP9 itself showed that DPP9 is endogenously expressed in keratinocytes. However, it was not possible to differentiate heterologously expressed DPP9 constructs from endogenous DPP9 due to the similar size of the HA-tagged and endogenous protein. To investigate NLRP1 inflammasome activation in these cells, the transgenic N/TERT-1 cells were stimulated with increasing concentrations of VbP. Treatment with the two highest concentrations of VbP led to IL-1 β secretion in all cells with significantly elevated IL-1 β levels for the mutant DPP9 of both isoforms (sDPP9 R252P, IDPP9 R281P) compared to the GFP expressing controls (Figure 23C). Notably, heterologous expression of wild-type DPP9 showed a slight but not significant decrease in IL-1 β secretion, suggesting that increased levels of DPP9 protect the cells from NLRP1 inflammasome activation at low concentrations of

VbP (Figure 23C). Activation of the NLRP1 inflammasome leads to IL-1 β secretion and triggers pyroptotic cell death. Therefore, pyroptosis was investigated by measuring LDH release and performing live cell microscopy on transgenic N/TERT-1 cells upon VbP stimulation. In line with IL-1 β secretion, N/TERT-1 cells expressing mutant DPP9 for both isoforms showed increased levels of LDH release compared to N/TERT-1 cells expressing GFP or wild-type DPP9 (Figure 23D).

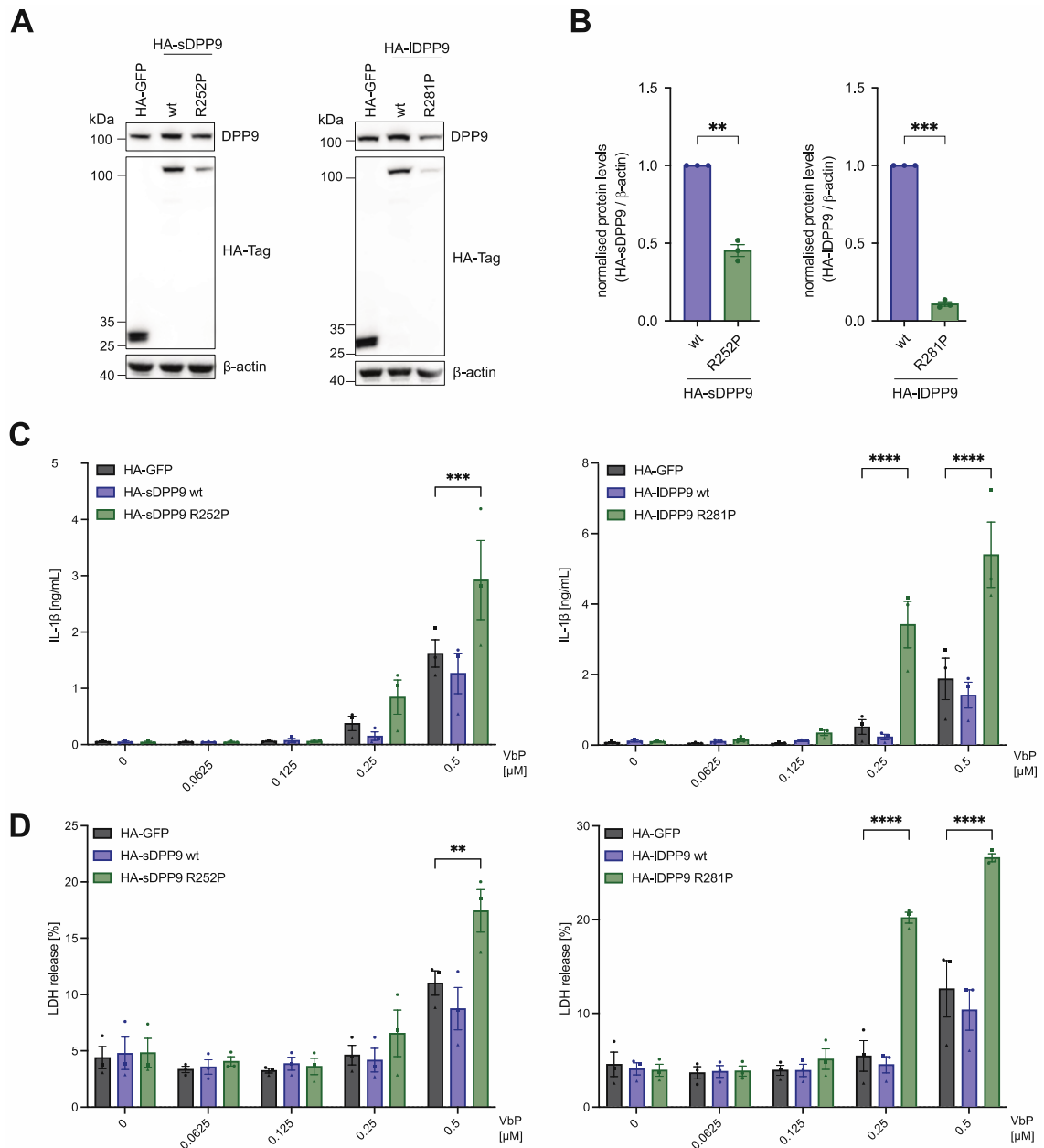


Figure 23: DPP9 R252P/R281P mutant functions in a dominant-negative manner on NLRP1 inflammasome activation. Using lentiviruses, N/TERT-1 keratinocytes were transduced with N-terminal HA-tagged GFP, wild-type DPP9, or mutant DPP9 (R252P/R281P). **(A)** The expression levels of these constructs were examined via immunoblotting, detecting DPP9 (top), HA-Tag (middle), and β -actin (bottom). One

representative immunoblot of three independent experiments is shown. **(B)** A normalised quantification of band intensities of HA-DPP9 in (A) from three independent experiments are summarised as mean \pm SEM. A paired t-test was performed. *** $p < 0.001$; ** $p < 0.01$. **(C, D)** Transgenic cells were treated for 24 hours with specified concentrations of Val-boroPro (VbP). Data from three independent experiments are summarised as mean \pm SEM. A 2-way ANOVA with Dunnett's multiple comparisons test was used to perform the statistics. **** $p < 0.0001$; *** $p < 0.001$, ** $p < 0.01$. Only significance is highlighted. **(C)** IL-1 β release was measured via ELISA. **(D)** LDH release was measured using a cytotoxicity assay. s = short isoform, l = long isoform.

Live-cell microscopy of the transgenic N/TERT-1 cells expressing HA-tagged GFP, wild-type DPP9, or mutant DPP9 was performed by indirect immunostaining of dying cells. For this purpose, propidium iodide (PI) staining was used, as pyroptotic cells are permeable to PI (Rosenberg et al., 2019). PI⁺ cells were quantified and revealed that cells expressing mutant DPP9 (sDPP9 R252P, IDPP9 R281P) started to die around six to ten hours after stimulation with a low concentration of VbP. In contrast, cells expressing wild-type DPP9 or GFP did not die within the 24 hours measured (Figure 24, A and C). The levels of cell death measured using PI positivity as a readout are consistent with cell death measured via LDH release (Figure 23 E; Figure 24, A and C). Fluorescence microscopy revealed that dying cells exhibit characteristics of pyroptosis, such as “ballooning” of the cells (Figure 24, E and F). Taken together, keratinocytes expressing both heterologous mutant DPP9 and endogenous DPP9 show elevated NLRP1 inflammasome activation and increased pyroptosis. This suggests that the heterozygous patient mutation functions in a dominant negative manner.

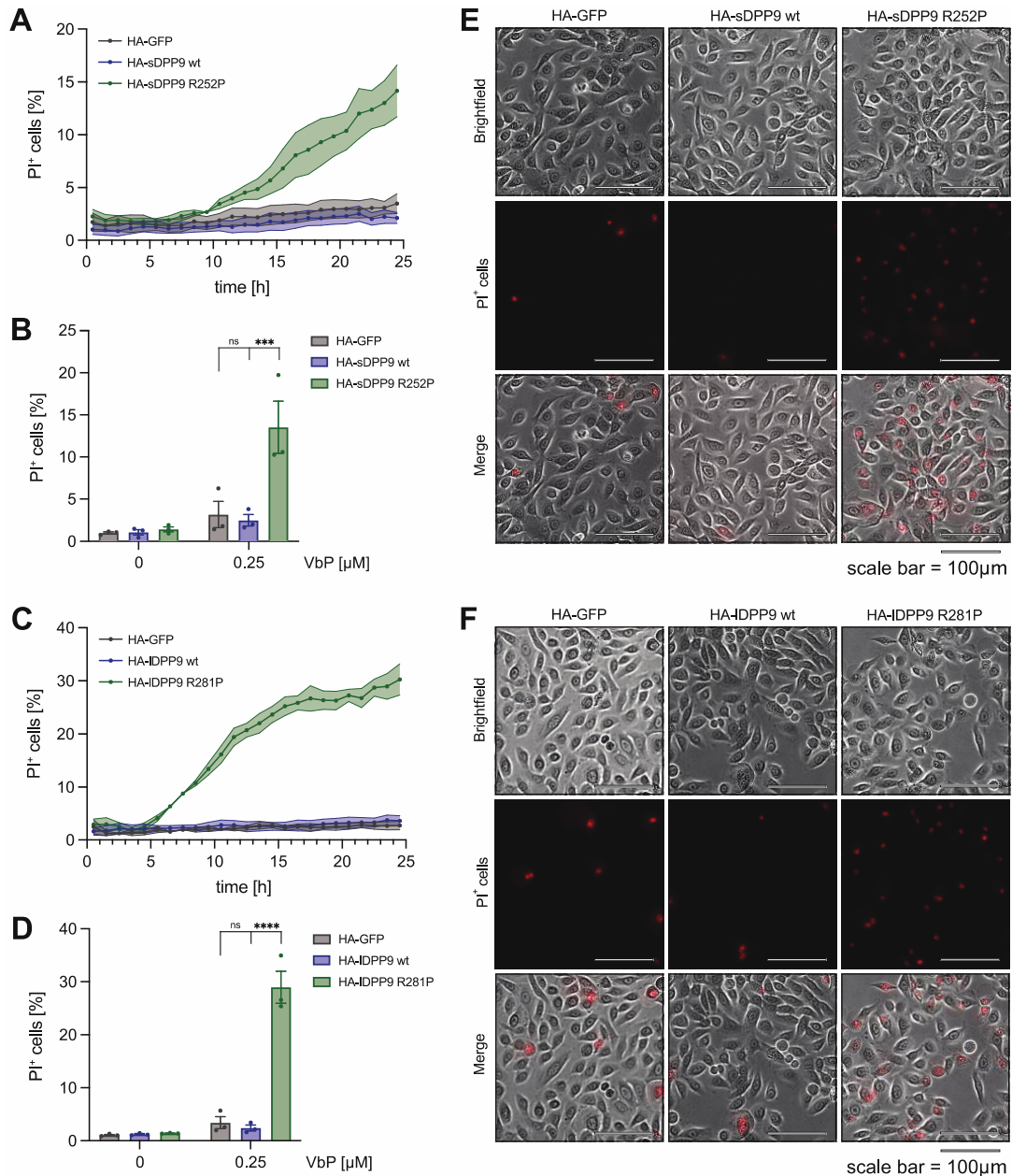


Figure 24: DPP9 R252P/R281P mutant enhances NLRP1 inflammasome-mediated pyroptosis. Using lentiviruses, N/TERT-1 keratinocytes were transduced with N-terminal HA-tagged GFP, wild-type DPP9, or mutant DPP9 (R252P/R281P). Transgenic cells were treated with indicated concentrations of VbP and quantified using fluorescence microscopy. **(A, C)** The percentage of PI⁺ cells was analysed by time-lapse microscopy over 24 hours. Data from three independent experiments are summarised as mean ± SEM. **(B, D)** The percentage of PI⁺ cells from (A, C) treated with Val-boroPro (0.25 μM) or untreated (0 μM) after 24 hours is depicted. Data from three independent experiments are summarised as mean ± SEM. A 2-way ANOVA with Dunnett's multiple comparisons test was used to perform the statistics. ****p < 0.0001; ***p < 0.001. **(E, F)** One representative field of view of three independent experiments from (A, C) after 24 hours of 0.25 μM VbP treatment is shown. Scale bars, 100 μm. s = short isoform, l = long isoform.

4.7 DPP9 R252P/R281P mutant exerts a dominant-negative effect on CARD8 inflammasome activation

Activation of CARD8 inflammasome by the DPP8/9 inhibitor VbP was shown in AML cell lines (Johnson et al., 2018) and resting lymphocytes (Johnson et al., 2020; Linder et al., 2020). A cellular model used to investigate the activation of the CARD8 inflammasome is the THP-1 cell line, a human leukaemia monocytic cell line (Okondo et al., 2017). VbP-induced inflammasome activation in THP-1 cells was shown to be dependent only on the CARD8 inflammasome. To investigate the ability of mutant DPP9 to suppress CARD8 inflammasome activation, transgenic THP-1 cells were generated. Immunoblotting of transduced THP-1 cells expressing HA-tagged GFP/ wild-type DPP9 (sDPP9/ IDPP9)/ or mutant DPP9 (sDPP9 R252P, IDPP9 R281P) confirmed expression of all heterologous constructs (Figure 25A). As observed for transgenic keratinocytes, immunoblotting of transgenic THP-1 cells showed that both the short and long isoform of mutant DPP9 were expressed at significantly lower levels than wild-type DPP9 with 62 % and 12 % of wild-type DPP9, respectively (Figure 25B). Immunoblotting revealed that DPP9 is endogenously expressed in THP-1 cells. However, it is not possible to distinguish between endogenous and heterologous DPP9 in the immunoblot, as described for the keratinocyte-based overexpression model. To investigate CARD8 inflammasome activation in these cells, THP-1 cells were primed with Pam3CSK4 and stimulated with increasing concentrations of VbP. VbP treatment resulted in significantly elevated IL-1 β levels for the mutant DPP9 of both isoforms (sDPP9 R252P, IDPP9 R281P) compared to the GFP-expressing control (Figure 25C). CARD8 inflammasome results in pyroptosis and the concomitant release of IL-1 β . Therefore, pyroptosis induction was examined by measuring LDH release in these cells. In line with IL-1 β secretion, THP-1 cells expressing either isoform of mutant DPP9 (sDPP9 R252P, IDPP9 R281P) showed increased levels of LDH release compared to THP-1 cells expressing GFP or wild-type DPP9 (Figure 25D). In summary, expression of mutant DPP9 in THP-1 cells leads to the release of the pro-inflammatory cytokine IL-1 β and LDH, suggesting that the heterozygous patient mutation acts in a dominant-negative manner to induce CARD8 inflammasome activation. Higher concentrations of VbP would result in pyroptosis

for THP-1 cells expressing GFP, as seen in the N/TERT-1 keratinocytes (Figure 23, C and D).

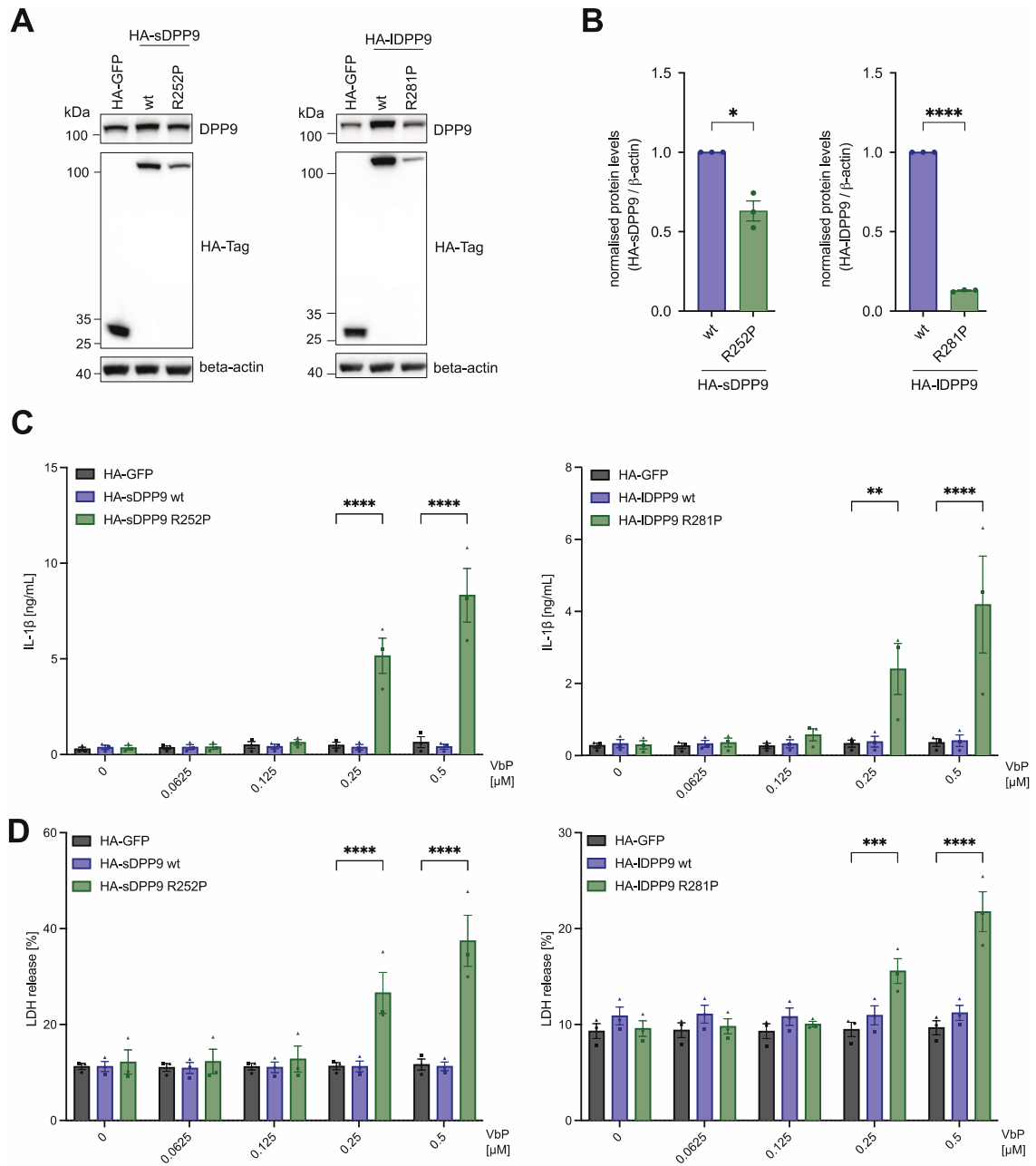


Figure 25: DPP9 R252P/R281P mutant functions in a dominant-negative manner on CARD8 inflammasome activation. Using lentiviruses, THP-1 cells were transduced with N-terminal HA-tagged GFP, wild-type DPP9, or mutant DPP9 (R252P/R281P). **(A)** The expression levels of these constructs were examined via immunoblotting, detecting DPP9 (top), HA-Tag (middle), and β -actin (bottom). One representative immunoblot of three independent experiments is shown. **(B)** A normalised quantification of DPP9 levels detected by immunoblotting (A) from three independent experiments are summarised as mean \pm SEM. A paired t-test was performed. **** p < 0.0001; * p < 0.05. **(C, D)** Transgenic cells were primed for 2 hours with Pam3CSK4 and then treated for 24 hours with specified concentrations of VbP. Data from three independent experiments are summarised as mean \pm SEM. A 2-way ANOVA with Dunnett's multiple comparisons test was used to perform the statistics. **** p < 0.0001; *** p < 0.001, ** p < 0.01. Only significance is shown. **(C)** IL-1 β release was measured via ELISA. **(D)** LDH release was measured using a cytotoxicity assay. s = short isoform, l = long isoform.

4.8 DPP9 knockout in keratinocytes leads to increased inflammation

N/TERT-1 cells are an excellent cellular model for NLRP1 inflammasome activation and have been used in several recent studies. Experiments using transgenic expression of the patient mutation in DPP9 in wild-type N/TERT-1 cells suggest that the mutation has a dominant-negative effect. To investigate whether DPP9 is the key factor for keeping NLRP1 in check in N/TERT-1 keratinocytes, a knockout of DPP9 was performed using the CRISPR/ Cas9 system: wild-type N/TERT-1 cells (WT) were electroporated with Cas9 and two sgRNAs targeting *DPP9*. Immunoblotting confirmed that the DPP9 knockout (KO) was successful, with very low DPP9 levels remaining (Figure 26A). Treatment of DPP9 KO cells with VbP showed a significantly higher release of IL-1 β compared to DPP9 wild-type cells (Figure 26B). There are several DPP9-independent modes for NLRP1 inflammasome activation, including anisomycin (ANS) and the synthetic dsRNA ligand Poly(I:C), as previously shown for N/TERT-1 keratinocytes (Bauernfried and Hornung, 2021). Treatment of N/TERT-1 cells with anisomycin (ANS) and Poly(I:C) led to inflammasome activation and concomitant IL-1 β release in both wild-type and DPP9 knockout cells (Figure 26C). However, DPP9 KO cells did not show elevated levels of IL-1 β release compared to wild-type cells, consistent with a DPP9-independent mode of NLRP1 activation (Figure 26C). Collectively, VbP stimulation of DPP9 knockout N/TERT-1 keratinocytes led to an increase in IL-1 β release compared to wild-type cells. This suggests that the knockout of DPP9 renders the remaining wild-type or heterozygous cells more susceptible to VbP-induced pyroptosis, leading to increased IL-1 β release.

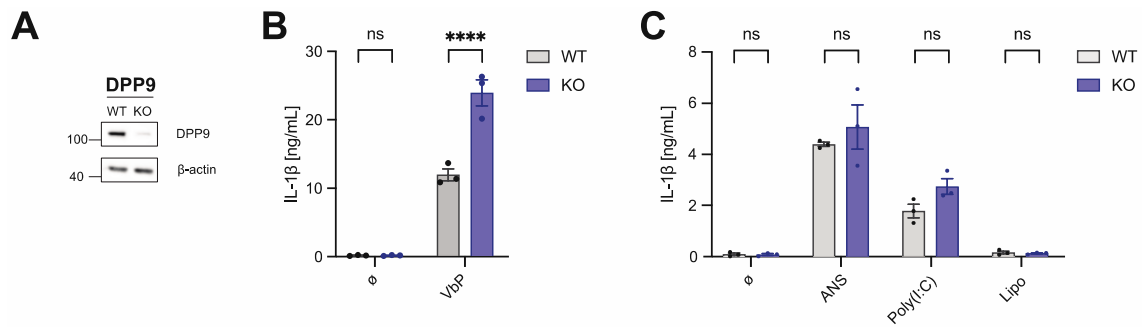


Figure 26: DPP9 knockout in N/TERT-1 keratinocytes results in increased IL-1 β release for DPP9-dependent NLRP1 inflammasome activation. N/TERT-1 keratinocytes were nucleofected with sgRNAs targeting DPP9 using CRISPR/Cas9. **(A)** The expression level of endogenous DPP9 was determined via immunoblotting, probing for DPP9 (top), and β -actin (bottom). One representative immunoblot of three independent experiments is shown. **(B)** DPP9 knockout (KO) and unmodified N/TERT-1 keratinocytes (WT) were treated for 24 hours with 4 μ M VbP. IL-1 β release from three independent experiments is summarised as mean \pm SEM. A 2-way ANOVA with Dunnett's multiple comparisons test was used to perform the statistics. **** $p < 0.0001$; ns = not significant. **(C)** DPP9 knockout (KO) and unmodified N/TERT-1 keratinocytes (WT) were treated for 24 hours with 4 μ M anisomycin (ANS) or transfected with 400 ng Poly(I:C) or Lipofectamine (Lipo) alone. IL-1 β release from three independent experiments is summarised as mean \pm SEM. A 2-way ANOVA with Sidak's multiple comparisons test was used to perform the statistics. ns = not significant.

4.9 DPP8 and DPP9 have redundant functions in N/TERT-1 keratinocytes

DPP8 and DPP9 share many structural similarities and have been shown to be redundant in their enzymatic activity. Several cell lines, for instance, the monocytic THP-1 cell line, express both homologues and inhibition of DPP8 and DPP9 has been shown to induce inflammasome activation (Okondo et al., 2017). To investigate the impact and possible redundancy of DPP9 and its homologue DPP8 in N/TERT-1 keratinocytes, DPP8 and DPP9 knockout (KO) as well as DPP8 and DPP9 double KO (dKO) cells were generated using the CRISPR/ Cas9 system with two guide RNAs per gene. In addition to N/TERT-1 wild-type cells, DPP8 and DPP9 knockouts were also generated in N/TERT-1 NLRP1 KO cells. Immunoblotting confirmed the NLRP1 KO in the N/TERT-1 NLRP1 KO cells and revealed a pool knockout of DPP9 (KO) with very low remaining DPP9 levels for the DPP9 KO cells as well as the DPP8/9 dKO cells (Figure 27A). DPP8 knockout was confirmed using Sanger sequencing, showing high efficiency of the two guide

RNAs in the DPP8 KO and DPP8/9 dKO cells (Figure 27B). To examine the growth of these knockout cells, three independent KOs for each genotype were created and counted at each split. Cell counts were normalised to the control KO cells (Ctrl). Data revealed a high initial cell death within the first three days for DPP8, DPP9 and DPP8/9 dKO cells after electroporation compared to the control cells (Figure 27C). DPP8/9 dKO cells still showed reduced cell count at day 8, whereas the cell counts of single knockouts are comparable to the control cells. These data indicate that functional DPP8 and DPP9 are important for N/TERT-1 keratinocytes, and one homologue is sufficient for the survival of the cells.

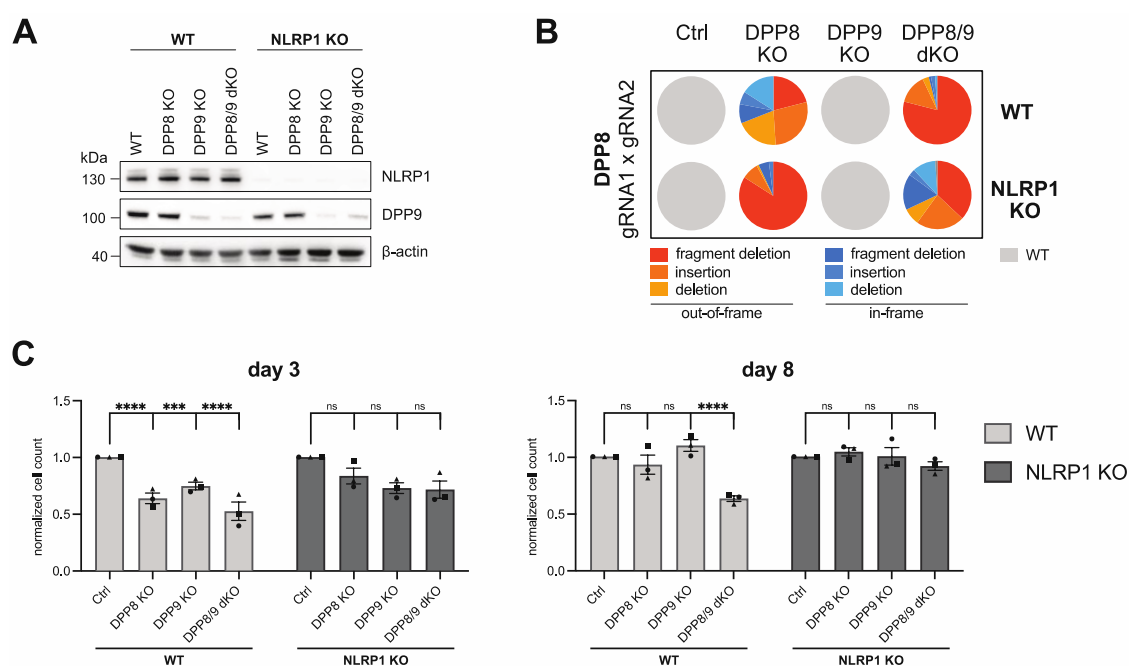


Figure 27: Knockout of DPP8 and 9 in N/TERT-1 keratinocytes. N/TERT-1 keratinocytes, wild-type (WT) or NLRP1 knockout (NLRP1 KO), were nucleofected with sgRNAs targeting either DPP8 or DPP9 or both using CRISPR/Cas9. **(A)** The expression levels of NLRP1, DPP9, and β -actin were determined via immunoblotting on day 8, probing for NLRP1 (top), DPP9 (middle), and β -actin (bottom). One representative immunoblot of three independent experiments is shown. **(B)** DPP8 knockout was confirmed using Sanger Sequencing on day 8, displaying out-of-frame (orange), in-frame (blue) variants, and wild-type (WT) (grey). **(C)** After nucleofection, the cells were seeded with the same cell count and counted three days and eight days after nucleofection. Cell counts were normalised to the control (Ctrl). Data from three independent experiments are summarised as mean \pm SEM. A 2-way ANOVA with Dunnett's multiple comparisons test was used to perform the statistics on cell counts before normalisation. ****p < 0.0001; ***p < 0.001; ns = not significant.

To examine whether the knockout of one of the two homologues or the double knockout of DPP8 and 9 results in IL-1 β release as expected for pyroptosis, these knockout cells in the wild-type background were seeded. This revealed an increased IL-1 β release for DPP8 knockout and DPP8/9 double knockout cells, not only in the stimulated cells but also in the unstimulated cells (Figure 28A). Since

DPP9 knockout alone led to an increase in IL-1 β secretion in N/TERT-1 keratinocytes (Figure 26), these cells were stimulated with a low concentration of VbP. This resulted in an elevated IL-1 β release for all knockout cell lines compared to the wild-type control cells. Strikingly, the release of IL-1 β is markedly increased in the double knockout cells. Subsequent immunoblotting of these cells revealed higher pro-IL-1 β levels in DPP8 KO and DPP8/9 dKO cells (Figure 28, B and C).

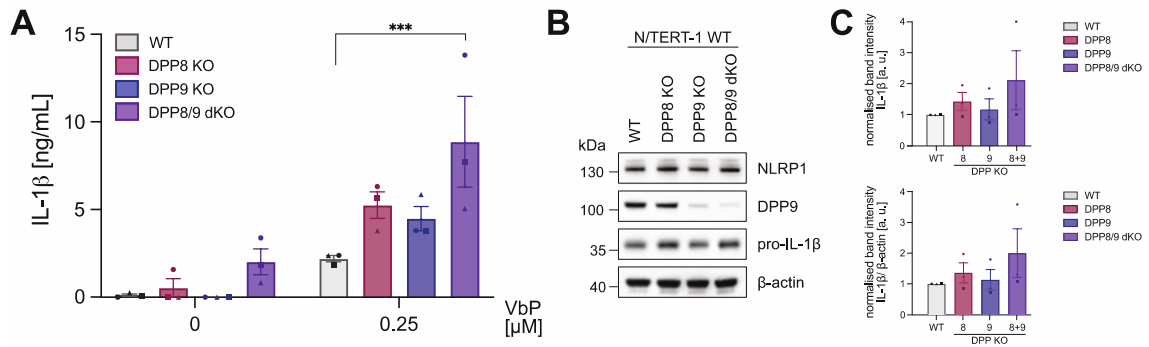


Figure 28: Knockout of DPP8 and 9 in N/TERT-1 keratinocytes results in increased IL-1 β release. N/TERT-1 keratinocytes were nucleofected with sgRNAs targeting either DPP8 or DPP9 or both using CRISPR/Cas9. **(A)** Eight days after nucleofection, these cells were stimulated for 24 hours with VbP (0.25 μ M) or left untreated. IL-1 β release from three independent experiments is summarised as mean \pm SEM. A 2-way ANOVA with Dunnett's multiple comparisons test was used to perform the statistics. **** p < 0.0001; *** p < 0.001. Only significance is shown. **(B)** The expression levels of NLRP1, DPP9, pro-IL-1 β , and β -actin were determined via immunoblotting, probing for NLRP1 (top), DPP9 (middle up), pro-IL-1 β (middle down) and β -actin (bottom). One representative immunoblot of three independent experiments is shown. **(C)** A normalised quantification of pro-IL-1 β levels detected by immunoblotting (B) from three independent experiments is summarised as mean \pm SEM.

Collectively, VbP stimulation of DPP8/9 dKO N/TERT-1 keratinocytes led to a significant increase in IL-1 β release compared to wild-type cells. This suggests that the pool knockout of DPP8 and 9 renders the wild-type or heterozygous cells more susceptible to VbP-induced pyroptosis. The slightly elevated levels of pro-IL-1 β in these cells are an indication that priming of these cells can occur.

5 Discussion

Every day, bacteria and viruses invade the human body, challenging the immune system. Therefore, our immune system requires precise regulation and rapid action to protect against various threats (Murphy and Weaver, 2017). NLRP1 and CARD8 are unique, structurally similar inflammasome sensors that undergo auto-proteolytic cleavage (Taabazuing et al., 2020). Under *steady-state* conditions, the auto-processed non-covalently linked fragments of NLRP1/CARD8 are bound and inhibited by dipeptidyl-peptidases 8 and 9 (DPP8/9). While various studies have demonstrated that disrupting this inhibition induces inflammasome activation *in vitro*, the impact of DPP8/9 on inflammasome regulation *in vivo* is not fully understood.

5.1 Role of DPP9 in regulating inflammasome activation *in vivo*

Two recent studies, including our study, provided insights into the role of DPP9 in inflammasome regulation in patients (Harapas et al., 2022; Wolf et al., 2023). In our study, the molecular basis of a *de novo* mutation in *DPP9*, a substitution of arginine (Arg, R) to proline (Pro, P) at position 252 (R252P), was elucidated. To this end, the role of the R252P mutation on the stability of DPP9 was assessed by investigating R252P in the crystal structure of DPP9 and performing inflammasome activation assays with overexpression of either wild-type or mutant DPP9. To further investigate the impact of the DPP9 mutant in physiological models, we employed different human cell lines, including N/TERT-1 keratinocytes and THP-1 cells. Therefore, we expressed heterologous constructs of wild-type or mutant DPP9 using lentiviral transduction. Subsequently, VbP-induced inflammasome activation was examined in these cells. To study inflammasome activation caused by DPP9 deficiency, CRISPR/Cas9 genome editing was used in N/TERT-1 keratinocytes.

Overall, the study revealed the functional basis for the *de novo* DPP9 R252P mutation, providing insight into the role of DPP9 in regulating inflammasome activation *in vivo*.

5.1.1 DPP9 R252P mutation impairs protein stability

Analysing the patient's DPP9 R252P mutation revealed high conservation of arginine at position 252 (R252) across different species using multiple species alignment, indicating that this residue is important for the function or structure of DPP9. Looking at the crystal structures of DPP9 (PDB ID: 6EOQ, 6EOR, 6QZV, 7A3F), R252 is located in a hydrophobic pocket in the core of the protein near the active site and establishes polar contacts with structurally close amino acid residues (Figure 14, Figure 15). Compared to the wild-type arginine, the substituted proline is uncharged and forms a distinctive cyclic structure, which disrupts secondary structure elements, such as α -helices and β -sheets (Morgan and Rubenstein, 2013). Transient and transgenic overexpression of DPP9 constructs in several cell lines, including HEK293T, THP-1 and N/TERT-1, revealed a significantly lower abundance of the mutant DPP9 protein compared to the wild-type protein (Figure 18, Figure 23, Figure 25). This indicates that the proline mutation impairs the stability of DPP9 not only in an overexpression system in HEK293T cells but also in cell lines with functional NLRP1 or CARD8 inflammasome signalling. These data are in line with the analysis of patient-derived induced pluripotent stem cells (iPSCs) of our patient, which also showed decreased DPP9 levels (Wolf et al., 2023), confirming that the R252P mutation in *DPP9* impairs the DPP9 protein stability. To better understand the impact of the DPP9 mutation on protein stability, the wild-type and mutant DPP9 proteins could be purified. For the characterisation of the protein stability, the recombinant proteins could be used to evaluate how they respond to stress factors such as temperature and agitation and to observe changes in their structure and behaviour. Techniques such as differential scanning calorimetry (DSC) assess thermal stability, while dynamic light scattering (DLS) and size exclusion chromatography (SEC) track aggregation of the protein.

5.1.2 DPP9 R252P mutation results in inflammasome activation in a dominant-negative manner

In addition to decreased DPP9 levels, the patient presented elevated serum levels of pro-inflammatory cytokines, including IL-1 β and IL-18, as well as markedly elevated LDH levels (Wolf et al., 2023). LDH in serum is a hallmark of cell damage, which is often, but not invariably, a component of inflammatory processes, it is released into the bloodstream when cells are damaged or destroyed. IL-1 β , however, plays a central role in inflammation and is often used as a specific marker for inflammatory conditions; importantly, both LDH and IL-1 β are consequences of inflammasome activation. Given that DPP9 is a critical negative regulator of NLRP1 and CARD8 (Taabazuing et al., 2020), we hypothesised that the severe inflammatory phenotype of the patient is caused by inflammasome activation resulting from impaired DPP9 stability. *In vitro* inflammasome activation assays revealed that the DPP9 mutant indeed lacks the capability to inhibit NLRP1 and CARD8 inflammasome activation measured by ASC speck formation as well as LDH and IL-1 β release (Figure 19, Figure 21, Figure 22). In accordance with our data, a recent study described four patients with loss-of-function mutations in DPP9 exhibiting immune-associated defects and dermatological anomalies due to aberrant NLRP1 inflammasome activation (Harapas et al., 2022). The patients in this study have biallelic loss-of-function mutations in DPP9, while their parents are healthy heterozygous carriers (Harapas et al., 2022). In contrast, our patient carried a *de novo* heterozygous DPP9 mutation (WT/R252P) that is not present in either parent (Figure 13) (Wolf et al., 2023) and leads to severe hyperinflammation in the patient. This led to the hypothesis that the heterozygous R252P mutation functions in a dominant-negative manner, interfering with the function of the wild-type protein, even when present in heterozygous individuals. Stimulation of transgenic N/TERT-1 keratinocytes and THP-1 cells with VbP revealed significantly increased IL-1 β release and cell death for cells expressing mutant DPP9 compared to GFP-expressing control cells (Figure 23, C and D; Figure 25, C and D). Notably, heterologous expression of wild-type DPP9 showed a slight decrease in IL-1 β release, suggesting that increased levels of DPP9 protect the cells from NLRP1 and CARD8 inflammasome activation at low concentrations of VbP (Figure 23C, Figure 25C). Live cell microscopy of transgenic N/TERT-1 keratinocytes revealed

the characteristic cell swelling known as “ballooning” upon VbP stimulation, which is indicative of pyroptosis (Figure 24). Collectively, our data indicate that the heterozygous patient mutation impairs DPP9 protein stability and functions in a dominant-negative manner on endogenous DPP9, causing the severe autoinflammation observed in the patient.

5.1.3 Patient mutation induces CARD8 inflammasome activation

As a dominant-negative mutation exerts a detrimental effect on the function of the protein, leading to a similar phenotype in cells as loss-of-function mutations, we used CRISPR/Cas9 to analyse DPP9 deficiency. Deletion of DPP9 in N/TERT-1 keratinocytes showed that DPP9 knockout cells are viable and functional (Figure 27C). In addition to DPP9, many cells express the DPP9 homologue DPP8, which shares 79 % similarity and has a comparable *in vitro* substrate specificity (Bjelke et al., 2006; H.-J. Lee et al., 2006). While deletion of DPP8 alone resulted in viable and functional cells such as the DPP9 deficient N/TERT-1 keratinocytes, DPP8/9 double knockout cells are impaired and showed increased IL-1 β release in unstimulated conditions (Figure 27C, Figure 28A). These data indicate that DPP8 can rescue DPP9 deficiency in immortalised keratinocytes, preventing inflammasome activation. The redundancy of DPP8 and DPP9 in N/TERT-1 keratinocytes is consistent with previous findings. Zhong et al. demonstrated elevated IL-1 β levels following the knockdown of DPP8 and DPP9 in immortalised keratinocytes (Zhong et al., 2018). DPP8-dependent rescue of patients with loss-of-function mutations in DPP9 could explain the milder skin manifestations that were observed in these patients (Harapas et al., 2022). In contrast, Linder et al. demonstrated in a genetic drop-out approach that DPP9 alone restrains CARD8 activation in T-cells, indicating that DPP8 does not rescue DPP9 deficiency in lymphocytes (Linder et al., 2020). This could lead to inflammation in the body due to accelerated inflammasome activation. In line with this, our patient exhibited severe signals of autoinflammation that were detected throughout the body, characterised by reduced levels of lymphocytes, including T- and B-cells, as well as significantly decreased numbers of neutrophils. Additionally, the patient had strongly elevated serum levels of LDH and pro-inflammatory cytokines (Wolf et al.,

2023). Compared to CARD8, NLRP1 inflammasome activation has been demonstrated in epithelial barrier cells (Griswold et al., 2022; Robinson et al., 2020; Zhong et al., 2016). Germline NLRP1 mutations have been described to result in skin lesions and skin cancer caused by NLRP1 inflammasome activation in patients (Zhong et al., 2016). Several gain-of-function mutations in NLRP1 have been previously shown to cause autoinflammation in patients, as described in Chapter 1.4.4 and Figure 11, highlighting a tissue-specific role of NLRP1. However, our patient did not exhibit skin abnormalities, which often develop early in life, often starting in infancy or childhood. To my best knowledge, no gain-of-function mutations of CARD8 have been described in patients yet. However, the severe phenotype in our patient would indicate a high risk for systemic inflammation upon unleashed CARD8 activation.

Of note, no variants were identified in other genes that are known to cause autoinflammation in the patient (Wolf et al., 2023). However, it is possible that variants in genes not yet linked to autoinflammation may contribute to the disease phenotype. In addition to restraining CARD8 and NLRP1 inflammasome activation, DPP9 is involved in various cellular processes, such as mitochondrial homeostasis and DNA repair, through its enzymatic peptidase activity. Studies using gene knock-in mice demonstrated that DPP9 activity is crucial for neonatal survival (Gall et al., 2013; Kim et al., 2017). Another study demonstrated that this neonatal lethality can largely be rescued by additional deletion of NLRP1 (Harapas et al., 2022). This indicates that NLRP1 inhibition is a major physiological role of DPP9, and that the loss of DPP9 function largely affects inflammasome activation.

Taken together, based on the absence of skin abnormalities and the presence of systemic autoinflammation, the patient's inflammasome activation is rather due to CARD8 than NLRP1 inflammasome activation. The high levels of LDH release in the patient could be the result of CARD8-mediated T-cell pyroptosis, which was shown to be dependent on DPP9 but independent of DPP8 activity. Thus, in these cells, DPP9 is crucial for inflammasome inhibition and diminished DPP9 expression is severe, as seen in the patient. Unfortunately, these are only assumptions based on the clinical phenotype of the patient, as more patient material was not available

for functional studies to decipher whether CARD8 or NLRP1 is the inflammasome sensor causing this severe autoinflammation.

5.1.4 DPP9 R252P mutation may interfere with NLRP1 binding

Inhibition of NLRP1 and CARD8 by DPP9 was shown to be dependent on both FIIND domain binding and DPP9 peptidase activity (Zhong et al., 2018). In their study, Zhong et al. demonstrated that an autoinflammation-causing NLRP1 mutation (P1214R) abrogates the binding to DPP9, resulting in inflammasome hyperactivation in the patient. To investigate whether the R252P mutation could impair the binding of NLRP1 and CARD8 to DPP9, structural models of the ternary complexes (described in Chapter 1.4.1 and Figure 6) were used. In brief, three interfaces mediate the ternary complex formation: (I) ZU5^A-DPP9, (II) UPA^B-DPP9, and one of which does not involve DPP9: (III) UPA^A-UPA^B. For CARD8, the two interfaces that bind DPP9 (I and II) are all located on one side of DPP9, spatially distant from the DPP9 R252P mutation (Figure 29A). Like CARD8, the two interfaces of NLRP1 binding to DPP9 are located on the same side of DPP9 (Figure 29B). However, NLRP1 has an extended N-terminus of UPA^B, which is inserted into the active site of DPP9 (Figure 29C) (Hollingsworth et al., 2021; Huang et al., 2021). The active site of DPP9, including the catalytically active serine at position 730 (S730), is structurally neighbouring the R252P mutation (shown in the magenta sphere representation). Hence, the R252P mutation does not interfere with interfaces I and II for CARD8 and interface I for NLRP1 (Figure 29A). But for NLRP1, the R252P mutation could interfere with interface II due to its extended N-terminus of NLRP1 UPA^B into the active site of DPP9 (Figure 29, B and C). To elucidate the impact of the mutation on the specific protein interactions of DPP9 with CARD8 or NLRP1, purified protein could be employed in *in vitro* assays to assess their binding capacities. However, the DPP9 R252P mutant is located next to the active site for both NLRP1 and CARD8. As described, this mutation leads to the instability of the DPP9 protein, which is most upstream in the signalling cascade. If the protein is not folded properly or destabilised and subsequently gets degraded, it is unable to form a ternary complex with NLRP1 or CARD8, resulting

in inflammasome activation. In conclusion, the activation of the inflammasome is due to instability rather than impaired direct binding of DPP9 to CARD8 or NLRP1.

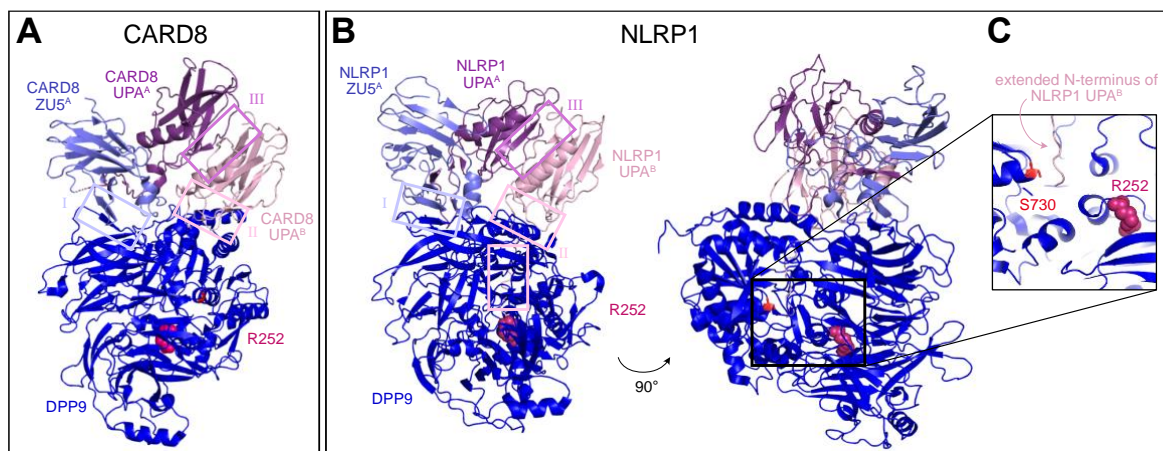


Figure 29: Ternary complexes of CARD8 and NLRP1 with DPP9. Cartoon representation of the CryoEM structures of the ternary complexes with highlighted R252P mutation in magenta sphere representation. **(A)** CARD8-DPP9 ternary complex (PDB ID: 7JKQ). **(B)** NLRP1-DPP9 ternary complex (PDB ID: 6X6A). **(C)** Insertion of the extended N-terminus of NLRP1 UPA^B into the DPP9 active site with S730 highlighted in red stick representation (PDB ID: 6X6A).

5.1.5 DPP9 loss-of-function mutations are intolerated

Investigation into genetic variations of *DPP9* based on the Genome Aggregation Database (gnomAD) revealed no individual with damaging homozygous rare variants and only one individual with two damaging heterozygous rare variants (gnomAD, Broad Institute). This suggests that *DPP9* is highly intolerant to loss-of-function or damaging mutations. Therefore, damaging variants of *DPP9*, such as loss-of-function variants, would likely have a severe biological effect (Karczewski et al., 2020). This underscores the importance of functional DPP9 in humans and explains the severe biological phenotype of previously described patients having biallelic loss-of-function mutations in *DPP9* (Harapas et al., 2022).

Collectively, rare variants that cause loss-of-function or instability of the DPP9 protein are detrimental to cells and likely result in a severe phenotype in patients, as evidenced by our patient (Wolf et al., 2023).

5.1.6 Minimal amounts of DPP8/9 are sufficient for DPP8/9 inhibition

As described, the secretion of the pro-inflammatory cytokine IL-1 β is a major component of inflammasome-induced pyroptosis (Okondo et al., 2017; Taabazuing et al., 2020). Interestingly, stimulation of DPP8/9 dKO keratinocytes with low concentrations of VbP resulted in an increase in IL-1 β release compared to wild-type cells (Figure 28A). It would be intuitive to assume that the functionality of VbP would be compromised in cells lacking DPP8/9. However, the data can be explained by residual levels of DPP8 or 9 present in these cells (Figure 27, A and B). Consequently, even minimal levels of DPP8/9 are sufficient to maintain DPP8/9 inhibition, which triggers VbP-induced inflammasome activation. This is due to the generation of these cells by pool knockout of DPP8 and DPP9 in a single step without single-cell knockout selection. This resulted in efficient but not complete knockout of both targets in each cell, leading to remaining wild-type or heterozygous cells. In line with this, Zhong et al. failed to generate viable clones of DPP8/9 double knockout keratinocytes using CRISPR/Cas9 (Zhong et al., 2018). This observation highlights the difference between two CRISPR/Cas9 knockout generation approaches: pool knockouts and single-cell clones. While pool knockouts allow fast and efficient knockout generation of large numbers of knockouts, the generation of single-cell clones takes longer but results in a homogeneous population with lethal knockout cell death.

Increased IL-1 β release for VbP-induced pyroptosis in the DPP8/9 dKO N/TERT-1 keratinocytes may additionally arise from IL-1 β priming of the remaining wild-type or heterozygous cells. Immunoblotting of cell lysates for pro-IL-1 β indeed revealed slightly elevated levels of pro-IL-1 β in DPP8/9 dKO cells (Figure 28, B and C), indicating that pyroptosis-driven IL-1 β release could create a positive feedback loop. IL-1 β is an important mediator of immune responses, triggering the activation of several signalling pathways in cells, including NF- κ B signalling, which induce the expression of IL-1 targets, such as IL-1 β itself (Weber et al., 2010). Positive feedback loops for IL-1 β amplify the IL-1 β response in cells through paracrine and autocrine signalling (Gaestel et al., 2009). This phenomenon has been observed in several cell types, such as human mononuclear cells (Dinarello et al., 1987).

Taken together, further experiments must be done to examine whether an IL-1 β feedback loop is the reason for the elevated IL-1 β levels in DPP8/9 dKO N/TERT-1 keratinocytes. These could include blocking or knocking out the IL-1R1 receptor and subsequently tests in co-culture experiments.

Taken together, VbP-induced increased IL-1 β release in DPP8/9 dKO N/TERT-1 keratinocytes indicates that minimal amounts of DPP8 or DPP9 are sufficient in these cells to maintain DPP8/9 inhibition.

5.2 Physiological role of DPP8/9 and NLRP1/CARD8 interaction

An important physiological role of DPP8/9 is regulating NLRP1 and CARD8 inflammasome activity by DPP8/9-NLRP1/CARD8 complex formation, which is the most proximal mode of activation of these inflammasomes. While this is not fully understood yet, inhibition of the NLRP1/CARD8 inflammasome activation likely evolved as a surveillance mechanism to fine-tune the immune response.

One physiological role of DPP8/9 inhibition could be continuously monitoring the cellular homeostasis, having an anti-microbial function. While it has been known for several years that destabilisation of the DPP8/9-NLRP1/CARD8 complex activates the NLRP1/CARD8 inflammasome, the physiological triggers are not yet known. Interestingly, it was shown that complex formation alone is not sufficient to inhibit NLRP1/CARD8 inflammasome activation, but also the protease activity of DPP9 is required (Andrew R. Griswold et al., 2019; Huang et al., 2021). This raises the question of whether DPP9 substrates may play a role in DPP8/9 inhibition, either directly by interfering with DPP8/9-NLRP1/CARD8 complex formation or indirectly by causing perturbations in cellular homeostasis. Cellular perturbations due to peptide accumulation and protein folding stress induced by aminopeptidase inhibitors have been linked to the binding of these peptides to DPP8/9, triggering NLRP1/CARD8 inflammasome activation (Orth-He et al., 2023; Rao et al., 2022). Revealing substrates of DPP8/9 could provide more insights into how disruptions of cellular homeostasis activate NLRP1 and CARD8. This supports the possibility

that any deviation from normal activity, such as inhibition of DPP8/9 by pathogenic or host-derived factors, could trigger an immune response mediated by activation of the NLRP1 or CARD8 inflammasome. Consistent with this idea, the ability of NLRs to detect cellular perturbation may reflect an ancient mechanism for sensing infection in animals, similar to the guard mechanism in the plant immune response (van Wersch et al., 2020). This surveillance mechanism would enable the immune system to rapidly detect and respond to cellular perturbations caused by external threats or internal dysregulation and to modulate the intensity of the immune response accordingly. One could speculate that this indirect sensing of cellular perturbation could be similar to the sensing of modifications in the RhoA GTPase signalling pathway by the pyrin inflammasome.

In line with finely modulating the immune response, inhibition of NLRP1/CARD8 by DPP8/9 protects from excessive inflammation. As described in the literature, uncontrolled inflammasome activation can lead to chronic inflammation associated with various pathological conditions, including autoimmune diseases and cancer. Germline gain-of-function mutations in *NLRP1* have previously been reported to cause skin inflammatory syndromes and increased susceptibility to skin cancer (Zhong et al., 2016), demonstrating the severity of uncontrolled NLRP1 inflammasome activation. By regulating NLRP1, DPP8/9 help to prevent excessive immune reaction in the body. While there are no published loss-of-function mutations in *DPP8*, DPP9 deficiency has recently been described to cause immune-associated defects and skin manifestations linked to NLRP1 and CARD8 inflammasome activation (Harapas et al., 2022; Wolf et al., 2023). Moreover, DPP9 was shown to be crucial for the neonatal survival of mice partly due to unleashed NLRP1 inflammasome activation (Harapas et al., 2022; Kim et al., 2017), demonstrating a species-overlapping regulatory mechanism of DPP9 regulating NLRP1 and CARD8. This indicates that DPP8/9 maintain tissue homeostasis by finely modulating the balance of immune responses and preventing chronic inflammation associated with auto-immune diseases.

Additionally, inhibition of NLRP1/CARD8 by DPP8/9 may confer an evolutionary advantage. In the ongoing race between pathogens and host immune defences, organisms that can effectively fight infections while maintaining a precise and

controlled immune response are at an advantage. Therefore, evolutionary pressures likely led to the development of regulatory mechanisms, such as the inhibition of NLRP1 and CARD8 by DPP8/9. This prevents the negative effects of chronic inflammation and could provide the ability to modulate the immune system to adapt to different environments and different pathogens.

Taken together, the physiological function of DPP8/9 in regulating NLRP1/CARD8 inflammasome activation is likely to fine-tune the immune response and act as a surveillance mechanism for cellular perturbations. The formation of the DPP8/9-NLRP1/CARD8 complex enables a precise and controlled immune response by monitoring cellular homeostasis and preventing excessive inflammation. By maintaining tissue homeostasis, DPP8 and DPP9 avoid tissue damage, thereby protecting against inflammatory diseases.

5.3 NLRP1 and CARD8 – Why both?

NLRP1 and CARD8 are both crucial inflammasome sensors that play important roles in innate immune defence. Both are kept in check by DPP8/9 and initiate an inflammatory response upon DPP9 inhibition, raising the question of why both sensors are present in the human immune system.

Having redundancy in the immune system is a common strategy to ensure a successful defence against invading pathogens and cellular stress signals. Indeed, both proteins are activated by DPP8/9 inhibition, indicating the redundancy of these sensors. Nevertheless, it has been demonstrated that these sensors exhibit distinct expression patterns and functionalities in different tissues. NLRP1 activation has been demonstrated to occur predominantly in epithelial barriers, such as keratinocytes (Drutman et al., 2019; Zhong et al., 2018). In contrast, the CARD8 inflammasome is activated in bone marrow-derived cells, such as T lymphocytes (Johnson et al., 2020; Linder et al., 2020). If both were solely responsible for detecting activity in DPP8/9, natural selection might have resulted in NLRP1 becoming smaller with fewer regulatory domains, like the inflammasome sensor CARD8. From an evolutionary perspective, natural selection often favours

simplicity and energy efficiency. For example, the expression of a smaller protein, such as CARD8, would consume less energy than the much longer NLRP1 protein. However, natural selection is not limited to energy efficiency but is governed by a balance between many factors, including environmental pressures, functional complexity, and adaptability. In numerous biological processes, complexity is essential for enabling a tightly controlled response to a diverse range of pathogens. As NLRP1 contains an additional NLR portion at its N-terminus, it is capable of detecting a wider range of threats. For instance, NLRP1 is able to recognise long dsRNA, which is generated as an intermediate during the replication of dsRNA viruses. Additionally, complex proteins may be more adaptable to evolutionary changes due to their increased capacity to undergo mutations in specific domains, thereby enabling them to evolve new capacities. Indeed, the linker region of primate NLRP1 indicates a strong pathogen-induced selective pressure during evolution (Chavarría-Smith et al., 2016).

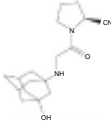
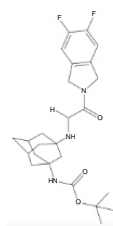
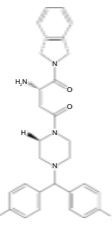
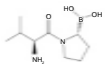
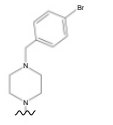
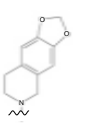
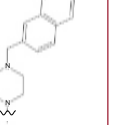
Taken together, the unique tissue-specific differences between CARD8 and NLRP1 suggest that the activation of the NLRP1 and CARD8 sensors is not redundant. In addition, the capacity of NLRP1 to respond to a broader array of potential threats highlights that the presence of both inflammasome sensors is beneficial for humans and that the two play a vital role in a tailored and effective immune response.

5.4 Dipeptidyl-peptidase (DPP) inhibitors

Over the years, inhibitors for dipeptidyl peptidases have been extensively studied. Initially, the majority of research was done on DPP4, utilising its DPP8 and DPP9 homologues as controls for DPP4 selectivity (Edmondson et al., 2004; Lankas et al., 2005). While recent research has concentrated on the identification of selective DPP8/9 inhibitors, this is challenging due to the high homology of DPP8/9, especially in their active sites (Bjelke et al., 2006).

5.4.1 Selective DPP8/9 inhibitors

Currently known inhibitors for DPP8/9 include Vildagliptin, Val-boroPro/Talabostat, and 1G244 (Figure 30). Whereas Vildagliptin and Talabostat are non-selective dipeptidyl peptidase (DPP) inhibitors and suppress other DPPs in addition to DPP8 and DPP9, 1G244 selectively inhibits DPP8 and DPP9 (Zolg et al., 2024). More research has focused on the development of selective inhibitors for differentiating between DPP8 and DPP9. Recent work using activity-based protein profiling (ABPP) has shown promising data on 4-oxo- β -lactams, having a higher specificity (4x to >21x depending on the 4-oxo- β -lactam derivative) for DPP8 than DPP9 (Figure 30) (Carvalho et al., 2022). The differential specificity of these compounds is proposed to be due to the strict ligand binding mode of DPP9 and the high structural instability of DPP8 upon ligand binding compared to DPP9. Three promising compounds (Compd. 6/9/12) were shown to trigger IL-1 β release as well as pyroptosis in murine bone marrow-derived dendritic cells (Carvalho et al., 2022). Additionally, a DPP9 selective inhibitor was derived from Vildagliptin, having a higher selectivity (176x) for DPP9 than DPP8 (Figure 30) (Benramdane et al., 2023).

	DPP9 sensitive		DPP8 sensitive				
Inhibitor	Vildagliptin	Compd. 42	1G244	Talabostat	Compd. 6	Compd. 9	Compd. 12
Structure							
Sensitivity Index (SI)	9.6	176.4	3.8	2.75	7.0	4.2	>21

4-oxo- β -lactam derivatives

Figure 30: Relevant DPP8/9 inhibitors and compounds. The structures of the inhibitors and compounds (Compd.) are depicted (drawn with molview.com). The sensitivity index (SI) for DPP9-sensitive inhibitors and DPP8-sensitive inhibitors was calculated as the ratio $IC_{50}(DPP8)/IC_{50}(DPP9)$ or $IC_{50}(DPP9)/IC_{50}(DPP8)$, respectively (similar for KI' values). IC_{50} values and inhibitor constants KI' were obtained from the literature (shown in Appendix).

Although more selective DPP8/9 inhibitors may be beneficial for the differentiation of independent functions of DPP8 and DPP9, the potential for their therapeutic usage remains uncertain.

5.4.2 Prospects for therapeutic applications

DPP9 plays an important role in biological processes, and its dysregulation is linked to pathophysiological conditions such as cancer and inflammasomopathy. Several cancer studies showed a correlation between high levels of DPP9 and a poor prognosis for the patients (Chang et al., 2023; Saso et al., 2020; Tang et al., 2017). The success of DPP4 inhibitors in treating type II diabetes mellitus (Lambeir et al., 2008) has raised interest in targeting related enzymes like DPP9 to treat diseases with DPP8/9 dysregulation, such as haematological tumours. Indeed, inhibition of DPP8/9 in cancer cells has demonstrated promising results, including reduced cell viability and proliferation in breast cancer cell lines using 1G244 (Sato et al., 2019) and the selective induction of pyroptosis in AML cells using Talabostat (Johnson et al., 2018). However, recent studies on the regulation of NLRP1/CARD8 inflammasome activation by DPP8/9 demonstrated that resting T lymphocytes undergo pyroptosis upon the inhibition of DPP9 (Johnson et al., 2020; Linder et al., 2020), which would be a detrimental side effect for therapy. In addition, other studies demonstrated that global inactivation of the enzymatic activity of DPP9 leads to neonatal lethality in mice (Gall et al., 2013; Harapas et al., 2022; Kim et al., 2017), which highlights the importance of functional DPP9 in cells. Although Talabostat (VbP) was in phase 2 clinical trials for several cancer cell types (Advanced Melanoma: NCT00083239, NCT00083252; Advanced Non-Small Cell Lung Cancer: NCT00080080), data on these studies and on long-term applications of DPP8/9 inhibitors are currently lacking. Therefore, while DPP9 possibly provides new treatment options for certain types of cancer, continued research is necessary to underscore the advantages of developing a safe and efficient inhibitor for clinical use.

5.5 Our work in the context of recent publications

Recently, Harapas and colleagues published a story on a similar topic (Harapas et al., 2022). Even though they also described DPP9 mutations causing uncontrolled inflammasome activation, there are differences between both studies (Harapas et

al., 2022; Wolf et al., 2023). Whereas the clinical phenotypes of the patients are similar in displaying pancytopenia and immune-associated defects, the patients described in the study of Harapas et al. exhibited skin manifestations, whereas the patient described in our study displayed a systemic hyperinflammation without skin involvement (Wolf et al., 2023). Genetic analysis revealed germline mutations in *DPP9* in all patients. Harapas et al. describe biallelic loss-of-function mutations with parents being heterozygous mutation carriers. In contrast, our patient presented a heterozygous *de novo* mutation, not present in either of the parents. This *de novo* mutation is heterozygous and functions in a dominant-negative manner on inflammasome activation. Whereas the clinical phenotype for the four patients of the other study can be explained by unleashed NLRP1 inflammasome activation due to the loss of DPP9, the severe inflammation in our patient is likely caused by uncontrolled CARD8 inflammasome activity due to impaired DPP9 stability.

Overall, both studies provide more insights into the regulatory role of DPP9 *in vivo* in inflammasome activation. Each of the studies clearly demonstrates that DPP9 is a crucial negative regulator of NLRP1 and CARD8 inflammasome activation.

5.6 Limitations of this study

Using functional assays in cell lines, we demonstrated that the DPP9 R252P mutation impairs the DPP9 protein stability, causing severe inflammasome activation. These results mostly explain the clinical phenotype of the patient, shedding light on the regulatory role of DPP9 *in vivo*.

This study describes only one patient with a *de novo* mutation in *DPP9* that is not present in their parents or any other unrelated individuals (Wolf et al., 2023). However, the biochemical and cellular assays align with the clinical phenotype of the patient. Furthermore, the functional data clearly demonstrates that impaired DPP9 stability as a result of the R252P mutation leads to inflammasome activation. This study does not include *in vivo* data; however, a recent study from Harapas and colleagues showed *in vivo* data using knock-in mice with catalytically inactive

DPP9. They demonstrated *in vivo* that DPP9 is essential for mouse survival rescued by the deletion of NLRP1 or its downstream inflammasome components ASC, GSDMD, and IL1R (Harapas et al., 2022).

DPP9 suppresses both closely related inflammasome sensors, NLRP1 and CARD8 (Taabazuing et al., 2020). Based on the clinical phenotype of the patient, we proposed that unleashed CARD8 inflammasome activity may have caused pyroptotic T cell death, as CARD8 pyroptosis was shown to induce T cell death and LDH release (Johnson et al., 2020; Linder et al., 2020). Due to the lack of patient cells for functional assays, no functional assays could be performed with primary material, deciphering CARD8 and NLRP1 inflammasome activation.

Apart from restraining NLRP1 and CARD8 inflammasome activation, human DPP9 is involved in various cellular processes, such as DNA repair and mitochondrial homeostasis, through its enzymatic activity. Although these were not studied in this research, and the patient's phenotype did not match any of them, we cannot entirely exclude the involvement of other DPP9 substrates.

Overall, the functional data clearly demonstrate inflammasome activation caused by DPP9 instability, which fits the phenotype of the patient.

6 Summary

DPP9 is a significant dipeptidyl peptidase in the body, involved in several biological pathways ranging from DNA repair to mitochondrial homeostasis. One of its crucial functions is the negative regulation of NLRP1 and CARD8 inflammasome activation. Inflammasome activation is a crucial process in the innate immune response, coordinating the maturation and release of the pro-inflammatory cytokines IL-1 β and IL-18. The role of DPP9 in regulating inflammasome activation has been demonstrated in several studies *in vitro*, using small molecule inhibitors, such as Val-boroPro in cell lines. Recently, the crystal structure of DPP9 with NLRP1 and CARD8 was solved, showing a ternary complex formation and providing insights into inflammasome activation upon inhibition of DPP9. However, its regulatory role in inflammasome activation *in vivo* is not yet fully understood.

In this study, we set out to investigate the molecular basis of a *de novo* mutation in *DPP9* that was found in a patient exhibiting severe infancy-onset hyperinflammation (Wolf et al., 2023). Multiple species alignment and structural analysis unveiled that the R252P/R281P mutation is located in a highly conserved region in the core of the protein. Overexpression of mutant DPP9 in different cell lines then revealed that the R252P/R281P mutation impairs the stability of the DPP9 protein. Using functional inflammasome assays, we demonstrated that destabilisation of DPP9 results in unleashed NLRP1 and CARD8 inflammasome activation with concomitant pyroptosis measured by LDH and IL-1 β release. In comparison to a recent study describing patients with biallelic loss-of-function mutations in *DPP9* with parents being healthy heterozygous mutation carriers, our patient harboured a heterozygous mutation in *DPP9*. Investigating the hypothesis that the mutation acts in a dominant-negative manner, we expressed transgenes in human cell lines. This revealed that the *DPP9* mutation indeed exerts a dominant-negative effect on endogenous *DPP9*. Based on the clinical phenotype of the patient, we proposed that the *DPP9* mutant resulted in unleashed CARD8 rather than NLRP1 inflammasome activity.

7 Bibliography

- Abbas, A.K., Lichtman, A.H., Pillai, S., 2018. Cellular and Molecular Immunology, Ninth Edition. ed. Elsevier, Philadelphia.
- Abbott, C.A., Yu, D.M.T., Woollatt, E., Sutherland, G.R., McCaughan, G.W., Gorrell, M.D., 2000. Cloning, expression and chromosomal localization of a novel human dipeptidyl peptidase (DPP) IV homolog, DPP8. *European Journal of Biochemistry* 267, 6140–6150. <https://doi.org/10.1046/j.1432-1327.2000.01617.x>
- Ablasser, A., Goldeck, M., Cavlar, T., Deimling, T., Witte, G., Röhl, I., Hopfner, K.-P., Ludwig, J., Hornung, V., 2013. cGAS produces a 2'-5'-linked cyclic dinucleotide second messenger that activates STING. *Nature* 498, 380–384. <https://doi.org/10.1038/nature12306>
- Adams, S., Miller, G.T., Jesson, M.I., Watanabe, T., Jones, B., Wallner, B.P., 2004. PT-100, a Small Molecule Dipeptidyl Peptidase Inhibitor, Has Potent Antitumor Effects and Augments Antibody-Mediated Cytotoxicity via a Novel Immune Mechanism. *Cancer Research* 64, 5471–5480. <https://doi.org/10.1158/0008-5472.CAN-04-0447>
- Adzhubei, I.A., Schmidt, S., Peshkin, L., Ramensky, V.E., Gerasimova, A., Bork, P., Kondrashov, A.S., Sunyaev, S.R., 2010. A method and server for predicting damaging missense mutations. *Nat Methods* 7, 248–249. <https://doi.org/10.1038/nmeth0410-248>
- Ajami, K., Abbott, C.A., McCaughan, G.W., Gorrell, M.D., 2004. Dipeptidyl peptidase 9 has two forms, a broad tissue distribution, cytoplasmic localization and DPIP-like peptidase activity. *Biochimica et Biophysica Acta (BBA) - Gene Structure and Expression* 1679, 18–28. <https://doi.org/10.1016/j.bbaexp.2004.03.010>
- Akira, S., Uematsu, S., Takeuchi, O., 2006. Pathogen recognition and innate immunity. *Cell* 124, 783–801. <https://doi.org/10.1016/j.cell.2006.02.015>
- Alnemri, E.S., Livingston, D.J., Nicholson, D.W., Salvesen, G., Thornberry, N.A., Wong, W.W., Yuan, J., 1996. Human ICE/CED-3 Protease Nomenclature. *Cell* 87, 171. [https://doi.org/10.1016/S0092-8674\(00\)81334-3](https://doi.org/10.1016/S0092-8674(00)81334-3)
- Amarante-Mendes, G.P., Adjemian, S., Branco, L.M., Zanetti, L.C., Weinlich, R., Bortoluci, K.R., 2018. Pattern Recognition Receptors and the Host Cell Death Molecular Machinery. *Front Immunol* 9, 2379. <https://doi.org/10.3389/fimmu.2018.02379>
- Ataide, M.A., Andrade, W.A., Zamboni, D.S., Wang, D., Souza, M. do C., Franklin, B.S., Elian, S., Martins, F.S., Pereira, D., Reed, G., Fitzgerald, K.A., Golenbock, D.T., Gazzinelli, R.T., 2014. Malaria-Induced NLRP12/NLRP3-Dependent Caspase-1 Activation Mediates Inflammation and

Hypersensitivity to Bacterial Superinfection. *PLOS Pathogens* 10, e1003885. <https://doi.org/10.1371/journal.ppat.1003885>

- Bachovchin, D.A., Koblan, L.W., Wu, W., Liu, Y., Li, Y., Zhao, P., Woznica, I., Shu, Y., Lai, J.H., Poplawski, S.E., Kiritsy, C.P., Healey, S.E., DiMare, M., Sanford, D.G., Munford, R.S., Bachovchin, W.W., Golub, T.R., 2014. A high-throughput, multiplexed assay for superfamily-wide profiling of enzyme activity. *Nat Chem Biol* 10, 656–663. <https://doi.org/10.1038/nchembio.1578>
- Baker, B., Zambryski, P., Staskawicz, B., Dinesh-Kumar, S.P., 1997. Signaling in Plant-Microbe Interactions. *Science* 276, 726–733. <https://doi.org/10.1126/science.276.5313.726>
- Ball, D.P., Taabazuing, C.Y., Griswold, A.R., Orth, E.L., Rao, S.D., Kotliar, I.B., Vostal, L.E., Johnson, D.C., Bachovchin, D.A., 2020. Caspase-1 interdomain linker cleavage is required for pyroptosis. *Life Science Alliance* 3. <https://doi.org/10.26508/lsa.202000664>
- Ball, D.P., Tsamouri, L.P., Wang, A.E., Huang, H.-C., Warren, C.D., Wang, Q., Edmondson, I.H., Griswold, A.R., Rao, S.D., Johnson, D.C., Bachovchin, D.A., 2022. Oxidized thioredoxin-1 restrains the NLRP1 inflammasome. *Science Immunology* 7, eabm7200. <https://doi.org/10.1126/sciimmunol.abm7200>
- Barry, K., Murphy, C., Mansell, A., 2023. NLRP1- A CINDERELLA STORY: a perspective of recent advances in NLRP1 and the questions they raise. *Commun Biol* 6, 1–7. <https://doi.org/10.1038/s42003-023-05684-3>
- Bauernfeind, F., Hornung, V., 2013. Of inflammasomes and pathogens – sensing of microbes by the inflammasome. *EMBO Molecular Medicine* 5, 814–826. <https://doi.org/10.1002/emmm.201201771>
- Bauernfried, S., Hornung, V., 2021. Human NLRP1: From the shadows to center stage. *Journal of Experimental Medicine* 219, e20211405. <https://doi.org/10.1084/jem.20211405>
- Bauernfried, S., Scherr, M.J., Pichlmair, A., Duderstadt, K.E., Hornung, V., 2021. Human NLRP1 is a sensor for double-stranded RNA. *Science* 371, eabd0811. <https://doi.org/10.1126/science.abd0811>
- Benramdane, S., De Loose, J., Filippi, N., Espadinha, M., Beyens, O., Rymenant, Y.V., Dirx, L., Bozdog, M., Feijens, P.-B., Augustyns, K., Caljon, G., De Winter, H., De Meester, I., Van der Veken, P., 2023. Highly Selective Inhibitors of Dipeptidyl Peptidase 9 (DPP9) Derived from the Clinically Used DPP4-Inhibitor Vildagliptin. *J. Med. Chem.* 66, 12717–12738. <https://doi.org/10.1021/acs.jmedchem.3c00609>
- Bergsbaken, T., Fink, S.L., Cookson, B.T., 2009. Pyroptosis: host cell death and inflammation. *Nat Rev Microbiol* 7, 99–109. <https://doi.org/10.1038/nrmicro2070>

- Bertin, J., Nir, W.-J., Fischer, C.M., Tayber, O.V., Errada, P.R., Grant, J.R., Keilty, J.J., Gosselin, M.L., Robison, K.E., Wong, G.H.W., Glucksmann, M.A., DiStefano, P.S., 1999. Human CARD4 Protein Is a Novel CED-4/Apaf-1 Cell Death Family Member That Activates NF- κ B *. *Journal of Biological Chemistry* 274, 12955–12958. <https://doi.org/10.1074/jbc.274.19.12955>
- Bigeard, J., Colcombet, J., Hirt, H., 2015. Signaling Mechanisms in Pattern-Triggered Immunity (PTI). *Molecular Plant* 8, 521–539. <https://doi.org/10.1016/j.molp.2014.12.022>
- Bjelke, J.R., Christensen, J., Nielsen, P.F., Branner, S., Kanstrup, A.B., Wagtmann, N., Rasmussen, H.B., 2006. Dipeptidyl peptidases 8 and 9: specificity and molecular characterization compared with dipeptidyl peptidase IV. *Biochemical Journal* 396, 391–399. <https://doi.org/10.1042/BJ20060079>
- Black, R.A., Kronheim, S.R., Sleath, P.R., 1989. Activation of interleukin-1 β by a co-induced protease. *FEBS Letters* 247, 386–390. [https://doi.org/10.1016/0014-5793\(89\)81376-6](https://doi.org/10.1016/0014-5793(89)81376-6)
- Bolgi, O., Silva-Garcia, M., Ross, B., Pilla, E., Kari, V., Killisch, M., Spitzner, M., Stark, N., Lenz, C., Weiss, K., Donzelli, L., Gorrell, M.D., Grade, M., Riemer, J., Urlaub, H., Dobbstein, M., Huber, R., Geiss-Friedlander, R., 2022. Dipeptidyl peptidase 9 triggers BRCA2 degradation and promotes DNA damage repair. *EMBO reports* 23, e54136. <https://doi.org/10.15252/embr.202154136>
- Bosso, M., Kirchhoff, F., 2020. Emerging Role of PYHIN Proteins as Antiviral Restriction Factors. *Viruses* 12, 1464. <https://doi.org/10.3390/v12121464>
- Bottazzi, B., Doni, A., Garlanda, C., Mantovani, A., 2010. An Integrated View of Humoral Innate Immunity: Pentraxins as a Paradigm. *Annual Review of Immunology* 28, 157–183. <https://doi.org/10.1146/annurev-immunol-030409-101305>
- Boucher, D., Monteleone, M., Coll, R.C., Chen, K.W., Ross, C.M., Teo, J.L., Gomez, G.A., Holley, C.L., Bierschenk, D., Stacey, K.J., Yap, A.S., Bezbradica, J.S., Schroder, K., 2018. Caspase-1 self-cleavage is an intrinsic mechanism to terminate inflammasome activity. *Journal of Experimental Medicine* 215, 827–840. <https://doi.org/10.1084/jem.20172222>
- Bouchier-Hayes, L., Conroy, H., Egan, H., Adrain, C., Creagh, E.M., MacFarlane, M., Martin, S.J., 2001. CARDINAL, a Novel Caspase Recruitment Domain Protein, Is an Inhibitor of Multiple NF- κ B Activation Pathways *. *Journal of Biological Chemistry* 276, 44069–44077. <https://doi.org/10.1074/jbc.M107373200>
- Boyden, E.D., Dietrich, W.F., 2006. Nalp1b controls mouse macrophage susceptibility to anthrax lethal toxin. *Nat Genet* 38, 240–244. <https://doi.org/10.1038/ng1724>

- Broz, P., Dixit, V.M., 2016. Inflammasomes: mechanism of assembly, regulation and signalling. *Nat Rev Immunol* 16, 407–420. <https://doi.org/10.1038/nri.2016.58>
- Broz, P., Moltke, J. von, Jones, J.W., Vance, R.E., Monack, D.M., 2010. Differential Requirement for Caspase-1 Autoproteolysis in Pathogen-Induced Cell Death and Cytokine Processing. *Cell Host & Microbe* 8, 471–483. <https://doi.org/10.1016/j.chom.2010.11.007>
- Bürckstümmer, T., Baumann, C., Blüml, S., Dixit, E., Dürnberger, G., Jahn, H., Planyavsky, M., Bilban, M., Colinge, J., Bennett, K.L., Superti-Furga, G., 2009. An orthogonal proteomic-genomic screen identifies AIM2 as a cytoplasmic DNA sensor for the inflammasome. *Nat Immunol* 10, 266–272. <https://doi.org/10.1038/ni.1702>
- Carvalho, L.A.R., Ross, B., Fehr, L., Bolgi, O., Wöhrle, S., Lum, K.M., Podlesainski, D., Vieira, A.C., Kiefersauer, R., Félix, R., Rodrigues, T., Lucas, S.D., Groß, O., Geiss-Friedlander, R., Cravatt, B.F., Huber, R., Kaiser, M., Moreira, R., 2022. Chemoproteomics-Enabled Identification of 4-Oxo- β -Lactams as Inhibitors of Dipeptidyl Peptidases 8 and 9. *Angewandte Chemie International Edition* 61, e202210498. <https://doi.org/10.1002/anie.202210498>
- Cavlar, T., Ablasser, A., Hornung, V., 2012. Induction of type I IFNs by intracellular DNA-sensing pathways. *Immunology & Cell Biology* 90, 474–482. <https://doi.org/10.1038/icb.2012.11>
- Cerretti, D.P., Kozlosky, C.J., Mosley, B., Nelson, N., Van Ness, K., Greenstreet, T.A., March, C.J., Kronheim, S.R., Druck, T., Cannizzaro, L.A., Huebner, K., Black, R.A., 1992. Molecular Cloning of the Interleukin-1 β Converting Enzyme. *Science* 256, 97–100. <https://doi.org/10.1126/science.1373520>
- Chang, K., Chen, Y., Zhang, X., Zhang, W., Xu, N., Zeng, B., Wang, Y., Feng, T., Dai, B., Xu, F., Ye, D., Wang, C., 2023. DPP9 Stabilizes NRF2 to Suppress Ferroptosis and Induce Sorafenib Resistance in Clear Cell Renal Cell Carcinoma. *Cancer Research* 83, 3940–3955. <https://doi.org/10.1158/0008-5472.CAN-22-4001>
- Charles A Janeway, J., Travers, P., Walport, M., Shlomchik, M.J., 2001. The complement system and innate immunity, in: *Immunobiology: The Immune System in Health and Disease*. 5th Edition. Garland Science.
- Chavarría-Smith, J., Mitchell, P.S., Ho, A.M., Daugherty, M.D., Vance, R.E., 2016. Functional and Evolutionary Analyses Identify Proteolysis as a General Mechanism for NLRP1 Inflammasome Activation. *PLOS Pathogens* 12, e1006052. <https://doi.org/10.1371/journal.ppat.1006052>
- Chavarría-Smith, J., Vance, R.E., 2013. Direct Proteolytic Cleavage of NLRP1B Is Necessary and Sufficient for Inflammasome Activation by Anthrax Lethal Factor. *PLOS Pathogens* 9, e1003452. <https://doi.org/10.1371/journal.ppat.1003452>

- Chen, J., Chen, Z.J., 2018. PtdIns4P on dispersed trans-Golgi network mediates NLRP3 inflammasome activation. *Nature* 564, 71–76. <https://doi.org/10.1038/s41586-018-0761-3>
- Cheung, M.S., Theodoropoulou, K., Lugin, J., Martinon, F., Busso, N., Hofer, M., 2017. Periodic Fever with Aphthous Stomatitis, Pharyngitis, and Cervical Adenitis Syndrome Is Associated with a CARD8 Variant Unable To Bind the NLRP3 Inflammasome. *The Journal of Immunology* 198, 2063–2069. <https://doi.org/10.4049/jimmunol.1600760>
- Chou, W.-C., Jha, S., Linhoff, M.W., Ting, J.P.-Y., 2023. The NLR gene family: from discovery to present day. *Nat Rev Immunol* 23, 635–654. <https://doi.org/10.1038/s41577-023-00849-x>
- Chow, W.Y., Forman, C.J., Bihan, D., Puzkarska, A.M., Rajan, R., Reid, D.G., Slatter, D.A., Colwell, L.J., Wales, D.J., Farndale, R.W., Duer, M.J., 2018. Proline provides site-specific flexibility for in vivo collagen. *Sci Rep* 8, 13809. <https://doi.org/10.1038/s41598-018-31937-x>
- Chowdhury, S., Chen, Y., Yao, T.-W., Ajami, K., Wang, X.M., Popov, Y., Schuppan, D., Bertolino, P., McCaughan, G.W., Yu, D.M., Gorrell, M.D., 2013. Regulation of dipeptidyl peptidase 8 and 9 expression in activated lymphocytes and injured liver. *World J Gastroenterol* 19, 2883–2893. <https://doi.org/10.3748/wjg.v19.i19.2883>
- Chui, A.J., Okondo, M.C., Rao, S.D., Gai, K., Griswold, A.R., Johnson, D.C., Ball, D.P., Taabazuing, C.Y., Orth, E.L., Vittimberga, B.A., Bachovchin, D.A., 2019. N-terminal degradation activates the NLRP1B inflammasome. *Science* 364, 82–85. <https://doi.org/10.1126/science.aau1208>
- Cirelli, K.M., Gorf, G., Hassan, M.A., Printz, M., Crown, D., Leppla, S.H., Grigg, M.E., Saeij, J.P.J., Moayeri, M., 2014. Inflammasome sensor NLRP1 controls rat macrophage susceptibility to *Toxoplasma gondii*. *PLoS Pathog* 10, e1003927. <https://doi.org/10.1371/journal.ppat.1003927>
- Clark, K.M., Kim, J.G., Wang, Q., Gao, H., Presti, R.M., Shan, L., 2023. Chemical inhibition of DPP9 sensitizes the CARD8 inflammasome in HIV-1-infected cells. *Nat Chem Biol* 19, 431–439. <https://doi.org/10.1038/s41589-022-01182-5>
- Connolly, D.J., Bowie, A.G., 2014. The emerging role of human PYHIN proteins in innate immunity: Implications for health and disease. *Biochemical Pharmacology* 92, 405–414. <https://doi.org/10.1016/j.bcp.2014.08.031>
- Dangl, J.L., Jones, J.D.G., 2001. Plant pathogens and integrated defence responses to infection. *Nature* 411, 826–833. <https://doi.org/10.1038/35081161>
- Danot, O., Marquenet, E., Vidal-Ingigliardi, D., Richet, E., 2009. Wheel of Life, Wheel of Death: A Mechanistic Insight into Signaling by STAND Proteins. *Structure* 17, 172–182. <https://doi.org/10.1016/j.str.2009.01.001>

- Decout, A., Katz, J.D., Venkatraman, S., Ablasser, A., 2021. The cGAS–STING pathway as a therapeutic target in inflammatory diseases. *Nat Rev Immunol* 21, 548–569. <https://doi.org/10.1038/s41577-021-00524-z>
- Degen, M., Santos, J.C., Pluhackova, K., Cebrero, G., Ramos, S., Jankevicius, G., Hartenian, E., Guillerm, U., Mari, S.A., Kohl, B., Müller, D.J., Schanda, P., Maier, T., Perez, C., Sieben, C., Broz, P., Hiller, S., 2023. Structural basis of NINJ1-mediated plasma membrane rupture in cell death. *Nature* 618, 1065–1071. <https://doi.org/10.1038/s41586-023-05991-z>
- Demarco, B., Grayczyk, J.P., Bjanec, E., Le Roy, D., Tonnus, W., Assenmacher, C.-A., Radaelli, E., Fettelet, T., Mack, V., Linkermann, A., Roger, T., Brodsky, I.E., Chen, K.W., Broz, P., 2020. Caspase-8–dependent gasdermin D cleavage promotes antimicrobial defense but confers susceptibility to TNF-induced lethality. *Science Advances* 6, eabc3465. <https://doi.org/10.1126/sciadv.abc3465>
- Dieudé, P., Guedj, M., Wipff, J., Ruiz, B., Riemekasten, G., Airo, P., Melchers, I., Hachulla, E., Cerinic, M.M., Diot, E., Hunzelmann, N., Caramaschi, P., Sibilia, J., Tiev, K., Mouthon, L., Riccieri, V., Cracowski, J.L., Carpentier, P.H., Distler, J., Amoura, Z., Tarner, I., Avouac, J., Meyer, O., Kahan, A., Boileau, C., Allanore, Y., 2011. NLRP1 influences the systemic sclerosis phenotype: a new clue for the contribution of innate immunity in systemic sclerosis-related fibrosing alveolitis pathogenesis. *Annals of the Rheumatic Diseases* 70, 668–674. <https://doi.org/10.1136/ard.2010.131243>
- Dinarello, C.A., 2007. Historical insights into cytokines. *European Journal of Immunology* 37, S34–S45. <https://doi.org/10.1002/eji.200737772>
- Dinarello, C.A., Ikejima, T., Warner, S.J., Orencole, S.F., Lonemann, G., Cannon, J.G., Libby, P., 1987. Interleukin 1 induces interleukin 1. I. Induction of circulating interleukin 1 in rabbits in vivo and in human mononuclear cells in vitro. *The Journal of Immunology* 139, 1902–1910. <https://doi.org/10.4049/jimmunol.139.6.1902>
- Diner, E.J., Burdette, D.L., Wilson, S.C., Monroe, K.M., Kellenberger, C.A., Hyodo, M., Hayakawa, Y., Hammond, M.C., Vance, R.E., 2013. The innate immune DNA sensor cGAS produces a non-canonical cyclic-di-nucleotide that activates human STING. *Cell Rep* 3, 1355–1361. <https://doi.org/10.1016/j.celrep.2013.05.009>
- D’Osueldo, A., Weichenberger, C.X., Wagner, R.N., Godzik, A., Wooley, J., Reed, J.C., 2011. CARD8 and NLRP1 Undergo Autoproteolytic Processing through a ZU5-Like Domain. *PLOS ONE* 6, e27396. <https://doi.org/10.1371/journal.pone.0027396>
- Drozdetskiy, A., Cole, C., Procter, J., Barton, G.J., 2015. JPred4: a protein secondary structure prediction server. *Nucleic Acids Research* 43, W389–W394. <https://doi.org/10.1093/nar/gkv332>

- Drutman, S.B., Haerynck, F., Zhong, F.L., Hum, D., Hernandez, N.J., Belkaya, S., Rapaport, F., de Jong, S.J., Creytens, D., Tavernier, S.J., Bonte, K., De Schepper, S., van der Werff ten Bosch, J., Lorenzo-Diaz, L., Wullaert, A., Bossuyt, X., Orth, G., Bonagura, V.R., Béziat, V., Abel, L., Jouanguy, E., Reversade, B., Casanova, J.-L., 2019. Homozygous NLRP1 gain-of-function mutation in siblings with a syndromic form of recurrent respiratory papillomatosis. *Proceedings of the National Academy of Sciences* 116, 19055–19063. <https://doi.org/10.1073/pnas.1906184116>
- Edmondson, S.D., Mastracchio, A., Beconi, M., Colwell, L.F., Habulihaz, B., He, H., Kumar, S., Leiting, B., Lyons, K.A., Mao, A., Marsilio, F., Patel, R.A., Wu, J.K., Zhu, L., Thornberry, N.A., Weber, A.E., Parmee, E.R., 2004. Potent and selective proline derived dipeptidyl peptidase IV inhibitors. *Bioorganic & Medicinal Chemistry Letters* 14, 5151–5155. <https://doi.org/10.1016/j.bmcl.2004.07.056>
- Elias, P.M., 2007. The skin barrier as an innate immune element. *Semin Immunopathol* 29, 3–14. <https://doi.org/10.1007/s00281-007-0060-9>
- Ewald, S.E., Chavarria-Smith, J., Boothroyd, J.C., 2014. NLRP1 Is an Inflammasome Sensor for *Toxoplasma gondii*. *Infection and Immunity* 82, 460–468. <https://doi.org/10.1128/iai.01170-13>
- Faustin, B., Lartigue, L., Bruey, J.-M., Luciano, F., Sergienko, E., Bailly-Maitre, B., Volkmann, N., Hanein, D., Rouiller, I., Reed, J.C., 2007. Reconstituted NALP1 Inflammasome Reveals Two-Step Mechanism of Caspase-1 Activation. *Molecular Cell* 25, 713–724. <https://doi.org/10.1016/j.molcel.2007.01.032>
- Feldmeyer, L., Keller, M., Niklaus, G., Hohl, D., Werner, S., Beer, H.-D., 2007. The Inflammasome Mediates UVB-Induced Activation and Secretion of Interleukin-1 β by Keratinocytes. *Current Biology* 17, 1140–1145. <https://doi.org/10.1016/j.cub.2007.05.074>
- Fenini, G., Grossi, S., Contassot, E., Biedermann, T., Reichmann, E., French, L.E., Beer, H.-D., 2018. Genome Editing of Human Primary Keratinocytes by CRISPR/Cas9 Reveals an Essential Role of the NLRP1 Inflammasome in UVB Sensing. *J Invest Dermatol* 138, 2644–2652. <https://doi.org/10.1016/j.jid.2018.07.016>
- Fernandes-Alnemri, T., Yu, J.-W., Datta, P., Wu, J., Alnemri, E.S., 2009. AIM2 activates the inflammasome and cell death in response to cytoplasmic DNA. *Nature* 458, 509–513. <https://doi.org/10.1038/nature07710>
- Finger, J.N., Lich, J.D., Dare, L.C., Cook, M.N., Brown, K.K., Duraiswami, C., Bertin, J.J., Gough, P.J., 2012. Autolytic Proteolysis within the Function to Find Domain (FIIND) Is Required for NLRP1 Inflammasome Activity*. *Journal of Biological Chemistry* 287, 25030–25037. <https://doi.org/10.1074/jbc.M112.378323>

- Finger, Y., Habich, M., Gerlich, S., Urbanczyk, S., van de Logt, E., Koch, J., Schu, L., Lapacz, K.J., Ali, M., Petrungaro, C., Salscheider, S.L., Pichlo, C., Baumann, U., Mielenz, D., Dengjel, J., Brachvogel, B., Hofmann, K., Riemer, J., 2020. Proteasomal degradation induced by DPP9-mediated processing competes with mitochondrial protein import. *The EMBO Journal* 39, e103889. <https://doi.org/10.15252/embj.2019103889>
- Flannagan, R.S., Jaumouillé, V., Grinstein, S., 2012. The Cell Biology of Phagocytosis. *Annual Review of Pathology: Mechanisms of Disease* 7, 61–98. <https://doi.org/10.1146/annurev-pathol-011811-132445>
- Gaestel, M., Kotlyarov, A., Kracht, M., 2009. Targeting innate immunity protein kinase signalling in inflammation. *Nat Rev Drug Discov* 8, 480–499. <https://doi.org/10.1038/nrd2829>
- Gai, K., Okondo, M.C., Rao, S.D., Chui, A.J., Ball, D.P., Johnson, D.C., Bachovchin, D.A., 2019. DPP8/9 inhibitors are universal activators of functional NLRP1 alleles. *Cell Death Dis* 10, 587. <https://doi.org/10.1038/s41419-019-1817-5>
- Gall, M.G., Chen, Y., Ribeiro, A.J.V. de, Zhang, H., Bailey, C.G., Spielman, D.S., Yu, D.M.T., Gorrell, M.D., 2013. Targeted Inactivation of Dipeptidyl Peptidase 9 Enzymatic Activity Causes Mouse Neonate Lethality. *PLOS ONE* 8, e78378. <https://doi.org/10.1371/journal.pone.0078378>
- Gao, P., Ascano, M., Wu, Y., Barchet, W., Gaffney, B.L., Zillinger, T., Serganov, A.A., Liu, Y., Jones, R.A., Hartmann, G., Tuschl, T., Patel, D.J., 2013. Cyclic [G(2',5')pA(3',5')p] Is the Metazoan Second Messenger Produced by DNA-Activated Cyclic GMP-AMP Synthase. *Cell* 153, 1094–1107. <https://doi.org/10.1016/j.cell.2013.04.046>
- Geijtenbeek, T.B.H., Gringhuis, S.I., 2009. Signalling through C-type lectin receptors: shaping immune responses. *Nat Rev Immunol* 9, 465–479. <https://doi.org/10.1038/nri2569>
- Geiss-Friedlander, R., Parmentier, N., Möller, U., Urlaub, H., Eynde, B.J.V. den, Melchior, F., 2009. The Cytoplasmic Peptidase DPP9 Is Rate-limiting for Degradation of Proline-containing Peptides *. *Journal of Biological Chemistry* 284, 27211–27219. <https://doi.org/10.1074/jbc.M109.041871>
- Girardin, S.E., Boneca, I.G., Viala, J., Chamaillard, M., Labigne, A., Thomas, G., Philpott, D.J., Sansonetti, P.J., 2003. Nod2 Is a General Sensor of Peptidoglycan through Muramyl Dipeptide (MDP) Detection *. *Journal of Biological Chemistry* 278, 8869–8872. <https://doi.org/10.1074/jbc.C200651200>
- Gitlin, L., Barchet, W., Gilfillan, S., Cella, M., Beutler, B., Flavell, R.A., Diamond, M.S., Colonna, M., 2006. Essential role of mda-5 in type I IFN responses to polyriboinosinic:polyribocytidylic acid and encephalomyocarditis picornavirus. *Proceedings of the National Academy of Sciences* 103, 8459–8464. <https://doi.org/10.1073/pnas.0603082103>

gnomAD, gnomAD, Broad Institute. DPP9 variant co-occurrence.

Gorfu, G., Cirelli, K.M., Melo, M.B., Mayer-Barber, K., Crown, D., Koller, B.H., Masters, S., Sher, A., Leppla, S.H., Moayeri, M., Saeij, J.P.J., Grigg, M.E., 2014. Dual Role for Inflammasome Sensors NLRP1 and NLRP3 in Murine Resistance to *Toxoplasma gondii*. *mBio* 5, 10.1128/mbio.01117-13. <https://doi.org/10.1128/mbio.01117-13>

Goubau, D., Schlee, M., Deddouche, S., Pruijssers, A.J., Zillinger, T., Goldeck, M., Schuberth, C., Van der Veen, A.G., Fujimura, T., Rehwinkel, J., Iskarpatyoti, J.A., Barchet, W., Ludwig, J., Dermody, T.S., Hartmann, G., Reis e Sousa, C., 2014. Antiviral immunity via RIG-I-mediated recognition of RNA bearing 5'-diphosphates. *Nature* 514, 372–375. <https://doi.org/10.1038/nature13590>

Grandemange, S., Sanchez, E., Louis-Plence, P., Mau-Them, F.T., Bessis, D., Coubes, C., Frouin, E., Seyger, M., Girard, M., Puechberty, J., Costes, V., Rodière, M., Carbasse, A., Jeziorski, E., Portales, P., Sarrabay, G., Mondain, M., Jorgensen, C., Apparailly, F., Hoppenreijts, E., Tuitou, I., Geneviève, D., 2017. A new autoinflammatory and autoimmune syndrome associated with NLRP1 mutations: NAIAD (NLRP1-associated autoinflammation with arthritis and dyskeratosis). *Annals of the Rheumatic Diseases* 76, 1191–1198. <https://doi.org/10.1136/annrheumdis-2016-210021>

Green, B.D., Flatt, P.R., Bailey, C.J., 2006. Dipeptidyl peptidase IV (DPP IV) inhibitors: a newly emerging drug class for the treatment of type 2 diabetes. *Diabetes and Vascular Disease Research* 3, 159–165. <https://doi.org/10.3132/dvdr.2006.024>

Green, R., Rogers, E.J., 2013. Chapter Twenty Eight - Transformation of Chemically Competent *E. coli*, in: Lorsch, J. (Ed.), *Methods in Enzymology, Laboratory Methods in Enzymology: DNA*. Academic Press, pp. 329–336. <https://doi.org/10.1016/B978-0-12-418687-3.00028-8>

Grenier, J.M., Wang, L., Manji, G.A., Huang, W.-J., Al-Garawi, A., Kelly, R., Carlson, A., Merriam, S., Lora, J.M., Briskin, M., DiStefano, P.S., Bertin, J., 2002. Functional screening of five PYPAF family members identifies PYPAF5 as a novel regulator of NF- κ B and caspase-1. *FEBS Letters* 530, 73–78. [https://doi.org/10.1016/S0014-5793\(02\)03416-6](https://doi.org/10.1016/S0014-5793(02)03416-6)

Greulich, W., Wagner, M., Gaidt, M.M., Stafford, C., Cheng, Y., Linder, A., Carell, T., Hornung, V., 2019. TLR8 Is a Sensor of RNase T2 Degradation Products. *Cell* 179, 1264-1275.e13. <https://doi.org/10.1016/j.cell.2019.11.001>

Griswold, A.R., Ball, D.P., Bhattacharjee, A., Chui, A.J., Rao, S.D., Taabazuing, C.Y., Bachovchin, D.A., 2019. DPP9's Enzymatic Activity and Not Its Binding to CARD8 Inhibits Inflammasome Activation. *ACS Chem Biol* 14, 2424–2429. <https://doi.org/10.1021/acscchembio.9b00462>

- Griswold, A.R., Huang, H.-C., Bachovchin, D.A., 2022. The NLRP1 Inflammasome Induces Pyroptosis in Human Corneal Epithelial Cells. *Investigative Ophthalmology & Visual Science* 63, 2. <https://doi.org/10.1167/iovs.63.3.2>
- Gupta, M.N., Uversky, V.N., 2024. Biological importance of arginine: A comprehensive review of the roles in structure, disorder, and functionality of peptides and proteins. *International Journal of Biological Macromolecules* 257, 128646. <https://doi.org/10.1016/j.ijbiomac.2023.128646>
- Hanna, P.C., Acosta, D., Collier, R.J., 1993. On the role of macrophages in anthrax. *Proceedings of the National Academy of Sciences* 90, 10198–10201. <https://doi.org/10.1073/pnas.90.21.10198>
- Hanson, P.I., Whiteheart, S.W., 2005. AAA+ proteins: have engine, will work. *Nat Rev Mol Cell Biol* 6, 519–529. <https://doi.org/10.1038/nrm1684>
- Hara, H., Seregin, S.S., Yang, D., Fukase, K., Chamailard, M., Alnemri, E.S., Inohara, N., Chen, G.Y., Núñez, G., 2018. The NLRP6 Inflammasome Recognizes Lipoteichoic Acid and Regulates Gram-Positive Pathogen Infection. *Cell* 175, 1651-1664.e14. <https://doi.org/10.1016/j.cell.2018.09.047>
- Harapas, C.R., Robinson, K.S., Lay, K., Wong, J., Moreno Traspas, R., Nabavizadeh, N., Rass-Rothschild, A., Boisson, B., Drutman, S.B., Laohamonthonkul, P., Bonner, D., Xiong, J.R., Gorrell, M.D., Davidson, S., Yu, C.-H., Fleming, M.D., Gudera, J., Stein, J., Ben-Harosh, M., Groopman, E., Shimamura, A., Tamary, H., Kayserili, H., Hatipoğlu, N., Casanova, J.-L., Bernstein, J.A., Zhong, F.L., Masters, S.L., Reversade, B., 2022. DPP9 deficiency: An inflammasomopathy that can be rescued by lowering NLRP1/IL-1 signaling. *Science Immunology* 7, eabi4611. <https://doi.org/10.1126/sciimmunol.abi4611>
- Harton, J.A., Linhoff, M.W., Zhang, J., Ting, J.P.-Y., 2002. Cutting Edge: CATERPILLER: A Large Family of Mammalian Genes Containing CARD, Pyrin, Nucleotide-Binding, and Leucine-Rich Repeat Domains1. *The Journal of Immunology* 169, 4088–4093. <https://doi.org/10.4049/jimmunol.169.8.4088>
- Harton, J.A., Ting, J.P.-Y., 2000. Class II Transactivator: Mastering the Art of Major Histocompatibility Complex Expression. *Molecular and Cellular Biology* 20, 6185–6194. <https://doi.org/10.1128/MCB.20.17.6185-6194.2000>
- Hashimoto, C., Hudson, K.L., Anderson, K.V., 1988. The Toll gene of drosophila, required for dorsal-ventral embryonic polarity, appears to encode a transmembrane protein. *Cell* 52, 269–279. [https://doi.org/10.1016/0092-8674\(88\)90516-8](https://doi.org/10.1016/0092-8674(88)90516-8)
- He, Y., Zeng, M.Y., Yang, D., Motro, B., Núñez, G., 2016. NEK7 is an essential mediator of NLRP3 activation downstream of potassium efflux. *Nature* 530, 354–357. <https://doi.org/10.1038/nature16959>

- Heffernan, R., Yang, Y., Paliwal, K., Zhou, Y., 2017. Capturing non-local interactions by long short-term memory bidirectional recurrent neural networks for improving prediction of protein secondary structure, backbone angles, contact numbers and solvent accessibility. *Bioinformatics* 33, 2842–2849. <https://doi.org/10.1093/bioinformatics/btx218>
- Heilig, R., Broz, P., 2018. Function and mechanism of the pyrin inflammasome. *European Journal of Immunology* 48, 230–238. <https://doi.org/10.1002/eji.201746947>
- Hellmich, K.A., Levinsohn, J.L., Fattah, R., Newman, Z.L., Maier, N., Sastalla, I., Liu, S., Leppla, S.H., Moayeri, M., 2012. Anthrax Lethal Factor Cleaves Mouse Nlrp1b in Both Toxin-Sensitive and Toxin-Resistant Macrophages. *PLOS ONE* 7, e49741. <https://doi.org/10.1371/journal.pone.0049741>
- Hemmi, H., Takeuchi, O., Kawai, T., Kaisho, T., Sato, S., Sanjo, H., Matsumoto, M., Hoshino, K., Wagner, H., Takeda, K., Akira, S., 2000. A Toll-like receptor recognizes bacterial DNA. *Nature* 408, 740–745. <https://doi.org/10.1038/35047123>
- Herlin, T., Jørgensen, S.E., Høst, C., Mitchell, P.S., Christensen, M.H., Laustsen, M., Larsen, D.A., Schmidt, F.I., Christiansen, M., Mogensen, T.H., 2020. Autoinflammatory disease with corneal and mucosal dyskeratosis caused by a novel NLRP1 variant. *Rheumatology* 59, 2334–2339. <https://doi.org/10.1093/rheumatology/kez612>
- Hochheiser, I.V., Pilsl, M., Hagelueken, G., Moecking, J., Marleaux, M., Brinkschulte, R., Latz, E., Engel, C., Geyer, M., 2022. Structure of the NLRP3 decamer bound to the cytokine release inhibitor CRID3. *Nature* 604, 184–189. <https://doi.org/10.1038/s41586-022-04467-w>
- Hollingsworth, L.R., Sharif, H., Griswold, A.R., Fontana, P., Mintseris, J., Dagbay, K.B., Paulo, J.A., Gygi, S.P., Bachovchin, D.A., Wu, H., 2021. DPP9 sequesters the C terminus of NLRP1 to repress inflammasome activation. *Nature* 592, 778–783. <https://doi.org/10.1038/s41586-021-03350-4>
- Hornung, V., Ablasser, A., Charrel-Dennis, M., Bauernfeind, F., Horvath, G., Caffrey, D.R., Latz, E., Fitzgerald, K.A., 2009. AIM2 recognizes cytosolic dsDNA and forms a caspase-1-activating inflammasome with ASC. *Nature* 458, 514–518. <https://doi.org/10.1038/nature07725>
- Hornung, V., Bauernfeind, F., Halle, A., Samstad, E.O., Kono, H., Rock, K.L., Fitzgerald, K.A., Latz, E., 2008. Silica crystals and aluminum salts activate the NALP3 inflammasome through phagosomal destabilization. *Nat Immunol* 9, 847–856. <https://doi.org/10.1038/ni.1631>
- Hornung, V., Ellegast, J., Kim, S., Brzózka, K., Jung, A., Kato, H., Poeck, H., Akira, S., Conzelmann, K.-K., Schlee, M., Endres, S., Hartmann, G., 2006. 5'-Triphosphate RNA Is the Ligand for RIG-I. *Science* 314, 994–997. <https://doi.org/10.1126/science.1132505>

- Hotter, D., Bosso, M., Jønsson, K.L., Krapp, C., Stürzel, C.M., Das, A., Littwitz-Salomon, E., Berkhout, B., Russ, A., Wittmann, S., Gramberg, T., Zheng, Y., Martins, L.J., Planelles, V., Jakobsen, M.R., Hahn, B.H., Dittmer, U., Sauter, D., Kirchhoff, F., 2019. IFI16 Targets the Transcription Factor Sp1 to Suppress HIV-1 Transcription and Latency Reactivation. *Cell Host Microbe* 25, 858-872.e13. <https://doi.org/10.1016/j.chom.2019.05.002>
- Hsiao, J.C., Neugroschl, A.R., Chui, A.J., Taabazuing, C.Y., Griswold, A.R., Wang, Q., Huang, H.-C., Orth-He, E.L., Ball, D.P., Hiotis, G., Bachovchin, D.A., 2022. A ubiquitin-independent proteasome pathway controls activation of the CARD8 inflammasome. *Journal of Biological Chemistry* 298. <https://doi.org/10.1016/j.jbc.2022.102032>
- Hu, Z., Zhou, Q., Zhang, C., Fan, S., Cheng, W., Zhao, Y., Shao, F., Wang, H.-W., Sui, S.-F., Chai, J., 2015. Structural and biochemical basis for induced self-propagation of NLRC4. *Science* 350, 399–404. <https://doi.org/10.1126/science.aac5489>
- Huang, M., Zhang, X., Toh, G.A., Gong, Q., Wang, J., Han, Z., Wu, B., Zhong, F., Chai, J., 2021. Structural and biochemical mechanisms of NLRP1 inhibition by DPP9. *Nature* 592, 773–777. <https://doi.org/10.1038/s41586-021-03320-w>
- Inohara, N., Koseki, T., Peso, L. del, Hu, Y., Yee, C., Chen, S., Carrio, R., Merino, J., Liu, D., Ni, J., Núñez, G., 1999. Nod1, an Apaf-1-like Activator of Caspase-9 and Nuclear Factor- κ B *. *Journal of Biological Chemistry* 274, 14560–14567. <https://doi.org/10.1074/jbc.274.21.14560>
- Ishii, K.J., Coban, C., Kato, H., Takahashi, K., Torii, Y., Takeshita, F., Ludwig, H., Sutter, G., Suzuki, K., Hemmi, H., Sato, S., Yamamoto, M., Uematsu, S., Kawai, T., Takeuchi, O., Akira, S., 2006. A Toll-like receptor-independent antiviral response induced by double-stranded B-form DNA. *Nat Immunol* 7, 40–48. <https://doi.org/10.1038/ni1282>
- Ishii, K.J., Kawagoe, T., Koyama, S., Matsui, K., Kumar, H., Kawai, T., Uematsu, S., Takeuchi, O., Takeshita, F., Coban, C., Akira, S., 2008. TANK-binding kinase-1 delineates innate and adaptive immune responses to DNA vaccines. *Nature* 451, 725–729. <https://doi.org/10.1038/nature06537>
- Ito, S., Hara, Y., Kubota, T., 2014. CARD8 is a negative regulator for NLRP3 inflammasome, but mutant NLRP3 in cryopyrin-associated periodic syndromes escapes the restriction. *Arthritis Res Ther* 16, R52. <https://doi.org/10.1186/ar4483>
- Jenster, L.-M., Lange, K.-E., Normann, S., vom Hemdt, A., Wuerth, J.D., Schiffelers, L.D.J., Tesfamariam, Y.M., Gohr, F.N., Klein, L., Kalthéuner, I.H., Ebner, S., Lapp, D.J., Mayer, J., Moeking, J., Ploegh, H.L., Latz, E., Meissner, F., Geyer, M., Kümmerer, B.M., Schmidt, F.I., 2022. P38 kinases mediate NLRP1 inflammasome activation after ribotoxic stress response and virus infection. *Journal of Experimental Medicine* 220, e20220837. <https://doi.org/10.1084/jem.20220837>

- Jin, T., Perry, A., Jiang, J., Smith, P., Curry, J.A., Unterholzner, L., Jiang, Z., Horvath, G., Rathinam, V.A., Johnstone, R.W., Hornung, V., Latz, E., Bowie, A.G., Fitzgerald, K.A., Xiao, T.S., 2012. Structures of the HIN Domain:DNA Complexes Reveal Ligand Binding and Activation Mechanisms of the AIM2 Inflammasome and IFI16 Receptor. *Immunity* 36, 561–571. <https://doi.org/10.1016/j.immuni.2012.02.014>
- Jin, Y., Birlea, S.A., Fain, P.R., Spritz, R.A., 2007a. Genetic Variations in *NALP1* Are Associated with Generalized Vitiligo in a Romanian Population. *Journal of Investigative Dermatology* 127, 2558–2562. <https://doi.org/10.1038/sj.jid.5700953>
- Jin, Y., Mailloux, C.M., Gowan, K., Riccardi, S.L., LaBerge, G., Bennett, D.C., Fain, P.R., Spritz, R.A., 2007b. *NALP1* in Vitiligo-Associated Multiple Autoimmune Disease. *New England Journal of Medicine* 356, 1216–1225. <https://doi.org/10.1056/NEJMoa061592>
- Johnson, D.C., Okondo, M.C., Orth, E.L., Rao, S.D., Huang, H.-C., Ball, D.P., Bachovchin, D.A., 2020. DPP8/9 inhibitors activate the CARD8 inflammasome in resting lymphocytes. *Cell Death Dis* 11, 1–10. <https://doi.org/10.1038/s41419-020-02865-4>
- Johnson, D.C., Taabazuing, C.Y., Okondo, M.C., Chui, A.J., Rao, S.D., Brown, F.C., Reed, C., Peguero, E., de Stanchina, E., Kentsis, A., Bachovchin, D.A., 2018. DPP8/DPP9 inhibitor-induced pyroptosis for treatment of acute myeloid leukemia. *Nat Med* 24, 1151–1156. <https://doi.org/10.1038/s41591-018-0082-y>
- Jones, D.T., 1999. Protein secondary structure prediction based on position-specific scoring matrices1. *Journal of Molecular Biology* 292, 195–202. <https://doi.org/10.1006/jmbi.1999.3091>
- Jorgensen, I., Miao, E.A., 2015. Pyroptotic cell death defends against intracellular pathogens. *Immunological Reviews* 265, 130–142. <https://doi.org/10.1111/imr.12287>
- Justa-Schuch, D., Möller, U., Geiss-Friedlander, R., 2014. The amino terminus extension in the long dipeptidyl peptidase 9 isoform contains a nuclear localization signal targeting the active peptidase to the nucleus. *Cell. Mol. Life Sci.* 71, 3611–3626. <https://doi.org/10.1007/s00018-014-1591-6>
- Justa-Schuch, D., Silva-Garcia, M., Pilla, E., Engelke, M., Kilisch, M., Lenz, C., Möller, U., Nakamura, F., Urlaub, H., Geiss-Friedlander, R., 2016. DPP9 is a novel component of the N-end rule pathway targeting the tyrosine kinase Syk. *eLife* 5, e16370. <https://doi.org/10.7554/eLife.16370>
- Karczewski, K.J., Francioli, L.C., Tiao, G., Cummings, B.B., Alföldi, J., Wang, Q., Collins, R.L., Laricchia, K.M., Ganna, A., Birnbaum, D.P., Gauthier, L.D., Brand, H., Solomonson, M., Watts, N.A., Rhodes, D., Singer-Berk, M., England, E.M., Seaby, E.G., Kosmicki, J.A., Walters, R.K., Tashman, K., Farjoun, Y., Banks, E., Poterba, T., Wang, A., Seed, C., Whiffin, N., Chong,

- J.X., Samocha, K.E., Pierce-Hoffman, E., Zappala, Z., O'Donnell-Luria, A.H., Minikel, E.V., Weisburd, B., Lek, M., Ware, J.S., Vittal, C., Armean, I.M., Bergelson, L., Cibulskis, K., Connolly, K.M., Covarrubias, M., Donnelly, S., Ferriera, S., Gabriel, S., Gentry, J., Gupta, N., Jeandet, T., Kaplan, D., Llanwarne, C., Munshi, R., Novod, S., Petrillo, N., Roazen, D., Ruano-Rubio, V., Saltzman, A., Schleicher, M., Soto, J., Tibbetts, K., Tolonen, C., Wade, G., Talkowski, M.E., Neale, B.M., Daly, M.J., MacArthur, D.G., 2020. The mutational constraint spectrum quantified from variation in 141,456 humans. *Nature* 581, 434–443. <https://doi.org/10.1038/s41586-020-2308-7>
- Kato, H., Takeuchi, O., Mikamo-Satoh, E., Hirai, R., Kawai, T., Matsushita, K., Hiiragi, A., Dermody, T.S., Fujita, T., Akira, S., 2008. Length-dependent recognition of double-stranded ribonucleic acids by retinoic acid-inducible gene-I and melanoma differentiation-associated gene 5. *Journal of Experimental Medicine* 205, 1601–1610. <https://doi.org/10.1084/jem.20080091>
- Kato, H., Takeuchi, O., Sato, S., Yoneyama, M., Yamamoto, M., Matsui, K., Uematsu, S., Jung, A., Kawai, T., Ishii, K.J., Yamaguchi, O., Otsu, K., Tsujimura, T., Koh, C.-S., Reis e Sousa, C., Matsuura, Y., Fujita, T., Akira, S., 2006. Differential roles of MDA5 and RIG-I helicases in the recognition of RNA viruses. *Nature* 441, 101–105. <https://doi.org/10.1038/nature04734>
- Kayagaki, N., Kornfeld, O.S., Lee, B.L., Stowe, I.B., O'Rourke, K., Li, Q., Sandoval, W., Yan, D., Kang, J., Xu, M., Zhang, J., Lee, W.P., McKenzie, B.S., Ulas, G., Payandeh, J., Roose-Girma, M., Modrusan, Z., Reja, R., Sagolla, M., Webster, J.D., Cho, V., Andrews, T.D., Morris, L.X., Miosge, L.A., Goodnow, C.C., Bertram, E.M., Dixit, V.M., 2021. NINJ1 mediates plasma membrane rupture during lytic cell death. *Nature* 591, 131–136. <https://doi.org/10.1038/s41586-021-03218-7>
- Kayagaki, N., Stowe, I.B., Lee, B.L., O'Rourke, K., Anderson, K., Warming, S., Cuellar, T., Haley, B., Roose-Girma, M., Phung, Q.T., Liu, P.S., Lill, J.R., Li, H., Wu, J., Kummerfeld, S., Zhang, J., Lee, W.P., Snipas, S.J., Salvesen, G.S., Morris, L.X., Fitzgerald, L., Zhang, Y., Bertram, E.M., Goodnow, C.C., Dixit, V.M., 2015. Caspase-11 cleaves gasdermin D for non-canonical inflammasome signalling. *Nature* 526, 666–671. <https://doi.org/10.1038/nature15541>
- Kim, M., Minoux, M., Piaia, A., Kueng, B., Gapp, B., Weber, D., Haller, C., Barbieri, S., Namoto, K., Lorenz, T., Wirsching, J., Bassilana, F., Dietrich, W., Rijli, F.M., Ksiazek, I., 2017. DPP9 enzyme activity controls survival of mouse migratory tongue muscle progenitors and its absence leads to neonatal lethality due to suckling defect. *Developmental Biology* 431, 297–308. <https://doi.org/10.1016/j.ydbio.2017.09.001>
- Kleifeld, O., Doucet, A., auf dem Keller, U., Prudova, A., Schilling, O., Kainthan, R.K., Starr, A.E., Foster, L.J., Kizhakkedathu, J.N., Overall, C.M., 2010. Isotopic labeling of terminal amines in complex samples identifies protein N-termini and protease cleavage products. *Nat Biotechnol* 28, 281–288. <https://doi.org/10.1038/nbt.1611>

- Koonin, E.V., Aravind, L., 2000. The NACHT family – a new group of predicted NTPases implicated in apoptosis and MHC transcription activation. *Trends in Biochemical Sciences* 25, 223–224. [https://doi.org/10.1016/S0968-0004\(00\)01577-2](https://doi.org/10.1016/S0968-0004(00)01577-2)
- Kulsuptrakul, J., Turcotte, E.A., Emerman, M., Mitchell, P.S., 2023. A human-specific motif facilitates CARD8 inflammasome activation after HIV-1 infection. *eLife* 12, e84108. <https://doi.org/10.7554/eLife.84108>
- Lambeir, A.-M., Scharpé, S., De Meester, I., 2008. DPP4 inhibitors for diabetes—What next? *Biochemical Pharmacology* 76, 1637–1643. <https://doi.org/10.1016/j.bcp.2008.07.029>
- Lamkanfi, M., Dixit, V.M., 2012. Inflammasomes and Their Roles in Health and Disease. *Annual Review of Cell and Developmental Biology* 28, 137–161. <https://doi.org/10.1146/annurev-cellbio-101011-155745>
- Lankas, G.R., Leiting, B., Roy, R.S., Eiermann, G.J., Beconi, M.G., Biftu, T., Chan, C.-C., Edmondson, S., Feeney, W.P., He, H., Ippolito, D.E., Kim, D., Lyons, K.A., Ok, H.O., Patel, R.A., Petrov, A.N., Pryor, K.A., Qian, X., Reigle, L., Woods, A., Wu, J.K., Zaller, D., Zhang, X., Zhu, L., Weber, A.E., Thornberry, N.A., 2005. Dipeptidyl Peptidase IV Inhibition for the Treatment of Type 2 Diabetes: Potential Importance of Selectivity Over Dipeptidyl Peptidases 8 and 9. *Diabetes* 54, 2988–2994. <https://doi.org/10.2337/diabetes.54.10.2988>
- Lee, H.-J., Chen, Y.-S., Chou, C.-Y., Chien, C.-H., Lin, C.-H., Chang, G.-G., Chen, X., 2006. Investigation of the Dimer Interface and Substrate Specificity of Prolyl Dipeptidase DPP8 *. *Journal of Biological Chemistry* 281, 38653–38662. <https://doi.org/10.1074/jbc.M603895200>
- Lee, S.H., Jeong, S.K., Ahn, S.K., 2006. An Update of the Defensive Barrier Function of Skin. *Yonsei Med J* 47, 293–306. <https://doi.org/10.3349/ymj.2006.47.3.293>
- Lemaitre, B., Nicolas, E., Michaut, L., Reichhart, J.-M., Hoffmann, J.A., 1996. The Dorsoventral Regulatory Gene Cassette *spätzle/Toll/cactus* Controls the Potent Antifungal Response in *Drosophila* Adults. *Cell* 86, 973–983. [https://doi.org/10.1016/S0092-8674\(00\)80172-5](https://doi.org/10.1016/S0092-8674(00)80172-5)
- Levinsohn, J.L., Newman, Z.L., Hellmich, K.A., Fattah, R., Getz, M.A., Liu, S., Sastalla, I., Leppla, S.H., Moayeri, M., 2012. Anthrax Lethal Factor Cleavage of Nlrp1 Is Required for Activation of the Inflammasome. *PLOS Pathogens* 8, e1002638. <https://doi.org/10.1371/journal.ppat.1002638>
- Levy, M., Thaïss, C.A., Zeevi, D., Dohnalová, L., Zilberman-Schapira, G., Mahdi, J.A., David, E., Savidor, A., Korem, T., Herzig, Y., Pevsner-Fischer, M., Shapiro, H., Christ, A., Harmelin, A., Halpern, Z., Latz, E., Flavell, R.A., Amit, I., Segal, E., Elinav, E., 2015. Microbiota-Modulated Metabolites Shape the Intestinal Microenvironment by Regulating NLRP6 Inflammasome Signaling. *Cell* 163, 1428–1443. <https://doi.org/10.1016/j.cell.2015.10.048>

- Li, M., Lay, K., Zimmer, A., Technau-Hafsi, K., Wong, J., Reimer-Taschenbrecker, A., Rohr, J., Abdalla, E., Fischer, J., Reversade, B., Has, C., 2023. A homozygous p.Leu813Pro gain-of-function NLRP1 variant causes phenotypes of different severity in two siblings. *British Journal of Dermatology* 188, 259–267. <https://doi.org/10.1093/bjd/ljac039>
- Liddicoat, B.J., Piskol, R., Chalk, A.M., Ramaswami, G., Higuchi, M., Hartner, J.C., Li, J.B., Seeburg, P.H., Walkley, C.R., 2015. RNA editing by ADAR1 prevents MDA5 sensing of endogenous dsRNA as nonself. *Science* 349, 1115–1120. <https://doi.org/10.1126/science.aac7049>
- Lilue, J., Doran, A.G., Fiddes, I.T., Abrudan, M., Armstrong, J., Bennett, R., Chow, W., Collins, J., Collins, S., Czechanski, A., Danecek, P., Diekhans, M., Dolle, D.-D., Dunn, M., Durbin, R., Earl, D., Ferguson-Smith, A., Flicek, P., Flint, J., Frankish, A., Fu, B., Gerstein, M., Gilbert, J., Goodstadt, L., Harrow, J., Howe, K., Ibarra-Soria, X., Kolmogorov, M., Lelliott, C.J., Logan, D.W., Loveland, J., Mathews, C.E., Mott, R., Muir, P., Nachtweide, S., Navarro, F.C.P., Odom, D.T., Park, N., Pelan, S., Pham, S.K., Quail, M., Reinholdt, L., Romoth, L., Shirley, L., Sisu, C., Sjoberg-Herrera, M., Stanke, M., Steward, C., Thomas, M., Threadgold, G., Thybert, D., Torrance, J., Wong, K., Wood, J., Yalcin, B., Yang, F., Adams, D.J., Paten, B., Keane, T.M., 2018. Sixteen diverse laboratory mouse reference genomes define strain-specific haplotypes and novel functional loci. *Nat Genet* 50, 1574–1583. <https://doi.org/10.1038/s41588-018-0223-8>
- Linder, A., Bauernfried, S., Cheng, Y., Albanese, M., Jung, C., Keppler, O.T., Hornung, V., 2020. CARD8 inflammasome activation triggers pyroptosis in human T cells. *The EMBO Journal* 39, e105071. <https://doi.org/10.15252/embj.2020105071>
- Listen, P., Roy, N., Tamai, K., Lefebvre, C., Baird, S., Cherton-Horvat, G., Farahani, R., McLean, M., Lkeda, J.-E., Mackenzie, A., Korneluk, R.G., 1996. Suppression of apoptosis in mammalian cells by NAIP and a related family of IAP genes. *Nature* 379, 349–353. <https://doi.org/10.1038/379349a0>
- Lopes Fischer, N., Naseer, N., Shin, S., Brodsky, I.E., 2020. Effector-triggered immunity and pathogen sensing in metazoans. *Nat Microbiol* 5, 14–26. <https://doi.org/10.1038/s41564-019-0623-2>
- Lu, A., Magupalli, V.G., Ruan, J., Yin, Q., Atianand, M.K., Vos, M.R., Schröder, G.F., Fitzgerald, K.A., Wu, H., Egelman, E.H., 2014. Unified Polymerization Mechanism for the Assembly of ASC-Dependent Inflammasomes. *Cell* 156, 1193–1206. <https://doi.org/10.1016/j.cell.2014.02.008>
- Magitta, N.F., Bøe Wolff, A.S., Johansson, S., Skinningsrud, B., Lie, B.A., Myhr, K.-M., Undlien, D.E., Joner, G., Njølstad, P.R., Kvien, T.K., Førre, Ø., Knappskog, P.M., Husebye, E.S., 2009. A coding polymorphism in NALP1 confers risk for autoimmune Addison's disease and type 1 diabetes. *Genes Immun* 10, 120–124. <https://doi.org/10.1038/gene.2008.85>

- Manji, G.A., Wang, L., Geddes, B.J., Brown, M., Merriam, S., Al-Garawi, A., Mak, S., Lora, J.M., Briskin, M., Jurman, M., Cao, J., DiStefano, P.S., Bertin, J., 2002. PYPAF1, a PYRIN-containing Apaf1-like Protein That Assembles with ASC and Regulates Activation of NF- κ B *. *Journal of Biological Chemistry* 277, 11570–11575. <https://doi.org/10.1074/jbc.M112208200>
- Mantovani, A., Garlanda, C., 2023. Humoral Innate Immunity and Acute-Phase Proteins. *New England Journal of Medicine* 388, 439–452. <https://doi.org/10.1056/NEJMra2206346>
- Mao, L., Kitani, A., Similuk, M., Oler, A.J., Albenberg, L., Kelsen, J., Aktay, A., Quezado, M., Yao, M., Montgomery-Recht, K., Fuss, I.J., Strober, W., 2018. Loss-of-function CARD8 mutation causes NLRP3 inflammasome activation and Crohn's disease. *J Clin Invest* 128, 1793–1806. <https://doi.org/10.1172/JCI98642>
- Mariathasan, S., Weiss, D.S., Newton, K., McBride, J., O'Rourke, K., Roose-Girma, M., Lee, W.P., Weinrauch, Y., Monack, D.M., Dixit, V.M., 2006. Cryopyrin activates the inflammasome in response to toxins and ATP. *Nature* 440, 228–232. <https://doi.org/10.1038/nature04515>
- Martinon, F., Agostini, L., Meylan, E., Tschopp, J., 2004. Identification of Bacterial Muramyl Dipeptide as Activator of the NALP3/Cryopyrin Inflammasome. *Current Biology* 14, 1929–1934. <https://doi.org/10.1016/j.cub.2004.10.027>
- Martinon, F., Burns, K., Tschopp, J., 2002. The Inflammasome: A Molecular Platform Triggering Activation of Inflammatory Caspases and Processing of proIL- β . *Molecular Cell* 10, 417–426. [https://doi.org/10.1016/S1097-2765\(02\)00599-3](https://doi.org/10.1016/S1097-2765(02)00599-3)
- Martinon, F., Pétrilli, V., Mayor, A., Tardivel, A., Tschopp, J., 2006. Gout-associated uric acid crystals activate the NALP3 inflammasome. *Nature* 440, 237–241. <https://doi.org/10.1038/nature04516>
- Masters, S.L., Gerlic, M., Metcalf, D., Preston, S., Pellegrini, M., O'Donnell, J.A., McArthur, K., Baldwin, T.M., Chevrier, S., Nowell, C.J., Cengia, L.H., Henley, K.J., Collinge, J.E., Kastner, D.L., Feigenbaum, L., Hilton, D.J., Alexander, W.S., Kile, B.T., Croker, B.A., 2012. NLRP1 Inflammasome Activation Induces Pyroptosis of Hematopoietic Progenitor Cells. *Immunity* 37, 1009–1023. <https://doi.org/10.1016/j.immuni.2012.08.027>
- Maver, A., Lavtar, P., Ristić, S., Stopinšek, S., Simčič, S., Hočevar, K., Sepčič, J., Drulović, J., Pekmezović, T., Novaković, I., Alenka, H., Rudolf, G., Šega, S., Starčević-Čizmarević, N., Palandačić, A., Zamolo, G., Kapović, M., Likar, T., Peterlin, B., 2017. Identification of rare genetic variation of NLRP1 gene in familial multiple sclerosis. *Sci Rep* 7, 3715. <https://doi.org/10.1038/s41598-017-03536-9>
- McGovern, D.P.B., Butler, H., Ahmad, T., Paolucci, M., Heel, D.A. van, Negoro, K., Hysi, P., Ragoussis, J., Travis, S.P.L., Cardon, L.R., Jewell, D.P., 2006a. TUCAN (CARD8) Genetic Variants and Inflammatory Bowel Disease.

Gastroenterology 131, 1190–1196.
<https://doi.org/10.1053/j.gastro.2006.08.008>

McGovern, D.P.B., Butler, H., Ahmad, T., Paolucci, M., van Heel, D.A., Negro, K., Hysi, P., Ragoussis, J., Travis, S.P.L., Cardon, L.R., Jewell, D.P., 2006b. *TUCAN (CARD8) Genetic Variants and Inflammatory Bowel Disease*. *Gastroenterology* 131, 1190–1196.
<https://doi.org/10.1053/j.gastro.2006.08.008>

McHale, L., Tan, X., Koehl, P., Michelmore, R.W., 2006. Plant NBS-LRR proteins: adaptable guards. *Genome Biol* 7, 212. <https://doi.org/10.1186/gb-2006-7-4-212>

Medzhitov, R., Preston-Hurlburt, P., Janeway, C.A., 1997. A human homologue of the *Drosophila* Toll protein signals activation of adaptive immunity. *Nature* 388, 394–397. <https://doi.org/10.1038/41131>

Moayeri, M., Crown, D., Newman, Z.L., Okugawa, S., Eckhaus, M., Cataisson, C., Liu, S., Sastalla, I., Leppla, S.H., 2010. Inflammasome Sensor Nlrp1b-Dependent Resistance to Anthrax Is Mediated by Caspase-1, IL-1 Signaling and Neutrophil Recruitment. *PLOS Pathogens* 6, e1001222. <https://doi.org/10.1371/journal.ppat.1001222>

Moecking, J., Laohamonthonkul, P., Chalker, K., White, M.J., Harapas, C.R., Yu, C.-H., Davidson, S., Hrovat-Schaale, K., Hu, D., Eng, C., Huntsman, S., Calleja, D.J., Horvat, J.C., Hansbro, P.M., O'Donoghue, R.J.J., Ting, J.P., Burchard, E.G., Geyer, M., Gerlic, M., Masters, S.L., 2021. NLRP1 variant M1184V decreases inflammasome activation in the context of DPP9 inhibition and asthma severity. *Journal of Allergy and Clinical Immunology* 147, 2134–2145.e20. <https://doi.org/10.1016/j.jaci.2020.12.636>

Moecking, J., Laohamonthonkul, P., Meşe, K., Hagelueken, G., Steiner, A., Harapas, C.R., Sandow, J.J., Graves, J.D., Masters, S.L., Geyer, M., 2022. Inflammasome sensor NLRP1 disease variant M1184V promotes autoproteolysis and DPP9 complex formation by stabilizing the FIIND domain. *Journal of Biological Chemistry* 298. <https://doi.org/10.1016/j.jbc.2022.102645>

Morgan, A.A., Rubenstein, E., 2013. Proline: The Distribution, Frequency, Positioning, and Common Functional Roles of Proline and Polyproline Sequences in the Human Proteome. *PLoS One* 8, e53785. <https://doi.org/10.1371/journal.pone.0053785>

Mulvihill, E., Sborgi, L., Mari, S.A., Pfreundschuh, M., Hiller, S., Müller, D.J., 2018. Mechanism of membrane pore formation by human gasdermin-D. *The EMBO Journal* 37, e98321. <https://doi.org/10.15252/emj.201798321>

Murphy, K., Weaver, C., 2017. *Janeway's immunobiology*, Ninth edition. ed. Garland Science, Taylor & Francis Group, LLC, New York, NY, USA.

- Nadkarni, R., Chu, W.C., Lee, C.Q.E., Mohamud, Y., Yap, L., Toh, G.A., Beh, S., Lim, R., Fan, Y.M., Zhang, Y.L., Robinson, K., Tryggvason, K., Luo, H., Zhong, F., Ho, L., 2022. Viral proteases activate the CARD8 inflammasome in the human cardiovascular system. *Journal of Experimental Medicine* 219, e20212117. <https://doi.org/10.1084/jem.20212117>
- Newman, Z.L., Printz, M.P., Liu, S., Crown, D., Breen, L., Miller-Randolph, S., Flodman, P., Leppla, S.H., Moayeri, M., 2010. Susceptibility to Anthrax Lethal Toxin-Induced Rat Death Is Controlled by a Single Chromosome 10 Locus That Includes rNlrp1. *PLOS Pathogens* 6, e1000906. <https://doi.org/10.1371/journal.ppat.1000906>
- Nie, L., Cai, S.-Y., Shao, J.-Z., Chen, J., 2018. Toll-Like Receptors, Associated Biological Roles, and Signaling Networks in Non-Mammals. *Front Immunol* 9, 1523. <https://doi.org/10.3389/fimmu.2018.01523>
- Ogura, Y., Inohara, N., Benito, A., Chen, F.F., Yamaoka, S., Núñez, G., 2001. Nod2, a Nod1/Apaf-1 Family Member That Is Restricted to Monocytes and Activates NF- κ B *. *Journal of Biological Chemistry* 276, 4812–4818. <https://doi.org/10.1074/jbc.M008072200>
- Okondo, M.C., Johnson, D.C., Sridharan, R., Go, E.B., Chui, A.J., Wang, M.S., Poplawski, S.E., Wu, W., Liu, Y., Lai, J.H., Sanford, D.G., Arciprete, M.O., Golub, T.R., Bachovchin, W.W., Bachovchin, D.A., 2017. DPP8 and DPP9 inhibition induces pro-caspase-1-dependent monocyte and macrophage pyroptosis. *Nat Chem Biol* 13, 46–53. <https://doi.org/10.1038/nchembio.2229>
- Okondo, M.C., Rao, S.D., Taabazuing, C.Y., Chui, A.J., Poplawski, S.E., Johnson, D.C., Bachovchin, D.A., 2018. Inhibition of Dpp8/9 Activates the Nlrp1b Inflammasome. *Cell Chem Biol* 25, 262-267.e5. <https://doi.org/10.1016/j.chembiol.2017.12.013>
- Olsen, C., Wagtmann, N., 2002. Identification and characterization of human *DPP9*, a novel homologue of dipeptidyl peptidase IV. *Gene* 299, 185–193. [https://doi.org/10.1016/S0378-1119\(02\)01059-4](https://doi.org/10.1016/S0378-1119(02)01059-4)
- Orning, P., Weng, D., Starheim, K., Ratner, D., Best, Z., Lee, B., Brooks, A., Xia, S., Wu, H., Kelliher, M.A., Berger, S.B., Gough, P.J., Bertin, J., Proulx, M.M., Goguen, J.D., Kayagaki, N., Fitzgerald, K.A., Lien, E., 2018. Pathogen blockade of TAK1 triggers caspase-8–dependent cleavage of gasdermin D and cell death. *Science* 362, 1064–1069. <https://doi.org/10.1126/science.aau2818>
- Orth-He, E.L., Huang, H.-C., Rao, S.D., Wang, Q., Chen, Q., O'Mara, C.M., Chui, A.J., Saoi, M., Griswold, A.R., Bhattacharjee, A., Ball, D.P., Cross, J.R., Bachovchin, D.A., 2023. Protein folding stress potentiates NLRP1 and CARD8 inflammasome activation. *Cell Reports* 42. <https://doi.org/10.1016/j.celrep.2022.111965>

- Pairo-Castineira, E., Clohisey, S., Klaric, L., Bretherick, A.D., Rawlik, K., Pasko, D., Walker, S., Parkinson, N., Fourman, M.H., Russell, C.D., Furniss, J., Richmond, A., Gountouna, E., Wrobel, N., Harrison, D., Wang, B., Wu, Y., Meynert, A., Griffiths, F., Oosthuyzen, W., Kousathanas, A., Moutsianas, L., Yang, Z., Zhai, R., Zheng, C., Grimes, G., Beale, R., Millar, J., Shih, B., Keating, S., Zechner, M., Haley, C., Porteous, D.J., Hayward, C., Yang, J., Knight, J., Summers, C., Shankar-Hari, M., Klenerman, P., Turtle, L., Ho, A., Moore, S.C., Hinds, C., Horby, P., Nichol, A., Maslove, D., Ling, L., McAuley, D., Montgomery, H., Walsh, T., Pereira, A.C., Renieri, A., Shen, X., Ponting, C.P., Fawkes, A., Tenesa, A., Caulfield, M., Scott, R., Rowan, K., Murphy, L., Openshaw, P.J.M., Semple, M.G., Law, A., Vitart, V., Wilson, J.F., Baillie, J.K., 2021. Genetic mechanisms of critical illness in COVID-19. *Nature* 591, 92–98. <https://doi.org/10.1038/s41586-020-03065-y>
- Pathan, N., Marusawa, H., Krajewska, M., Matsuzawa, S., Kim, H., Okada, K., Torii, S., Kitada, S., Krajewski, S., Welsh, K., Pio, F., Godzik, A., Reed, J.C., 2001. TUCAN, an Antiapoptotic Caspase-associated Recruitment Domain Family Protein Overexpressed in Cancer *. *Journal of Biological Chemistry* 276, 32220–32229. <https://doi.org/10.1074/jbc.M100433200>
- Pettersen, E.F., Goddard, T.D., Huang, C.C., Meng, E.C., Couch, G.S., Croll, T.I., Morris, J.H., Ferrin, T.E., 2021. UCSF ChimeraX: Structure visualization for researchers, educators, and developers. *Protein Science* 30, 70–82. <https://doi.org/10.1002/pro.3943>
- Pichlmair, A., Schulz, O., Tan, C.P., Näslund, T.I., Liljeström, P., Weber, F., Reis e Sousa, C., 2006. RIG-I-Mediated Antiviral Responses to Single-Stranded RNA Bearing 5'-Phosphates. *Science* 314, 997–1001. <https://doi.org/10.1126/science.1132998>
- Pilla, E., Möller, U., Sauer, G., Mattioli, F., Melchior, F., Geiss-Friedlander, R., 2012. A Novel SUMO1-specific Interacting Motif in Dipeptidyl Peptidase 9 (DPP9) That Is Important for Enzymatic Regulation *. *Journal of Biological Chemistry* 287, 44320–44329. <https://doi.org/10.1074/jbc.M112.397224>
- Pinilla, M., Mazars, R., Vergé, R., Gorse, L., Paradis, M., Suire, B., Santoni, K., Robinson, K.S., Toh, G.A., Prouvensier, L., Leon-Icaza, S.A., Hessel, A., Péricat, D., Murriss, M., Guet-Revillet, H., Henras, A., Buyck, J., Ravet, E., Zhong, F.L., Cougoule, C., Planès, R., Meunier, E., 2023. EEF2-inactivating toxins engage the NLRP1 inflammasome and promote epithelial barrier disruption. *Journal of Experimental Medicine* 220, e20230104. <https://doi.org/10.1084/jem.20230104>
- Pippig, D.A., Hellmuth, J.C., Cui, S., Kirchhofer, A., Lammens, K., Lammens, A., Schmidt, A., Rothenfusser, S., Hopfner, K.-P., 2009. The regulatory domain of the RIG-I family ATPase LGP2 senses double-stranded RNA. *Nucleic Acids Research* 37, 2014–2025. <https://doi.org/10.1093/nar/gkp059>
- Planès, R., Pinilla, M., Santoni, K., Hessel, A., Passemar, C., Lay, K., Paillette, P., Valadão, A.-L.C., Robinson, K.S., Bastard, P., Lam, N., Fadrique, R., Rossi, I., Pericat, D., Bagayoko, S., Leon-Icaza, S.A., Rombouts, Y., Perouzel, E.,

- Tiraby, M., Zhang, Q., Cicuta, P., Jouanguy, E., Neyrolles, O., Bryant, C.E., Floto, A.R., Goujon, C., Lei, F.Z., Martin-Blondel, G., Silva, S., Casanova, J.-L., Cougoule, C., Reversade, B., Marcoux, J., Ravet, E., Meunier, E., 2022. Human NLRP1 is a sensor of pathogenic coronavirus 3CL proteases in lung epithelial cells. *Mol Cell* 82, 2385-2400.e9. <https://doi.org/10.1016/j.molcel.2022.04.033>
- Pontillo, A., Reis, E.C., Bricher, P.N., Vianna, P., Diniz, S., Fernandes, K.S., Chies, J.A., Sandrim, V., 2015. NLRP1 L155H Polymorphism is a Risk Factor for Preeclampsia Development. *American Journal of Reproductive Immunology* 73, 577–581. <https://doi.org/10.1111/aji.12353>
- Rao, S.D., Chen, Q., Wang, Q., Orth-He, E.L., Saoi, M., Griswold, A.R., Bhattacharjee, A., Ball, D.P., Huang, H.-C., Chui, A.J., Covelli, D.J., You, S., Cross, J.R., Bachovchin, D.A., 2022. M24B aminopeptidase inhibitors selectively activate the CARD8 inflammasome. *Nat Chem Biol* 18, 565–574. <https://doi.org/10.1038/s41589-021-00964-7>
- Razmara, M., Srinivasula, S.M., Wang, L., Poyet, J.-L., Geddes, B.J., DiStefano, P.S., Bertin, J., Alnemri, E.S., 2002. CARD-8 Protein, a New CARD Family Member That Regulates Caspase-1 Activation and Apoptosis *. *Journal of Biological Chemistry* 277, 13952–13958. <https://doi.org/10.1074/jbc.M107811200>
- Rehwinkel, J., Gack, M.U., 2020. RIG-I-like receptors: their regulation and roles in RNA sensing. *Nat Rev Immunol* 20, 537–551. <https://doi.org/10.1038/s41577-020-0288-3>
- Reinhold, D., Gohl, A., Wrenger, S., Reinhold, A., Kühlmann, U.C., Faust, J., Neubert, K., Thielitz, A., Brocke, S., Täger, M., Ansorge, S., Bank, U., 2009. Role of dipeptidyl peptidase IV (DP IV)-like enzymes in T lymphocyte activation: investigations in DP IV/CD26-knockout mice. *Clinical Chemistry and Laboratory Medicine* 47, 268–274. <https://doi.org/10.1515/CCLM.2009.062>
- Robert Hollingsworth, L., David, L., Li, Y., Griswold, A.R., Ruan, J., Sharif, H., Fontana, P., Orth-He, E.L., Fu, T.-M., Bachovchin, D.A., Wu, H., 2021. Mechanism of filament formation in UPA-promoted CARD8 and NLRP1 inflammasomes. *Nat Commun* 12, 189. <https://doi.org/10.1038/s41467-020-20320-y>
- Robinson, K.S., Teo, D.E.T., Tan, K.S., Toh, G.A., Ong, H.H., Lim, C.K., Lay, K., Au, B.V., Lew, T.S., Chu, J.J.H., Chow, V.T.K., Wang, D.Y., Zhong, F.L., Reversade, B., 2020. Enteroviral 3C protease activates the human NLRP1 inflammasome in airway epithelia. *Science* 370, eaay2002. <https://doi.org/10.1126/science.aay2002>
- Robinson, K.S., Toh, G.A., Firdaus, M.J., Tham, K.C., Rozario, P., Lim, C.K., Toh, Y.X., Lau, Z.H., Binder, S.C., Mayer, J., Bonnard, C., Schmidt, F.I., Common, J.E.A., Zhong, F.L., 2023. Diphtheria toxin activates ribotoxic stress and

NLRP1 inflammasome-driven pyroptosis. *Journal of Experimental Medicine* 220, e20230105. <https://doi.org/10.1084/jem.20230105>

Robinson, K.S., Toh, G.A., Rozario, P., Chua, R., Bauernfried, S., Sun, Z., Firdaus, M.J., Bayat, S., Nadkarni, R., Poh, Z.S., Tham, K.C., Harapas, C.R., Lim, C.K., Chu, W., Tay, C.W.S., Tan, K.Y., Zhao, T., Bonnard, C., Sobota, R., Connolly, J.E., Common, J., Masters, S.L., Chen, K.W., Ho, L., Wu, B., Hornung, V., Zhong, F.L., 2022. ZAK α -driven ribotoxic stress response activates the human NLRP1 inflammasome. *Science* 377, 328–335. <https://doi.org/10.1126/science.abl6324>

Robinson, M.J., Osorio, F., Rosas, M., Freitas, R.P., Schweighoffer, E., Groß, O., Verbeek, J.S., Ruland, J., Tybulewicz, V., Brown, G.D., Moita, L.F., Taylor, P.R., Reis e Sousa, C., 2009. Dectin-2 is a Syk-coupled pattern recognition receptor crucial for Th17 responses to fungal infection. *Journal of Experimental Medicine* 206, 2037–2051. <https://doi.org/10.1084/jem.20082818>

Rogers, C., Fernandes-Alnemri, T., Mayes, L., Alnemri, D., Cingolani, G., Alnemri, E.S., 2017. Cleavage of DFNA5 by caspase-3 during apoptosis mediates progression to secondary necrotic/pyroptotic cell death. *Nat Commun* 8, 14128. <https://doi.org/10.1038/ncomms14128>

Rosales, C., Uribe-Querol, E., 2017. Phagocytosis: A Fundamental Process in Immunity. *Biomed Res Int* 2017, 9042851. <https://doi.org/10.1155/2017/9042851>

Rosenberg, M., Azevedo, N.F., Ivask, A., 2019. Propidium iodide staining underestimates viability of adherent bacterial cells. *Sci Rep* 9, 6483. <https://doi.org/10.1038/s41598-019-42906-3>

Ross, B., Krapp, S., Augustin, M., Kierfersauer, R., Arciniega, M., Geiss-Friedlander, R., Huber, R., 2018. Structures and mechanism of dipeptidyl peptidases 8 and 9, important players in cellular homeostasis and cancer. *Proceedings of the National Academy of Sciences* 115, E1437–E1445. <https://doi.org/10.1073/pnas.1717565115>

Rothenfusser, S., Goutagny, N., DiPerna, G., Gong, M., Monks, B.G., Schoenemeyer, A., Yamamoto, M., Akira, S., Fitzgerald, K.A., 2005. The RNA Helicase Lgp2 Inhibits TLR-Independent Sensing of Viral Replication by Retinoic Acid-Inducible Gene-1. *The Journal of Immunology* 175, 5260–5268. <https://doi.org/10.4049/jimmunol.175.8.5260>

Saito, T., Hirai, R., Loo, Y.-M., Owen, D., Johnson, C.L., Sinha, S.C., Akira, S., Fujita, T., Gale, M., 2007. Regulation of innate antiviral defenses through a shared repressor domain in RIG-I and LGP2. *Proceedings of the National Academy of Sciences* 104, 582–587. <https://doi.org/10.1073/pnas.0606699104>

Sandstrom, A., Mitchell, P.S., Goers, L., Mu, E.W., Lesser, C.F., Vance, R.E., 2019. Functional degradation: A mechanism of NLRP1 inflammasome activation

by diverse pathogen enzymes. *Science* 364, eaau1330.
<https://doi.org/10.1126/science.aau1330>

- Sarhan, J., Liu, B.C., Muendlein, H.I., Li, P., Nilson, R., Tang, A.Y., Rongvaux, A., Bunnell, S.C., Shao, F., Green, D.R., Poltorak, A., 2018. Caspase-8 induces cleavage of gasdermin D to elicit pyroptosis during *Yersinia* infection. *Proceedings of the National Academy of Sciences* 115, E10888–E10897. <https://doi.org/10.1073/pnas.1809548115>
- Saso, K., Miyoshi, N., Fujino, S., Sasaki, M., Yasui, M., Ohue, M., Ogino, T., Takahashi, H., Uemura, M., Matsuda, C., Mizushima, T., Doki, Y., Eguchi, H., 2020. Dipeptidyl Peptidase 9 Increases Chemoresistance and is an Indicator of Poor Prognosis in Colorectal Cancer. *Ann Surg Oncol* 27, 4337–4347. <https://doi.org/10.1245/s10434-020-08729-7>
- Sastalla, I., Crown, D., Masters, S.L., McKenzie, A., Leppla, S.H., Moayeri, M., 2013. Transcriptional analysis of the three Nlrp1 paralogs in mice. *BMC Genomics* 14, 188. <https://doi.org/10.1186/1471-2164-14-188>
- Sato, T., Tatekoshi, A., Takada, K., Iyama, S., Kamihara, Y., Jawaid, P., Rehman, M.U., Noguchi, K., Kondo, T., Kajikawa, S., Arita, K., Wada, A., Murakami, J., Arai, M., Yasuda, I., Dang, N.H., Hatano, R., Iwao, N., Ohnuma, K., Morimoto, C., 2019. DPP8 is a novel therapeutic target for multiple myeloma. *Sci Rep* 9, 18094. <https://doi.org/10.1038/s41598-019-54695-w>
- Satoh, T., Kato, H., Kumagai, Y., Yoneyama, M., Sato, S., Matsushita, K., Tsujimura, T., Fujita, T., Akira, S., Takeuchi, O., 2010. LGP2 is a positive regulator of RIG-I- and MDA5-mediated antiviral responses. *Proceedings of the National Academy of Sciences* 107, 1512–1517. <https://doi.org/10.1073/pnas.0912986107>
- Schattgen, S.A., Fitzgerald, K.A., 2011. The PYHIN protein family as mediators of host defenses. *Immunological Reviews* 243, 109–118. <https://doi.org/10.1111/j.1600-065X.2011.01053.x>
- Schlee, M., Roth, A., Hornung, V., Hagmann, C.A., Wimmenauer, V., Barchet, W., Coch, C., Janke, M., Mihailovic, A., Wardle, G., Juranek, S., Kato, H., Kawai, T., Poeck, H., Fitzgerald, K.A., Takeuchi, O., Akira, S., Tuschl, T., Latz, E., Ludwig, J., Hartmann, G., 2009. Recognition of 5' Triphosphate by RIG-I Helicase Requires Short Blunt Double-Stranded RNA as Contained in Panhandle of Negative-Strand Virus. *Immunity* 31, 25–34. <https://doi.org/10.1016/j.immuni.2009.05.008>
- Schmacke, N.A., O'Duill, F., Gaidt, M.M., Szymanska, I., Kamper, J.M., Schmid-Burgk, J.L., Mädler, S.C., Mackens-Kiani, T., Kozaki, T., Chauhan, D., Nagl, D., Stafford, C.A., Harz, H., Fröhlich, A.L., Pinci, F., Ginhoux, F., Beckmann, R., Mann, M., Leonhardt, H., Hornung, V., 2022. IKK β primes inflammasome formation by recruiting NLRP3 to the trans-Golgi network. *Immunity* 55, 2271–2284.e7. <https://doi.org/10.1016/j.immuni.2022.10.021>

- Schmalstieg, F.C., Goldman, A.S., 2008. Ilya Ilich Metchnikoff (1845-1915) and Paul Ehrlich (1854-1915): the centennial of the 1908 Nobel Prize in Physiology or Medicine. *J Med Biogr* 16, 96–103. <https://doi.org/10.1258/jmb.2008.008006>
- Schmid-Burgk, J.L., Chauhan, D., Schmidt, T., Ebert, T.S., Reinhardt, J., Endl, E., Hornung, V., 2016. A Genome-wide CRISPR (Clustered Regularly Interspaced Short Palindromic Repeats) Screen Identifies NEK7 as an Essential Component of NLRP3 Inflammasome Activation *. *Journal of Biological Chemistry* 291, 103–109. <https://doi.org/10.1074/jbc.C115.700492>
- Schmidt, A., Schwerd, T., Hamm, W., Hellmuth, J.C., Cui, S., Wenzel, M., Hoffmann, F.S., Michallet, M.-C., Besch, R., Hopfner, K.-P., Endres, S., Rothenfusser, S., 2009. 5'-triphosphate RNA requires base-paired structures to activate antiviral signaling via RIG-I. *Proceedings of the National Academy of Sciences* 106, 12067–12072. <https://doi.org/10.1073/pnas.0900971106>
- Schoultz, I., Verma, D., Halfvarsson, J., Törkvist, L., Fredrikson, M., Sjöqvist, U., Lördal, M., Tysk, C., Lerm, M., Söderkvist, P., Söderholm, J.D., 2009. Combined Polymorphisms in Genes Encoding the Inflammasome Components NALP3 and CARD8 Confer Susceptibility to Crohn's Disease in Swedish Men. *Official journal of the American College of Gastroenterology | ACG* 104, 1180.
- Schrödinger, L., DeLano, W., 2020. PYMOL.
- Sharif, H., Hollingsworth, L.R., Griswold, A.R., Hsiao, J.C., Wang, Q., Bachovchin, D.A., Wu, H., 2021. Dipeptidyl peptidase 9 sets a threshold for CARD8 inflammasome formation by sequestering its active C-terminal fragment. *Immunity* 54, 1392-1404.e10. <https://doi.org/10.1016/j.immuni.2021.04.024>
- Sharif-zak, M., Abbasi-jorjandi, M., Asadikaram, G., Ghoreishi, Z., Rezazadeh-Jabalbarzi, M., afsharipur, A., Rashidinejad, H., Khajepour, F., Jafarzadeh, A., Arefinia, N., Kheyrikhah, A., Abolhassani, M., 2022. CCR2 and DPP9 expression in the peripheral blood of COVID-19 patients: Influences of the disease severity and gender. *Immunobiology* 227, 152184. <https://doi.org/10.1016/j.imbio.2022.152184>
- Shi, H., Wang, Y., Li, X., Zhan, X., Tang, M., Fina, M., Su, L., Pratt, D., Bu, C.H., Hildebrand, S., Lyon, S., Scott, L., Quan, J., Sun, Q., Russell, J., Arnett, S., Jurek, P., Chen, D., Kravchenko, V.V., Mathison, J.C., Moresco, E.M.Y., Monson, N.L., Ulevitch, R.J., Beutler, B., 2016. NLRP3 activation and mitosis are mutually exclusive events coordinated by NEK7, a new inflammasome component. *Nat Immunol* 17, 250–258. <https://doi.org/10.1038/ni.3333>
- Shi, J., Zhao, Y., Wang, K., Shi, X., Wang, Y., Huang, H., Zhuang, Y., Cai, T., Wang, F., Shao, F., 2015. Cleavage of GSDMD by inflammatory caspases

- determines pyroptotic cell death. *Nature* 526, 660–665. <https://doi.org/10.1038/nature15514>
- Shi, J., Zhao, Y., Wang, Y., Gao, W., Ding, J., Li, P., Hu, L., Shao, F., 2014. Inflammatory caspases are innate immune receptors for intracellular LPS. *Nature* 514, 187–192. <https://doi.org/10.1038/nature13683>
- Srinivasula, S.M., Poyet, J.-L., Razmara, M., Datta, P., Zhang, Z., Alnemri, E.S., 2002. The PYRIN-CARD Protein ASC Is an Activating Adaptor for Caspase-1*. *Journal of Biological Chemistry* 277, 21119–21122. <https://doi.org/10.1074/jbc.C200179200>
- Stafford, C.A., Gassauer, A.-M., de Oliveira Mann, C.C., Tanzer, M.C., Fessler, E., Wefers, B., Nagl, D., Kuut, G., Sulek, K., Vasilopoulou, C., Schwojer, S.J., Wiest, A., Pfautsch, M.K., Wurst, W., Yabal, M., Fröhlich, T., Mann, M., Gisch, N., Jae, L.T., Hornung, V., 2022. Phosphorylation of muramyl peptides by NAGK is required for NOD2 activation. *Nature* 609, 590–596. <https://doi.org/10.1038/s41586-022-05125-x>
- Steimle, V., Otten, L.A., Zufferey, M., Mach, B., 1993. Complementation cloning of an MHC class II transactivator mutated in hereditary MHC class II deficiency (or bare lymphocyte syndrome). *Cell* 75, 135–146. [https://doi.org/10.1016/S0092-8674\(05\)80090-X](https://doi.org/10.1016/S0092-8674(05)80090-X)
- Sui, J., Li, H., Fang, Y., Liu, Y., Li, M., Zhong, B., Yang, F., Zou, Q., Wu, Y., 2012. NLRP1 gene polymorphism influences gene transcription and is a risk factor for rheumatoid arthritis in Han Chinese. *Arthritis & Rheumatism* 64, 647–654. <https://doi.org/10.1002/art.33370>
- Sun, L., Wu, J., Du, F., Chen, X., Chen, Z.J., 2013. Cyclic GMP-AMP Synthase Is a Cytosolic DNA Sensor That Activates the Type I Interferon Pathway. *Science* 339, 786–791. <https://doi.org/10.1126/science.1232458>
- Sundaram, B., Pandian, N., Mall, R., Wang, Y., Sarkar, R., Kim, H.J., Malireddi, R.K.S., Karki, R., Janke, L.J., Vogel, P., Kanneganti, T.-D., 2023. NLRP12-PANoptosome activates PANoptosis and pathology in response to heme and PAMPs. *Cell* 186, 2783-2801.e20. <https://doi.org/10.1016/j.cell.2023.05.005>
- Taabazuing, C.Y., Griswold, A.R., Bachovchin, D.A., 2020. The NLRP1 and CARD8 inflammasomes. *Immunological Reviews* 297, 13–25. <https://doi.org/10.1111/imr.12884>
- Takaoka, A., Wang, Z., Choi, M.K., Yanai, H., Negishi, H., Ban, T., Lu, Y., Miyagishi, M., Kodama, T., Honda, K., Ohba, Y., Taniguchi, T., 2007. DAI (DLM-1/ZBP1) is a cytosolic DNA sensor and an activator of innate immune response. *Nature* 448, 501–505. <https://doi.org/10.1038/nature06013>
- Takeuchi, O., Akira, S., 2010. Pattern Recognition Receptors and Inflammation. *Cell* 140, 805–820. <https://doi.org/10.1016/j.cell.2010.01.022>

- Tang, Z., Li, J., Shen, Q., Feng, J., Liu, H., Wang, W., Xu, L., Shi, G., Ye, X., Ge, M., Zhou, X., Ni, S., 2017. Contribution of upregulated dipeptidyl peptidase 9 (DPP9) in promoting tumorigenicity, metastasis and the prediction of poor prognosis in non-small cell lung cancer (NSCLC). *International Journal of Cancer* 140, 1620–1632. <https://doi.org/10.1002/ijc.30571>
- Taylor, P.R., Tsoni, S.V., Willment, J.A., Dennehy, K.M., Rosas, M., Findon, H., Haynes, K., Steele, C., Botto, M., Gordon, S., Brown, G.D., 2007. Dectin-1 is required for β -glucan recognition and control of fungal infection. *Nat Immunol* 8, 31–38. <https://doi.org/10.1038/ni1408>
- Tenthorey, J.L., Kofoed, E.M., Daugherty, M.D., Malik, H.S., Vance, R.E., 2014. Molecular Basis for Specific Recognition of Bacterial Ligands by NAIP/NLRC4 Inflammasomes. *Molecular Cell* 54, 17–29. <https://doi.org/10.1016/j.molcel.2014.02.018>
- Thornberry, N.A., Bull, H.G., Calaycay, J.R., Chapman, K.T., Howard, A.D., Kostura, M.J., Miller, D.K., Molineaux, S.M., Weidner, J.R., Aunins, J., Elliston, K.O., Ayala, J.M., Casano, F.J., Chin, J., Ding, G.J.-F., Egger, L.A., Gaffney, E.P., Limjuco, G., Palyha, O.C., Raju, S.M., Rolando, A.M., Salley, J.P., Yamin, T.-T., Lee, T.D., Shively, J.E., MacCross, M., Mumford, R.A., Schmidt, J.A., Tocci, M.J., 1992. A novel heterodimeric cysteine protease is required for interleukin-1 β processing in monocytes. *Nature* 356, 768–774. <https://doi.org/10.1038/356768a0>
- Tschopp, J., Martinon, F., Burns, K., 2003. NALPs: a novel protein family involved in inflammation. *Nat Rev Mol Cell Biol* 4, 95–104. <https://doi.org/10.1038/nrm1019>
- Tsu, B.V., Agarwal, R., Gokhale, N.S., Kulsuptrakul, J., Ryan, A.P., Fay, E.J., Castro, L.K., Beierschmitt, C., Yap, C., Turcotte, E.A., Delgado-Rodriguez, S.E., Vance, R.E., Hyde, J.L., Savan, R., Mitchell, P.S., Daugherty, M.D., 2023. Host-specific sensing of coronaviruses and picornaviruses by the CARD8 inflammasome. *PLOS Biology* 21, e3002144. <https://doi.org/10.1371/journal.pbio.3002144>
- Tsu, B.V., Beierschmitt, C., Ryan, A.P., Agarwal, R., Mitchell, P.S., Daugherty, M.D., 2021. Diverse viral proteases activate the NLRP1 inflammasome. *eLife* 10, e60609. <https://doi.org/10.7554/eLife.60609>
- Tuladhar, S., Kanneganti, T.-D., 2020. NLRP12 in innate immunity and inflammation. *Molecular Aspects of Medicine, Inflammasome* 76, 100887. <https://doi.org/10.1016/j.mam.2020.100887>
- Unterholzner, L., Keating, S.E., Baran, M., Horan, K.A., Jensen, S.B., Sharma, S., Sirois, C.M., Jin, T., Latz, E., Xiao, T.S., Fitzgerald, K.A., Paludan, S.R., Bowie, A.G., 2010. IFI16 is an innate immune sensor for intracellular DNA. *Nat Immunol* 11, 997–1004. <https://doi.org/10.1038/ni.1932>
- Upton, J.W., Kaiser, W.J., Mocarski, E.S., 2012. DAI/ZBP1/DLM-1 complexes with RIP3 to mediate virus-induced programmed necrosis that is targeted by

- murine cytomegalovirus vIRA. *Cell Host Microbe* 11, 290–297. <https://doi.org/10.1016/j.chom.2012.01.016>
- van Wersch, S., Tian, L., Hoy, R., Li, X., 2020. Plant NLRs: The Whistleblowers of Plant Immunity. *Plant Communications* 1, 100016. <https://doi.org/10.1016/j.xplc.2019.100016>
- Vasconcelos, N.M. de, Vliegen, G., Gonçalves, A., Hert, E.D., Martín-Pérez, R., Opdenbosch, N.V., Jallapally, A., Geiss-Friedlander, R., Lambeir, A.-M., Augustyns, K., Veken, P.V.D., Meester, I.D., Lamkanfi, M., 2019. DPP8/DPP9 inhibition elicits canonical Nlrp1b inflammasome hallmarks in murine macrophages. *Life Science Alliance* 2. <https://doi.org/10.26508/lsa.201900313>
- Vind, A.C., Snieckute, G., Blasius, M., Tiedje, C., Krogh, N., Bekker-Jensen, D.B., Andersen, K.L., Nordgaard, C., Tollenaere, M.A.X., Lund, A.H., Olsen, J.V., Nielsen, H., Bekker-Jensen, S., 2020. ZAK α Recognizes Stalled Ribosomes through Partially Redundant Sensor Domains. *Molecular Cell* 78, 700–713.e7. <https://doi.org/10.1016/j.molcel.2020.03.021>
- Vladimer, G.I., Weng, D., Paquette, S.W.M., Vanaja, S.K., Rathinam, V.A.K., Aune, M.H., Conlon, J.E., Burbage, J.J., Proulx, M.K., Liu, Q., Reed, G., Mecsas, J.C., Iwakura, Y., Bertin, J., Goguen, J.D., Fitzgerald, K.A., Lien, E., 2012. The NLRP12 Inflammasome Recognizes *Yersinia pestis*. *Immunity* 37, 96–107. <https://doi.org/10.1016/j.immuni.2012.07.006>
- Walker, N.P.C., Talanian, R.V., Brady, K.D., Dang, L.C., Bump, N.J., Ferenza, C.R., Franklin, S., Ghayur, T., Hackett, M.C., Hammill, L.D., Herzog, L., Hugunin, M., Houy, W., Mankovich, J.A., McGuinness, L., Orlewicz, E., Paskind, M., Pratt, C.A., Reis, P., Summani, A., Terranova, M., Welch, J.P., Xiong, L., Möller, A., Tracey, D.E., Kamen, R., Wong, W.W., 1994. Crystal structure of the cysteine protease interleukin-1 β -converting enzyme: A (p20/p10)₂ homodimer. *Cell* 78, 343–352. [https://doi.org/10.1016/0092-8674\(94\)90303-4](https://doi.org/10.1016/0092-8674(94)90303-4)
- Wang, C., Yu, C., Ye, F., Wei, Z., Zhang, M., 2012. Structure of the ZU5-ZU5-UPA-DD tandem of ankyrin-B reveals interaction surfaces necessary for ankyrin function. *Proc Natl Acad Sci U S A* 109, 4822–4827. <https://doi.org/10.1073/pnas.1200613109>
- Wang, L., Manji, G.A., Grenier, J.M., Al-Garawi, A., Merriam, S., Lora, J.M., Geddes, B.J., Briskin, M., DiStefano, P.S., Bertin, J., 2002. PYPAF7, a Novel PYRIN-containing Apaf1-like Protein That Regulates Activation of NF- κ B and Caspase-1-dependent Cytokine Processing *. *Journal of Biological Chemistry* 277, 29874–29880. <https://doi.org/10.1074/jbc.M203915200>
- Wang, P., Zhu, S., Yang, L., Cui, S., Pan, W., Jackson, R., Zheng, Y., Rongvaux, A., Sun, Q., Yang, G., Gao, S., Lin, R., You, F., Flavell, R., Fikrig, E., 2015. Nlrp6 regulates intestinal antiviral innate immunity. *Science* 350, 826–830. <https://doi.org/10.1126/science.aab3145>

- Wang, Q., Clark, K.M., Tiwari, R., Raju, N., Tharp, G.K., Rogers, J., Harris, R.A., Raveendran, M., Bosinger, S.E., Burdo, T.H., Silvestri, G., Shan, L., 2024. The CARD8 inflammasome dictates HIV/SIV pathogenesis and disease progression. *Cell* 187, 1223-1237.e16. <https://doi.org/10.1016/j.cell.2024.01.048>
- Wang, Q., Gao, H., Clark, K.M., Mugisha, C.S., Davis, K., Tang, J.P., Harlan, G.H., DeSelm, C.J., Presti, R.M., Kutluay, S.B., Shan, L., 2021. CARD8 is an inflammasome sensor for HIV-1 protease activity. *Science* 371, eabe1707. <https://doi.org/10.1126/science.abe1707>
- Wang, Q., Hsiao, J.C., Yardeny, N., Huang, H.-C., O'Mara, C.M., Orth-He, E.L., Ball, D.P., Zhang, Z., Bachovchin, D.A., 2023. The NLRP1 and CARD8 inflammasomes detect reductive stress. *Cell Reports* 42. <https://doi.org/10.1016/j.celrep.2022.111966>
- Wang, R., Wei, Z., Jin, H., Wu, H., Yu, C., Wen, W., Chan, L.-N., Wen, Z., Zhang, M., 2009. Autoinhibition of UNC5b Revealed by the Cytoplasmic Domain Structure of the Receptor. *Molecular Cell* 33, 692–703. <https://doi.org/10.1016/j.molcel.2009.02.016>
- Wang, Y., Gao, W., Shi, X., Ding, J., Liu, W., He, H., Wang, K., Shao, F., 2017. Chemotherapy drugs induce pyroptosis through caspase-3 cleavage of a gasdermin. *Nature* 547, 99–103. <https://doi.org/10.1038/nature22393>
- Wang, Y., Shao, F., 2021. NINJ1, rupturing swollen membranes for cataclysmic cell lysis. *Molecular Cell* 81, 1370–1371. <https://doi.org/10.1016/j.molcel.2021.03.005>
- Watanabe, H., Gaide, O., Pétrilli, V., Martinon, F., Contassot, E., Roques, S., Kummer, J.A., Tschopp, J., French, L.E., 2007. Activation of the IL-1 β -Processing Inflammasome Is Involved in Contact Hypersensitivity. *J Invest Dermatol* 127, 1956–1963. <https://doi.org/10.1038/sj.jid.5700819>
- Weber, A., Wasiliew, P., Kracht, M., 2010. Interleukin-1 (IL-1) Pathway. *Science Signaling* 3, cm1–cm1. <https://doi.org/10.1126/scisignal.3105cm1>
- Wilson, C.H., Indarto, D., Doucet, A., Pogson, L.D., Pitman, M.R., McNicholas, K., Menz, R.I., Overall, C.M., Abbott, C.A., 2013. Identifying Natural Substrates for Dipeptidyl Peptidases 8 and 9 Using Terminal Amine Isotopic Labeling of Substrates (TAILS) Reveals in Vivo Roles in Cellular Homeostasis and Energy Metabolism * \diamond . *Journal of Biological Chemistry* 288, 13936–13949. <https://doi.org/10.1074/jbc.M112.445841>
- Wilson, K.P., Black, J.-A.F., Thomson, J.A., Kim, E.E., Griffith, J.P., Navia, M.A., Murcko, M.A., Chambers, S.P., Aldape, R.A., Raybuck, S.A., Livingston, D.J., 1994. Structure and mechanism of interleukin-1 β converting enzyme. *Nature* 370, 270–275. <https://doi.org/10.1038/370270a0>
- Wolf, C., Fischer, H., Köhl, J.-S., Koss, S., Jamra, R.A., Starke, S., Schultz, J., Ehl, S., Neumann, K., Schuetz, C., Huber, R., Hornung, V., Lee-Kirsch, M.A.,

2023. Hemophagocytic lymphohistiocytosis–like hyperinflammation due to a de novo mutation in DPP9. *Journal of Allergy and Clinical Immunology* 152, 1336–1344.e5. <https://doi.org/10.1016/j.jaci.2023.07.013>
- Wu, C.C.-C., Peterson, A., Zinshteyn, B., Regot, S., Green, R., 2020. Ribosome Collisions Trigger General Stress Responses to Regulate Cell Fate. *Cell* 182, 404–416.e14. <https://doi.org/10.1016/j.cell.2020.06.006>
- Wu, J., Sun, L., Chen, X., Du, F., Shi, H., Chen, C., Chen, Z.J., 2013. Cyclic GMP-AMP Is an Endogenous Second Messenger in Innate Immune Signaling by Cytosolic DNA. *Science* 339, 826–830. <https://doi.org/10.1126/science.1229963>
- Wu, Q., Zhao, M., Huang, G., Zheng, Z., Chen, Y., Zeng, W., Lv, X., 2020. Fibroblast Activation Protein (FAP) Overexpression Induces Epithelial–Mesenchymal Transition (EMT) in Oral Squamous Cell Carcinoma by Down-Regulating Dipeptidyl Peptidase 9 (DPP9). *OncoTargets and Therapy* 13, 2599–2611. <https://doi.org/10.2147/OTT.S243417>
- Xiao, L., Magupalli, V.G., Wu, H., 2023. Cryo-EM structures of the active NLRP3 inflammasome disc. *Nature* 613, 595–600. <https://doi.org/10.1038/s41586-022-05570-8>
- Xu, H., Shi, J., Gao, H., Liu, Y., Yang, Z., Shao, F., Dong, N., 2019. The N-end rule ubiquitin ligase UBR2 mediates NLRP1B inflammasome activation by anthrax lethal toxin. *The EMBO Journal* 38, e101996. <https://doi.org/10.15252/emboj.2019101996>
- Xu, H., Yang, J., Gao, W., Li, L., Li, P., Zhang, L., Gong, Y.-N., Peng, X., Xi, J.J., Chen, S., Wang, F., Shao, F., 2014. Innate immune sensing of bacterial modifications of Rho GTPases by the Pyrin inflammasome. *Nature* 513, 237–241. <https://doi.org/10.1038/nature13449>
- Yamasaki, S., Matsumoto, M., Takeuchi, O., Matsuzawa, T., Ishikawa, E., Sakuma, M., Tateno, H., Uno, J., Hirabayashi, J., Mikami, Y., Takeda, K., Akira, S., Saito, T., 2009. C-type lectin Mincle is an activating receptor for pathogenic fungus, *Malassezia*. *Proceedings of the National Academy of Sciences* 106, 1897–1902. <https://doi.org/10.1073/pnas.0805177106>
- Yan, R., Xu, D., Yang, J., Walker, S., Zhang, Y., 2013. A comparative assessment and analysis of 20 representative sequence alignment methods for protein structure prediction. *Sci Rep* 3, 2619. <https://doi.org/10.1038/srep02619>
- Yoneyama, M., Fujita, T., 2008. Structural Mechanism of RNA Recognition by the RIG-I-like Receptors. *Immunity* 29, 178–181. <https://doi.org/10.1016/j.immuni.2008.07.009>
- Yoneyama, M., Kikuchi, M., Matsumoto, K., Imaizumi, T., Miyagishi, M., Taira, K., Foy, E., Loo, Y.-M., Gale, M., Jr, Akira, S., Yonehara, S., Kato, A., Fujita, T., 2005. Shared and Unique Functions of the DExD/H-Box Helicases RIG-I,

- MDA5, and LGP2 in Antiviral Innate Immunity. *The Journal of Immunology* 175, 2851–2858. <https://doi.org/10.4049/jimmunol.175.5.2851>
- Zhang, L., Chen, S., Ruan, J., Wu, J., Tong, A.B., Yin, Q., Li, Y., David, L., Lu, A., Wang, W.L., Marks, C., Ouyang, Q., Zhang, X., Mao, Y., Wu, H., 2015. Cryo-EM structure of the activated NAIP2-NLRC4 inflammasome reveals nucleated polymerization. *Science* 350, 404–409. <https://doi.org/10.1126/science.aac5789>
- Zhang, Xu, Shi, H., Wu, J., Zhang, Xuewu, Sun, L., Chen, C., Chen, Z.J., 2013. Cyclic GMP-AMP Containing Mixed Phosphodiester Linkages Is An Endogenous High-Affinity Ligand for STING. *Molecular Cell* 51, 226–235. <https://doi.org/10.1016/j.molcel.2013.05.022>
- Zhang, Z., Shibata, T., Fujimura, A., Kitaura, J., Miyake, K., Ohto, U., Shimizu, T., 2023. Structural basis for thioredoxin-mediated suppression of NLRP1 inflammasome. *Nature* 622, 188–194. <https://doi.org/10.1038/s41586-023-06532-4>
- Zhang, Z.-T., Ma, X.-J., Zong, Y., Du, X.-M., Hu, J.-H., Lu, G.-C., 2015. Is the CARD8 rs2043211 polymorphism associated with susceptibility to Crohn's disease? A meta-analysis. *Autoimmunity* 48, 524–531. <https://doi.org/10.3109/08916934.2015.1045581>
- Zhao, Y., Shao, F., 2015. The NAIP–NLRC4 inflammasome in innate immune detection of bacterial flagellin and type III secretion apparatus. *Immunological Reviews* 265, 85–102. <https://doi.org/10.1111/imr.12293>
- Zheng, D., Kern, L., Elinav, E., 2021. The NLRP6 inflammasome. *Immunology* 162, 281–289. <https://doi.org/10.1111/imm.13293>
- Zhong, F.L., Mamaï, O., Sborgi, L., Boussofara, L., Hopkins, R., Robinson, K., Szeverényi, I., Takeichi, T., Balaji, R., Lau, A., Tye, H., Roy, K., Bonnard, C., Ahl, P.J., Jones, L.A., Baker, P.J., Lacina, L., Otsuka, A., Fournie, P.R., Malecaze, F., Lane, E.B., Akiyama, M., Kabashima, K., Connolly, J.E., Masters, S.L., Soler, V.J., Omar, S.S., McGrath, J.A., Nedelcu, R., Gribaa, M., Denguezli, M., Saad, A., Hiller, S., Reversade, B., 2016. Germline NLRP1 Mutations Cause Skin Inflammatory and Cancer Susceptibility Syndromes via Inflammasome Activation. *Cell* 167, 187-202.e17. <https://doi.org/10.1016/j.cell.2016.09.001>
- Zhong, F.L., Robinson, K., Teo, D.E.T., Tan, K.-Y., Lim, C., Harapas, C.R., Yu, C.-H., Xie, W.H., Sobota, R.M., Au, V.B., Hopkins, R., D'Osualdo, A., Reed, J.C., Connolly, J.E., Masters, S.L., Reversade, B., 2018. Human DPP9 represses NLRP1 inflammasome and protects against autoinflammatory diseases via both peptidase activity and FIIND domain binding. *Journal of Biological Chemistry* 293, 18864–18878. <https://doi.org/10.1074/jbc.RA118.004350>
- Zhou, J.Y., Sarkar, M.K., Okamura, K., Harris, J.E., Gudjonsson, J.E., Fitzgerald, K.A., 2023. Activation of the NLRP1 inflammasome in human keratinocytes

by the dsDNA mimetic poly(dA:dT). Proceedings of the National Academy of Sciences 120, e2213777120. <https://doi.org/10.1073/pnas.2213777120>

Zimmermann, L., Stephens, A., Nam, S.-Z., Rau, D., Kübler, J., Lozajic, M., Gabler, F., Söding, J., Lupas, A.N., Alva, V., 2018. A Completely Reimplemented MPI Bioinformatics Toolkit with a New HHpred Server at its Core. Journal of Molecular Biology, Computation Resources for Molecular Biology 430, 2237–2243. <https://doi.org/10.1016/j.jmb.2017.12.007>

Zolg, S., Donzelli, L., Geiss-Friedlander, R., 2024. N-terminal processing by dipeptidyl peptidase 9: Cut and Go! Biochimie. <https://doi.org/10.1016/j.biochi.2024.03.002>

Żurawek, M., Fichna, M., Januszkiewicz-Lewandowska, D., Gryczyńska, M., Fichna, P., Nowak, J., 2010. A coding variant in *NLRP1* is associated with autoimmune Addison's disease. Human Immunology 71, 530–534. <https://doi.org/10.1016/j.humimm.2010.02.004>

8 List of abbreviations

AAA+	ATPases associated with various cellular activities
ABPP	Activity-based protein profiling
ADAR1	Adenosine deaminase acting on RNA 1
AIADK	Autoinflammation with arthritis and dyskeratosis
AIM2	Absent in melanoma 2
ALR	AIM2-like receptor
AML	Acute myeloid leukaemia
APC	Antigen presenting cell
AP-1	Activator protein-1
ASC	Apoptosis-associated speck-like protein containing a caspase recruitment domain (CARD)
ATP	Adenosine triphosphate
BIR	Baculovirus inhibitor of apoptosis repeat
CAPS	Cryopyrin-associated periodic syndromes
CARD	Caspase recruitment domain
CARDINAL	CARD inhibitor of NF- κ B-activating ligands
CCR2	CC chemokine receptor 2
cGAS	Nucleotidyltransferase cyclic GMP-AMP synthase
CIITA	Class II major histocompatibility complex transactivator
cGAMP	Cyclic GMP-AMP
CLR	C-type lectin receptor
CNVs	Copy number variations
CRD	Carbohydrate recognition domain
CRP	C-reactive protein
C3	Third complement component
DAI	DNA-dependent activator of IFN regulatory factors
DAMP	Damage-associated molecular pattern
DPP8/9	Dipeptidyl peptidases 8 and 9
dsRNA	Double-stranded RNA
DT	Diphtheria toxin
ETI	Effector-triggered immunity
ExoA	Exotoxin A
FAP	Fibroblast activation protein
FKLC	Familial keratosis lichenoides chronica
GFP	Green fluorescent protein

HA	Hemagglutinin
HIN	Hematopoietic interferon-inducible nuclear domain(s)
HIV-1	Human immunodeficiency virus
HMGB1	High mobility group box 1
IFI16	Interferon gamma-inducible protein 16
IKK ϵ	I κ B kinase- ϵ
IL-1	Interleukin-1
indels	Insertions/deletions
IRF	Interferon regulatory factors
ISGs	Interferon-stimulated genes
JRRP	Juvenile-onset recurrent respiratory papillomatosis
LDH	Lactate dehydrogenase
LF	Lethal factor
LRR	Leucine-rich repeat
MAC	Membrane attack complex
MAVS	Mitochondrial antiviral-signaling protein
MDP	Muramyl dipeptide
MHC	Major histocompatibility complex
MINCLE	Macrophage inducible Ca ²⁺ -dependent lectin receptor
MSPC	Multiple self-healing palmoplantar carcinoma
mtDNA	Mitochondrial DNA
MyD88	Myeloid differentiation primary response protein 88
NAGK	N-acetylglucosamine kinase
NAIP	Neuronal apoptosis inhibitory protein
NAIPs	NLR family apoptosis inhibitory proteins
NBD	Nucleotide-binding domain
NBS-LRR	Nucleotide-binding sequence LRR
NEK7	NIMA-related kinase 7
NF- κ B	nuclear factor kappa light-chain enhancer of activated B cells
NINJ1	Ninjurin-1
NLR	NOD-like receptors
NLRAs	NLR family acidic transactivation domain-containing proteins
NLRBs	NLR family BIR domain-containing proteins
NLRCs	NLR family CARD containing proteins
NLRPs	NLR family PYD containing proteins
NLS	Nuclear localisation signal
NNRTIs	Non-nucleoside reverse transcriptase inhibitors
NOD	Nucleotide-binding oligomerisation domain

NSCLC	Non-small cell lung cancer
nsSNPs	Nonsynonymous SNPs
OSCC	Oral squamous cell carcinoma
PAMP	Pathogen-associated molecular pattern
PI	Propidium iodide
PIDD	p53-inducible protein with a death domain
PRR	Pattern-recognition receptor
PSSP	Protein secondary structure prediction
PTI	Pattern-triggered immunity
PYD	Pyrin domain
PYPAF	PYRIN-containing APAF-1-like proteins
RFP	Red fluorescent protein
RIG	Retinoic acid-inducible gene
RLR	Retinoic acid-inducible gene (RIG)-I-like receptors
RNP	Ribonucleoprotein
SIV-1	Simian immunodeficiency virus 1
SNPs	Single-Nucleotide Polymorphisms
SNVs	Single nucleotide variants
ssRNA	Single-stranded RNA
STAND	Signal transduction ATPases with numerous domains
TBK1	TANK-binding kinase 1
TGN	Trans-Golgi network
TIR	Toll/IL-1 receptor
TLR	Toll-like receptor
TNF	Tumor necrosis factor
TRIF	TIR domain-containing adaptor-inducing IFN β
TRX-1	Thioredoxin-1
TUCAN	Tumour-upregulated CARD-containing antagonist of caspase-9
T3SS	Type-III secretion system
UPA	Conserved in UNC5, PIDD and Ankyrins
ZBP1	Z-DNA binding protein 1
ZU5	Found in ZO-1 (zona occludens 1) and UNC5 (uncoordinated protein
5)	

9 Acknowledgements

First, I want to thank Prof. Dr. Veit Hornung for allowing me to do my Ph.D. thesis in his lab and for all his support throughout the years of my Ph.D. He always had an open door to discuss results and problems and always found the time for me when I needed it. Thanks for the constructive suggestions, especially during the paper time.

Next, I would like to thank our very nice collaborators, Dr. Christine Wolf and Prof. Dr. Min Ae Lee-Kirsch, for approaching us about this collaboration and contributing to the publication of this story.

I would also like to thank my TAC committee, Prof. Dr. Andreas Pichlmair and Prof. Dr. Oliver Keppler, for the enjoyable atmosphere and helpful discussions during our meetings. Special thanks here to Andreas for already believing in me during my bachelor studies and his support throughout the years.

I would also like to thank our lab technicians, especially Claudia Ludwig and Larissa Hansbauer, who made my life so much easier! Claudia Ludwig for her help with ELISAs, Western blots and cloning whenever I needed it. Special thanks to Jochen Rech for teaching me how to use the microscopes and the robot and for always helping me with problems, even on weekends. Additionally, I would like to thank Dr. Zhiqi Sun for the fruitful discussions with me in the cell culture while splitting cells and Dr. Andreas Linder for getting me started in the lab and for his support with the T cell project. Special thanks to the rest of the Hornung group, current and alumni, for their support, scientific discussions, and social evenings, especially the adventure game group and the hospital lunch group ☺ It was enjoyable to work with you guys! Special thanks to Dr Ciana Diskin and Julia Kamper, who read my thesis, gave good comments and cheered me up during the writing process. Thanks to Dr Katja Lammens, who took the time to proofread the structural part of my thesis.

Very special thanks to Holger ☺ You not only cheered me up and put a smile on my face every day but also helped me survive even stressful times with injuries, moving, and writing my thesis! Thanks for our excellent day-to-day life!

Furthermore, I would like to thank my lovely friends for causing my good mood at work ;)

Ultimately, I would like to thank my parents and family for their endless support during my studies, especially my Master's thesis abroad, which would not have been possible without them!

10 Appendix

10.1 PolyPhen-2 report for the short isoform of DPP9

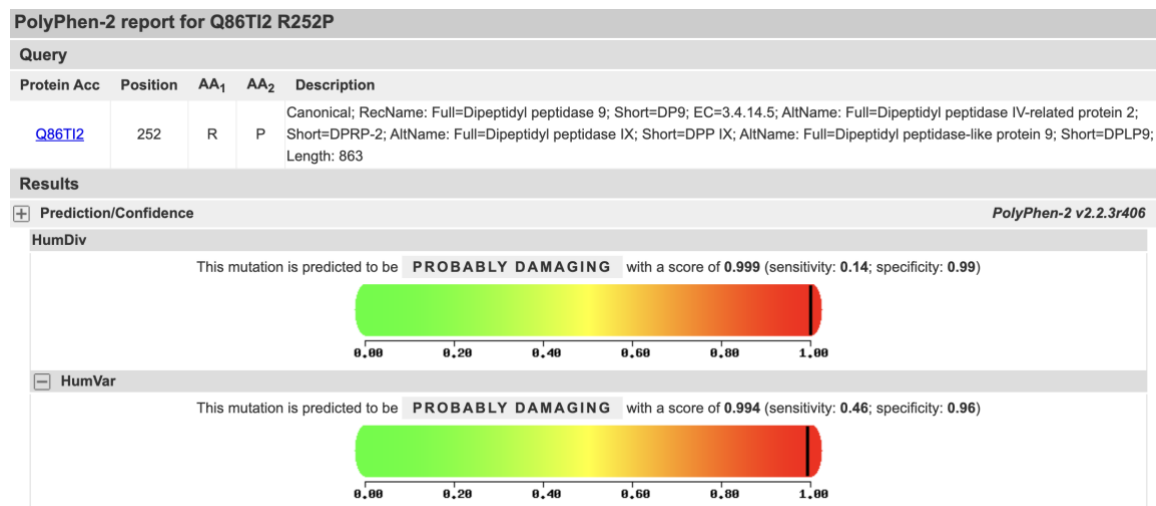


Figure 31: *In silico* analysis of the DPP9 mutant (R252P). PolyPhen-2 report for the short isoform of DPP9 (Q86T12; ENST00000593973.2).

10.2 IC₅₀ and K_i' values of relevant DPP8 and DPP9 inhibitors

The following IC₅₀ and K_i' values were obtained from the literature.

Table 16: IC₅₀ and K_i' values of DPP8/9 inhibitors.

Inhibitor / Compound	IC ₅₀ [μM] DPP8	IC ₅₀ [μM] DPP9	Sensitivity Index (SI)	Reference
Vildagliptin	2.2 ± 0.4	0.23 ± 0.08	9.6 (DPP8/DPP9)	(Benramdane et al., 2023)
Compd. 42	0.6 ± 0.4	0.0034 ± 0.0006	176.4 (DPP8/DPP9)	(Benramdane et al., 2023)
G1244	0.014	0.053	3.8 (DPP9/DPP8)	(Benramdane et al., 2023)
Talabostat	0.004	0.011	2.75 (DPP9/DPP8)	Selleckchem

Compound	KI' [nM] DPP8	KI' [nM] DPP9	Sensitivity Index (SI)	Reference
Compd. 6	26.3 ± 2.6	184 ± 38.4	7.0	(Carvalho et al., 2022)
Compd. 9	2.7 ± 0.6	11.4 ± 3.5	4.2	(Carvalho et al., 2022)
Compd. 12	95.0 ± 15.5	>2000	>21	(Carvalho et al., 2022)

10.3 Batch processing scripts for ImageJ

The following scripts were adopted from the ImageJ forum for the best processing of the images taken for this thesis.

Brightfield

// Macro to quantify cells in brightfield images

```
run("Clear Results");
setBatchMode(true);
inputDirectory = getDirectory("Choose a Directory of Images");
fileList = getFileList(inputDirectory);
for (i = 0; i < fileList.length; i++)
{
    processImage(fileList[i]);
}
updateResults();
setBatchMode(false);

outputFile = File.openDialog("Save results file");
saveAs("results",outputFile);

function processImage(imageFile)
{
    // store the number of results before executing the commands, so we can
    add the filename just to the new results
    prevNumResults = nResults;

    open(imageFile);
    setVoxelSize(0.7, 0.7, 1, "um");
```

```

filename = getTitle();

run("Bandpass Filter...", "filter_large=40 filter_small=3 suppress=None
tolerance=5 autoscale saturate");

setAutoThreshold("IsoData");
run("Set Measurements...", "area mean perimeter shape limit
redirect=None decimal=4");
run("Analyze Particles...", "size=30-Infinity circularity=0.5-1.00 display
include");

for (row = prevNumResults; row < nResults; row++)
{
    setResult("Filename", row, filename);
}

close("");
}

```

PI⁺ cells

// Macro to quantify PI positive cells in images

```

run("Clear Results");
setBatchMode(true);
inputDirectory = getDirectory("Choose a Directory of Images");
fileList = getFileList(inputDirectory);

for (i = 0; i < fileList.length; i++)
{
    processImage(fileList[i]);
}

updateResults();
setBatchMode(false);
outputFile = File.openDialog("Save results file");

saveAs("results",outputFile);

function processImage(imageFile)
{
    prevNumResults = nResults;

    open(imageFile);
}

```



```
setVoxelSize(0.7, 0.7, 1, "um");
filename = getTitle();

setAutoThreshold("Moments dark");
run("Set Measurements...", "area mean perimeter shape limit
redirect=None decimal=4");

run("Analyze Particles...", "size=30-Infinity circularity=0-1.00 display");

for (row = prevNumResults; row < nResults; row++)
{
    setResult("Filename", row, filename);
}

close("");
}
```